CATÓLICA
ESCOLA SUPERIOR DE BIOTECNOLOGIA
PORTO

OSMAC STRATEGIES TO DISCOVER NEW NATURAL PRODUCTS

by

Dora de Fátima Medeiros Ferreira

July 2023

CATÓLICA
ESCOLA SUPERIOR DE BIOTECNOLOGIA
PORTO

OSMAC STRATEGIES TO DISCOVER NEW NATURAL PRODUCTS

Thesis presented to Escola Superior de Biotecnologia of the
Universidade Católica Portuguesa to fulfill the requirements of Master of Science degree in
Applied Microbiology

by

Dora de Fátima
Medeiros Ferreira

Supervisors (CIIMAR): Mariana Reis, PhD – supervisor

Ralph Urbatzka, PhD – co-supervisor

Joana Almeida, PhD – co-supervisor

Tutor (Escola Superior de Biotecnologia): Prof. Rui Morais, PhD

July 2023

Resumo

As cianobactérias são microrganismos fotossintéticos capazes de produzir uma larga gama de produtos secundários, desde toxinas a outros compostos com aplicações biotecnológicas e farmacêuticas reconhecidas. Recentes avanços na Genómica e Bioinformática têm vindo a demonstrar que os genomas das cianobactérias codificam para mais conjuntos de genes biossintéticos (BGCs) do que os compostos identificados até agora, possivelmente porque, em condições de laboratório estes podem estar crípticos ou silenciados. Tendo em conta que os metabolitos secundários podem ser produzidos em resposta a condições de stress ambiental, estratégias OSMaC (*One Strain, Many Compounds*) podem ajudar a desvendar o potencial biossintético destes microrganismos. Esta abordagem baseia-se no facto de que, em diferentes condições de cultura, a mesma estirpe pode sintetizar diferentes moléculas.

O CIIMAR alberga uma importante coleção de culturas de cianobactérias (LEGE-CC), que tem vindo a ser investigada para descoberta de novos compostos bioativos. Estudos anteriores guiados por bioatividade descobriram que as estirpes *Lusitaniella coriacea* LEGE 01767 e *Leptothoe* sp. LEGE 181152 produzem diferentes grupos de compostos cuja estrutura indica um possível papel ecológico de agentes quelantes de metais. Adicionalmente, o genoma de *Leptothoe* sp. LEGE 181152 contém um BGC cujo produto não foi identificado.

O objetivo principal deste trabalho foi utilizar OSMaC em duas estirpes da Coleção de Culturas LEGE-CC (CIIMAR) para (i) estudar a produção de lusichelinas (**1-5**) na estirpe *Lusitaniella coriacea* LEGE 01767 e (ii) modulação do metabolismo secundário da estirpe *Leptothoe* sp. LEGE 181152 para indução da expressão de BGCs crípticos/silenciados. Para isto, uma metodologia foi seguida que envolveu exploração genómica, cultivo em diferentes condições de cultura e análises metabolómicas por espectroscopia de massa.

A estirpe *Lusitaniella coriacea* LEGE 01767 foi cultivada em condições normais de cultura (Z8-TM), de ferro limitado e sem ferro, bem como em 0, 5, 200 e 450 nM de sulfato de cobre, para avaliar o seu efeito na produção de lusichelinas **1-5**. Considerando a hipótese inicial de que estes compostos estariam envolvidos na quelação de ferro, era de esperar um aumento da sua presença nas condições sem ferro e com ferro limitado. No entanto, isto não se verificou e o auge da sua produção deu-se nas condições normais de cultura, o que aponta para a quelação de ferro não ser o seu principal papel biológico. As concentrações de 200 e 450 nM de sulfato parecem causar alguma toxicidade na cianobactéria. Nestas condições, foi identificado um potencial novo composto com a mesma massa exata da lusichelina **5**.

A estirpe *Leptothoe* sp. LEGE 181152 foi cultivada em diferentes condições de luz: luz branca, azul e vermelha em ciclos de 16/8h luz/escuridão e em 24h de luz contínua. Verificou-se uma grande modulação do metaboloma nas várias condições, sendo que a luz azul e vermelha parecem exercer um efeito mais pronunciado do que a luz branca. Adicionalmente, a luz contínua causou mais alterações metabolómicas do que o ciclo 16/8h luz/escuridão. Um novo grupo de compostos halogenados, predominante nas condições de luz azul, foi descoberto. Os extratos referentes às diferentes condições experimentais não revelaram bioatividade, quer anticancerígena, quer

antibacteriana. No entanto, os extratos das condições de luz vermelha apresentaram atividade contra a adesão de larvas de mexilhão (*Mytilus galloprovincialis*).
Concluindo, a manipulação das condições de cultura nestas duas estirpes provocou alterações nas suas capacidades biossintéticas, o que se refletiu no seu potencial bioativo e permitiu a identificação de potenciais novos compostos.

Palavras-chave: Produtos naturais, cianobactérias, estratégias OSMaC, sideróforos.

Abstract

Cyanobacteria are photosynthetic microorganisms known to produce a wide range of secondary metabolites, from toxins to other compounds with recognized biotechnological and pharmaceutical applications. Recent advances in Genomics and Bioinformatics have shown that cyanobacterial genomes encode for more biosynthetic gene clusters (BGCs) than the identified compounds so far, possibly because some are cryptic or silent under standard laboratory conditions. Given that secondary metabolites can be produced as a response to environmental stress conditions, employing the OSMaC (One Strain, Many Compounds) strategy might help unlocking the full biosynthetic potential of these microorganisms. This approach underlies that, in different culture conditions, a single strain can produce different molecules.

CIIMAR harbors an important cyanobacterial culture collection (LEGE-CC) that has been investigated for the discovery of new bioactive compounds. Previous bioactivity-guided studies discovered that strains *Lusitaniella coriacea* LEGE 01767 and *Leptothoe* sp. LEGE 181152 produce different groups of compounds whose structure indicates a possible role as metal chelating agents. Additionally, the genome of *Leptothoe* sp. LEGE 181152 contains a BGC whose product has not been found.

The main goal of this work was to use OSMaC on two strains from the LEGE-CC Culture Collection (CIIMAR) to (i) study the production of lusichelins (**1-5**) on *Lusitaniella coriacea* LEGE 01767 (ii) modulate the secondary metabolism *Leptothoe* sp. LEGE 181152 to induce expression of cryptic/silent BGCs in. To achieve this, a workflow was followed involving genome mining, cultivation under different culture conditions and metabolomic analyses by mass spectrometry.

Lusitaniella coriacea LEGE 01767 was cultivated under standard (Z8-TM), iron-limited and iron-depleted conditions, as well as with 0, 5, 200 and 450 nM copper sulfate, to evaluate their effect on production of lusichelins **1-5**. Given the initial hypothesis that lusichelins are involved in iron chelation, an increase of their presence in iron-limited and iron-depleted conditions was expected. However, it did not occur, and peak production was detected on standard conditions. This points to iron chelation not being their main biological purpose. The conditions with 200 and 450 nM of copper sulfate seemed to cause some toxicity to the cyanobacterium. In these, a potential new compound with the same exact mass of lusichelin **5** was identified.

Leptothoe sp. LEGE 181152 was cultivated under different light conditions: white, blue, and red light in 16/8h light/dark cycle and 24h of continuous light. In these conditions, major modulation of the metabolome was verified, with blue and red light having a more pronounced effect than the white light. Moreover, continuous light stimulated more changes in the metabolome than the 16/8h light/dark cycle. A new group of halogenated compounds, predominant in blue light conditions, was discovered. The extracts from these different experimental conditions did not reveal anticancer or antibacterial activity. However, extracts from the red light conditions presented anti-settlement activity in mussel larvae (*Mytilus galloprovincialis*).

Ultimately, the manipulation of the culture conditions in these two strains caused alterations in their biosynthetic capabilities, which reflected in their bioactive potential and allowed the identification of potential new compounds.

Keywords: Natural products, cyanobacteria, OSMaC strategies, siderophores.

Acknowledgements

Antes de mais gostaria de agradecer à minha orientadora Doutora Mariana Reis, por todo o acompanhamento durante a realização deste trabalho. Obrigada também por todos os conhecimentos e conselhos transmitidos, que certamente serão fundamentais para o progresso do meu percurso académico e profissional. Aos meus coorientadores Doutor Ralph Urbatzka e Doutora Joana Almeida, por toda a disponibilidade e ajuda sempre que necessário. Ao Prof. Doutor Rui Morais, pela orientação interna por parte da Escola Superior de Biotecnologia.

À Leonor Ferreira, que acompanhou o desenvolvimento deste trabalho durante todo o ano. Obrigada pela paciência, pelos ensinamentos e pela amizade. À Sandra Pereira, por toda a ajuda, mas particularmente pelo acompanhamento durante os ensaios de atividade antibacteriana e contra a adesão de larvas de mexilhão. A todos os meus outros colegas do BBE, que, para além de sempre disponíveis para ajudar, sempre proporcionaram um ambiente de trabalho descontraído e animado, que tornou os dias complicados mais leves. Um agradecimento especial aos meus colegas e amigos Ricardo Figueiredo, Lucas Solidade, Catarina Fonseca, Pedro Cruz, Filipe Henriques, Rúben Luz e, mais uma vez, Leonor Ferreira.

Aos meus pais, irmã e avó Honória, por todo o apoio, compreensão e orgulho que sempre tiveram em mim.

À Helena Rocha e Mariana Sousa, que foram fundamentais durante o primeiro ano do Mestrado.

Por fim, às minhas amigas Filipa Marques, Lécia Rodrigues, Raquel Ramos e Leonor Lobo, que desde a Licenciatura são presenças constantes na minha vida. Continuaram a sê-lo durante o Mestrado e certamente continuarão durante o Doutoramento que se avizinha.

Agradeço também ao programa BYT*plus* do CIIMAR e à Fundação Amadeus Dias pela bolsa BYT*plus*.

Contents

List of abbreviations

A - Adenylation

ABC - ATP-binding cassette

ACP - Acyl-carrier protein

AT - Acyltransferase

BBE - Blue Biotechnology and Ecotoxicology

BGCs - Biosynthetic gene clusters

BlastP - Protein BLAST

C - Condensation

cAMP - Cyclic AMP

CIIMAR - Interdisciplinary Centre of Marine and Environmental Research

CoA - Coenzyme A

Crp/Fnr - cAMP receptor protein/ fumarate and nitrate reductase regulator protein

DH - Dehydratase

DMSO - Dimethyl sulfoxide

E – Epimerase

EIC - Extracted Ion Chromatograms

ER - Enoylreductase

FBMN - Feature-Based Molecular Networking

Fur - Ferric Uptake Regulator

GNPS - Global Natural Products Social Molecular Networking

IM - Internal membrane

KR - Ketoreductase

KS - Ketosynthase

LC-HRESIMS/MS - Liquid chromatography-high resolution electrospray ionization tandem mass spectrometry

LEGE-CC - Blue Biotechnology and Ecotoxicology Culture Collection

LogP - Octanol-water partition coefficient

MFS - Major Facilitator Superfamily

MS - Mass Spectrometry

MT - Methyltransferase

MTT - (3-(4,5-dimethylthiazol-2-yl)-2,5-diphenyltetrazolium bromide

NIS - NRPS independent siderophore

NPs - Natural Products

NRPS - Non-ribosomal peptide synthetase

NRPs - Non-ribosomal peptides

NRPS/PKS - Hybrid non-ribosomal peptide synthetase/polyketide synthetase

OM - Outer membrane

OSMaC - One Strain, Many Compounds

PCA - Principal Component Analysis

PCP - Peptidyl carrier protein

PKS - Polyketide synthetase

PKs - Polyketides

RT - Retention time

TBDT - TonB-dependant transporter

TFBS - Transcription Factor Binding Sites

TM - Tropic Marin

WGS - Whole genome sequencing

ZurR - Zinc-responsive repressor

1. Introduction

1.1 Cyanobacteria

Cyanobacteria are prokaryotic, Gram-negative, and photoautotrophic organisms (1,2). Some also present ability to fix nitrogen which, in addition to carbon fixation, makes them one of the most important groups of organisms on Earth, playing crucial roles on carbon and nitrogen cycles (3,4). Nitrogen fixation in cyanobacteria is an anaerobic process, while oxygen is produced through photosynthesis (5). Cyanobacteria can separate these two processes temporally, through a circadian clock, or spatially, by having specialized cells called heterocysts (5).

Other types of specialized cells might occur, such as akinetes (associated with stress responses) (6) and hormogonia (involved in reproduction) (7). However, cyanobacteria mostly reproduce through binary fusion (8). Morphologically, they are mainly classified as unicellular, filamentous, or colonial (9), but might possess other distinctive characteristics used for their taxonomic classification (8).

Morphology used to be the main criterion for the classification of cyanobacteria, but the advances in genetics and molecular biology demonstrated that not always morphological likeness reflects genetic closeness (10,11). To date, the most updated cyanobacterial classification system is the one published by Mareš *et al.* in 2022, in which a polyphasic phylogenomic approach was employed (11). The most notable changes were the proposal of ten new orders and fifteen families (11).

Cyanobacteria are ubiquitously distributed, being found in terrestrial and aquatic (marine, brackish and freshwater) habitats, as well as in extreme environments, such as deserts, hot springs, and polar settings (12). Symbiotic relations can also be established with organisms like sponges, macroalgae, protozoans and others (13).

Algal blooms and toxin production are the main reasons for which cyanobacteria are known, both having negative impacts on the environment and human health (14). However, their ability to produce other natural products (NPs) with various pharmaceutical and biotechnological applications has been recognized and is now a thriving research topic (15).

1.2 Cyanobacterial Natural Products

NPs can be defined as primary or secondary metabolites produced by living organisms (16). For centuries, plants were used as medicine in many civilizations, with little knowledge as to why they were effective (17). However, in 1826, the purification and commercialization of morphine from opium, which became the first pure drug, was a turning point (17). Later, in the beginning of the 20th century, the discovery of penicillin from *Penicillium notatum* by Alexander Fleming turned the attention to microorganisms as sources of bioactive NPs (17). Nowadays, they are routinely studied as lead compounds in drug discovery, due to their affinity and specificity to biological targets, as well as their large chemical diversity (18,19).

The marine environment is an especially interesting source of NPs (20). Various pharmaceuticals available in the market today originated from marine organisms, such as mollusks, sponges, or tunicates (20). Curiously though, there is reason to believe that in some cases microorganisms

associated with these species were the true producers of compounds (20,21). An example of this is dolastatin 10, the lead-compound of various anticancer drugs available nowadays in the market or in clinical trials (e.g. Adcetris®) (20,22). It was originally isolated from a sea hare (*Dolabella auricularia*), but later it was discovered that a marine cyanobacterium (*Symploca* sp. VP642), part of the sea hare's diet, was the actual synthesizer (23).

Cyanobacteria show a particularly attractive potential for novel NP production, since their distinct ecological niche translates into their unique metabolome (24,25). Until 2019, fourteen major bioactivities have been identified, with cytotoxicity alone comprising around 30% (Figure 1) (15). The Oscillatoriales and Nostocales orders are responsible for most of this production (41.2% and 34.6%, respectively) (Figure 1) (15). However, these data still have not taken into consideration the new taxa, and the general restructuration of cyanobacterial classification, proposed in 2022.

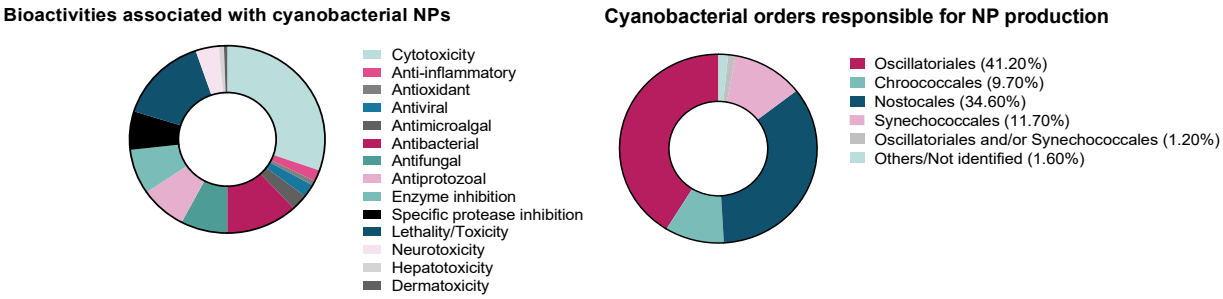

Figure 1. The percentage distribution of cyanobacterial bioactivities (on the left) and the orders responsible for them (on the right). Adapted from (15).

Besides showing a great deal of activities, cyanobacterial NPs are also chemically and structurally diverse (24). As of 2019, 260 metabolite families had been described, fitting into one of these chemical classes: peptides, depsipeptides, lipopeptides, lipids, macrolides/lactones, alkaloids, terpenes, polysaccharides, polyketides, and others (Figure 2) (15). The most common biosynthetic pathways are the non-ribosomal peptide synthetase (NRPS) and polyketide synthetase (PKS) pathways, and their hybrids (NRPS/PKS) (24).

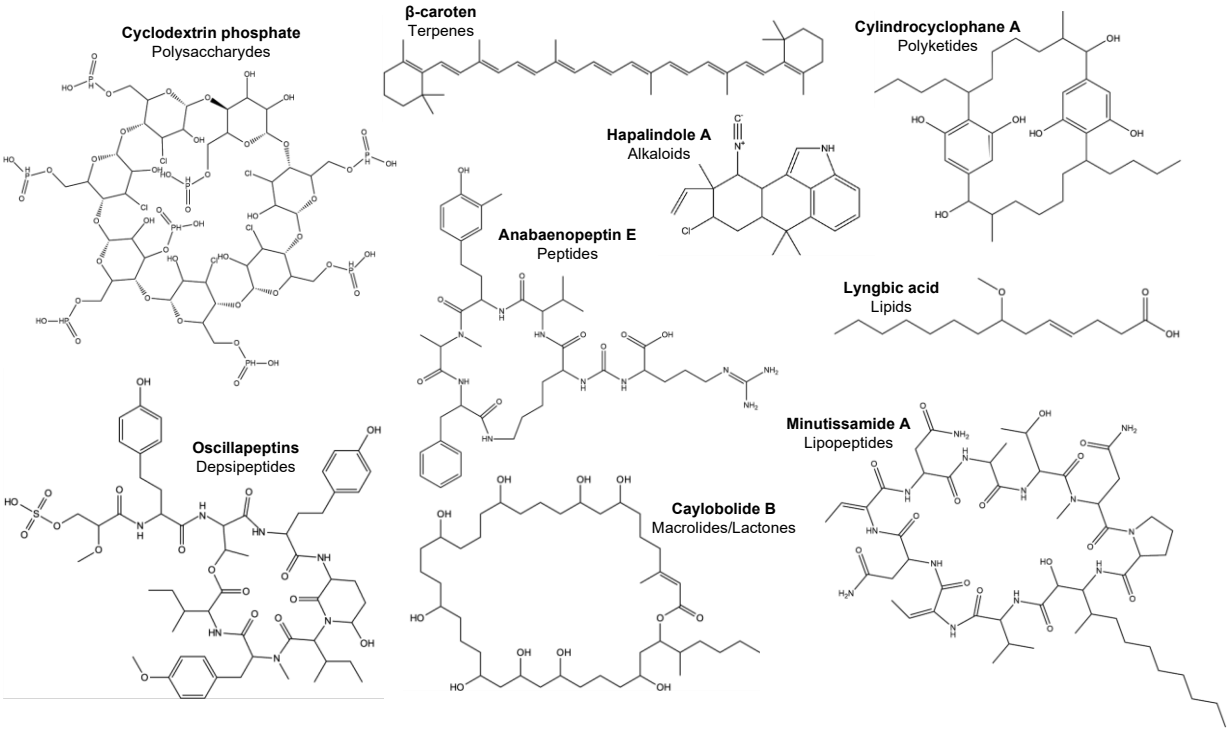

Figure 2. Examples of structures of cyanobacterial metabolites of each chemical class.

1.2.1 NRPS/PKS biosynthetic pathways

Non-ribosomal peptides (NRPs) are peptide secondary metabolites, synthesized by NRPS independently of mRNA (26). Since the building blocks for this synthesis can be any amino acid – both proteinogenic and non-proteinogenic -, the chemical diversity of this type of compounds is enormous (27). Polyketides (PKs) are natural products synthesized from acyl-coenzyme A (CoA) thioesters by PKS, in a process homologous to fatty acid synthesis (28).

In NRPs, at least a core module containing an adenylation (A), a peptidyl carrier protein (PCP) and a condensation (C) domain is necessary (29). The A domain selects and adenylates an amino acid, which is then linked to a phosphopantetheinyl group on the PCP domain (30). After, the formation of an amide bond between the amino acid and the peptide attached to the PCP domain of the preceding module is catalyzed by the C domain (30). In PKs, the essential domains are the acyltransferase (AT), acyl-carrier protein (ACP) and ketosynthase (KS) domains: the AT domain loads an acyl-CoA - the starter unit - on the ACP, and the KS domain performs decarboxylative Claisen condensation, to elongate the carbon chain (Figure 3) (31).

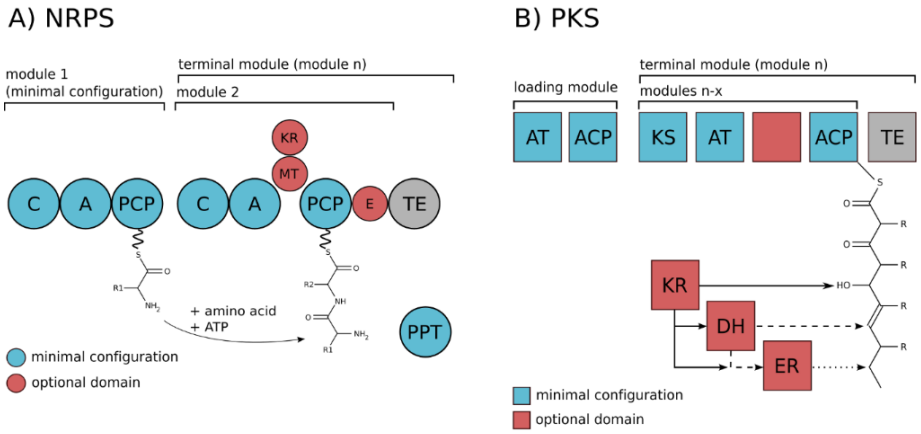

Figure 3. Schematization of NRPS and PKS pathways. Abbreviations: C – condensation, A – adenylation, PCP – peptidyl carrier protein, MT - Methyltransferase, KR - ketoreductase, E – epimerase, AT - acyltransferase, ACP - acyl-carrier protein, KS – ketosynthase,, DH - dehydratase, ER - enoylreductase. Taken from (32).

In the final module of either a PK or a NRP, a thioesterase (TE) releases the molecule from the final PCP domain, through hydrolysis or cyclization (29). Additional tailoring domains may occur (Table 1), expanding the structural diversity of these compounds (27,30).

Table 1. Optional domains in NRPS and PKS pathways, and their function (27,33).

Domain	Function	Pathway
Dehydratase (DH)	Elimination β-hydroxyl group to form α-β double bond	PKS
Enoylreductase (ER)	Creation of fully reduced β-methylene group	PKS
Ketoreductase (KR)	Reduction of β-ketone group to alcohol	PKS and NRPS
Epimerase (E)	Epimerization (change in configuration of one chiral center)	NRPS
Methyltransferase (MT)	Methylation of the peptide backbone	NRPS

1.3 OSMaC strategies

The biosynthesis of secondary metabolites is usually energetically expensive and so it is triggered to confer an adaptive response to changes in the environmental conditions to compete with other organisms, etc (34). The genes necessary for their synthesis are typically organized in adjacent clusters in the genome, forming biosynthetic gene clusters (BGCs) (35). These usually contain core biosynthetic genes, “tailoring” genes (encoding for enzymes that perform additional modifications), as well as transport and regulatory genes (35).

With the technology available nowadays - whole genome sequencing (WGS) and bioinformatic tools, like antiSMASH -, prediction of the NP encoded in a certain BGC, and assessment of its putative novelty is possible (36,37). However, orphan BGCs, whose products are unknown, can be cryptic (given too poor BGC expression the NP is hidden in the hodgepodge of metabolites) or silent (no BGC expression). Silent BGCs are frequently associated with cultivation in standard laboratory conditions

(34). Due to this, we know that only a small fraction of NPs is yet discovered and accessing the full biosynthetic potential of microorganisms is a major theme in NPs research nowadays (38,39). For this, two main types of approaches can be applied: genetic engineering-based (e.g. heterologous expression) or culture-based, which are summarized by the OSMaC concept (One Strain, Many Compounds) (34). The latter, originally introduced by Zeeck and colleagues in 2002, postulates that microbial physiology is altered in different culture conditions, and, consequently, so is their metabolome (40). Thus, varying physical parameters, the nutrient regimen, adding chemical elicitors, or even co-culturing with other organisms can elicit the expression of BGCs and unveil the ones that are cryptic or silent (Figure 4) (34).

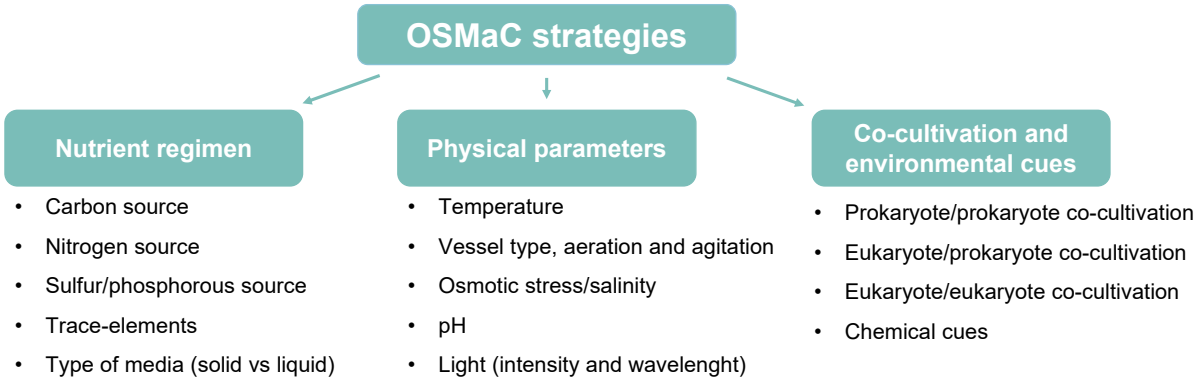

Figure 4. Summary of strategies included in the OSMaC concept.

By manipulating the culture conditions, the authors who presented the idea of OSMaC were able to isolate more than 100 compounds of great chemical diversity, from just 6 microorganisms (40). After that, this strategy has been employed successfully in several microorganisms, such as *Streptomyces* sp., *Vibrio* sp. and *Aspergillus* sp. (41–43). As an example, the addition of 1 mM NaBr to a culture of *Aspergillus flavipes* induced the production of eight different cytochalasans (two unknown), with anticancer activity (43). In cyanobacteria, though, very few reports of employment of OSMaC strategies were found (44,45).

1.4 Cyanobacterial siderophores

Iron is an essential nutrient for the metabolism of most organisms, being involved in various important processes such as DNA and RNA synthesis, respiration, nitrogen fixation, photosynthesis, and detoxification of superoxide radicals (46). Cyanobacteria, as photosynthetic organisms, have particularly high iron requirements (47).

Iron bioavailability in aquatic environments is an issue: their oxygenated and circumneutral pH conditions lower the solubility of iron and Fe^{2+} (a more bioavailable form) is rapidly oxidated to Fe^{3+}, which forms other insoluble complexes (48–50). Fe^{2+} can enter the cells through porins by passive diffusion and, if a concentration gradient is present, Fe^{3+} can also be transported by this mode (51,52). Yet, this is not enough, and cyanobacteria need additional strategies to overcome this limitation (48).

Siderophores - low-molecular weight, iron-chelating molecules - are one of them (48). These compounds are secreted into the environment, where they complex with Fe^{3+}/Fe^{2+} (48). Then, they are

transported through the outer membrane into the periplasm by TonB-dependent transporters, where they bind with siderophore-binding proteins (52,53). After, they cross the periplasmatic membrane through an ABC-type transporter and, in the cytoplasm, the complex is dissociated (Figure 5) (52,54). Alternatively, in some cyanobacteria (such as *Synechocystis* 6803) it has been discovered that iron can be reduced to Fe^{2+} in the periplasmastic membrane, through an alternate respiratory terminal oxidase (54).

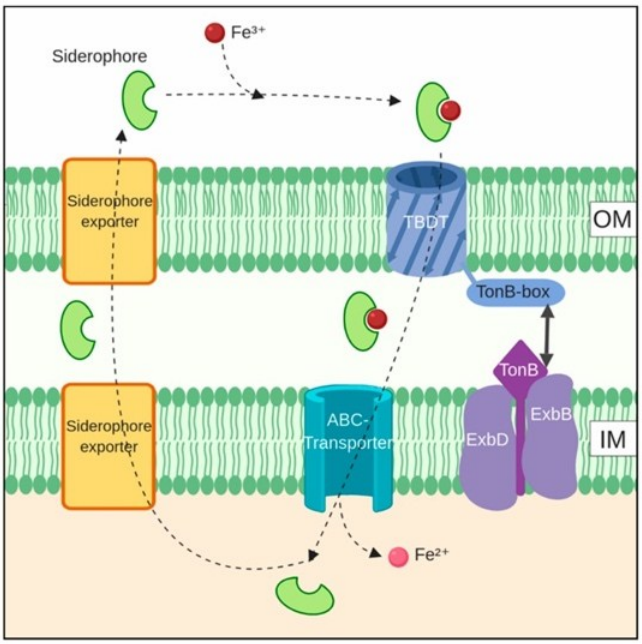

Figure 5. Schematic representation of siderophore cycling in a generic microorganism. TBDT – TonB-dependent transporter, OM – outer membrane, IM – internal membrane. Taken from (55).

1.4.1 Chemistry and biosynthesis of siderophores

Siderophores are classified as one of these four major chemical classes: hydroxamate, catecholate, phenolate and carboxylate (Figure 6) (48). These categories are attributed based on the moieties involved in the chelation and sometimes a mixture of functional groups is present (48,56). Although all these have been isolated from bacteria, in cyanobacteria only hydroxamates and catecholate siderophores have been reported so far (48).

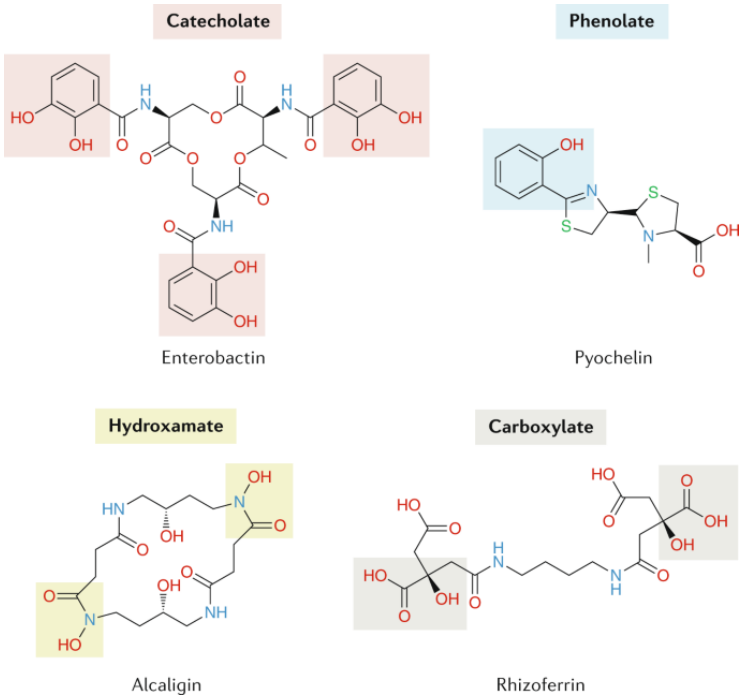

Figure 6. Examples of siderophores of each of the four chemical classes: hydroxamate, catecholate, phenolate and carboxylate. Taken from (57).

Hydroxamate siderophores, such as the cyanobacterial siderophores schizokinen and synechobactin are the most widespread type in nature (48,58). Their chelating moieties usually contain hydroxylated and acylated alkylamines and, when bound to iron, it is thought that a hexavalent octahedron is formed with the oxygens of the hydroxamate and α-hydroxycarboxylate groups (48). Catechol siderophores, like anachelin, can chelate iron by forming mono, bis or tris catechol-iron complexes (48,59). The iron affinity of catechol groups is usually higher than hydroxamate siderophores, but they are also more susceptible to pH (48).

The biosynthesis of siderophores can occur through NRPS and NRPS/PKS pathways or, alternatively, in an NRPS independent manner (NIS) (49). The first two have been associated with both catecholate and hydroxamate siderophores, while NIS biosynthesis is only reported to yield hydroxamate-type siderophores so far (49).

1.4.2 Regulation of siderophore synthesis

As it is logical, siderophoregenesis is primarily regulated by intracellular and extracellular levels of iron, with lower iron concentrations resulting in increased siderophore production (49). However, excessive intracellular iron harms the microbial metabolism, so maintaining homeostasis is essential (47,49).

The most universal way microorganisms have of assuring this is through a transcription factor named ferric uptake regulator (Fur) (60). In iron-replete conditions, iron binds to the monomeric form of Fur, which dimerizes, transforming into a conformation with affinity to Fur boxes - specific binding sites in the promotor region of genes (46,61). When this occurs, the transcription of siderophore and other iron-related genes is blocked (46,61).

However, iron concentration is not the only way to regulate the production of siderophores, and factors like temperature, pH, nitrogen sources and presence of heavy metals can also affect it (49).

1.4.3 Biotechnological importance of siderophores

Besides the obvious function of meeting the demanding iron requirements cyanobacteria have, siderophores can chelate other metals, diminishing their toxicity (49). An example of this is schizokinen, a dihydroxamate-type siderophore produced by *Anabaena* PCC 7120, which binds to copper (62). This ability is clearly interesting from a biotechnological point of view and studies have demonstrated the potential of a siderophore produced by *Anabaena oryzae* in cadmium-sequestering solutions (63).
Moreover, several bacterial siderophores have recognized antimicrobial activity and siderophore-antibiotic conjugates inspired by the Trojan horse strategy have also been used against antibiotic-resistant pathogens (64). Examples of this are ampicillin/amoxicillin-enterobactin conjugates (Figure 7) that presented enhanced selective activity against *Escherichia coli* strains (65). As enterobactin is a native siderophore of these strains, the conjugate hijacks the iron-uptake pathways, being delivered into the cell, where the antibiotic exerts its activity (65).

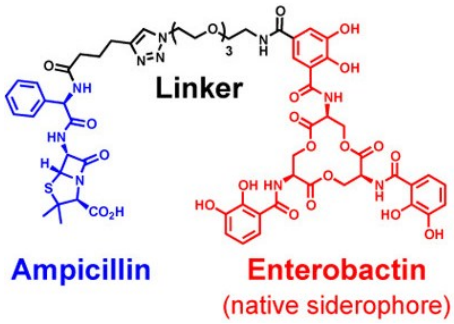

Figure 7. Structure of ampicillin-enterobactin conjugate. Adapted from (65).

Moreover, siderophores have shown promising applicability in the treatment of diseases like cancer (66), malaria (67), and tuberculosis (68), as well as in solutions to overcome biomedical biofouling (69).

1.5 Cyanobacteria under study

1.5.1 *Lusitaniella coriacea* LEGE 07167

Lusitaniella coriacea LEGE 07167 is a LEGE-CC marine cyanobacterial strain. It was collected as a rock surface scraping on a tide puddle at Praia dos Lavadores, Portugal. In previous work of the group, a group of compounds named lusichelins were isolated from this strain (Figure 8). Lusichelins **1** and **2** are stereoisomers, just like **3** and **4**. Lusichelins **1/2** contain an additional methylation in relation to lusichelin **5**. Lusichelin **5** has also been isolated in a complex with iron (*m/z* 597.9919 $[M+H]^+$), which, in addition to the presence of various putative siderophore-associated genes in its BGC, has led to the hypothesis that this compound is a siderophore.

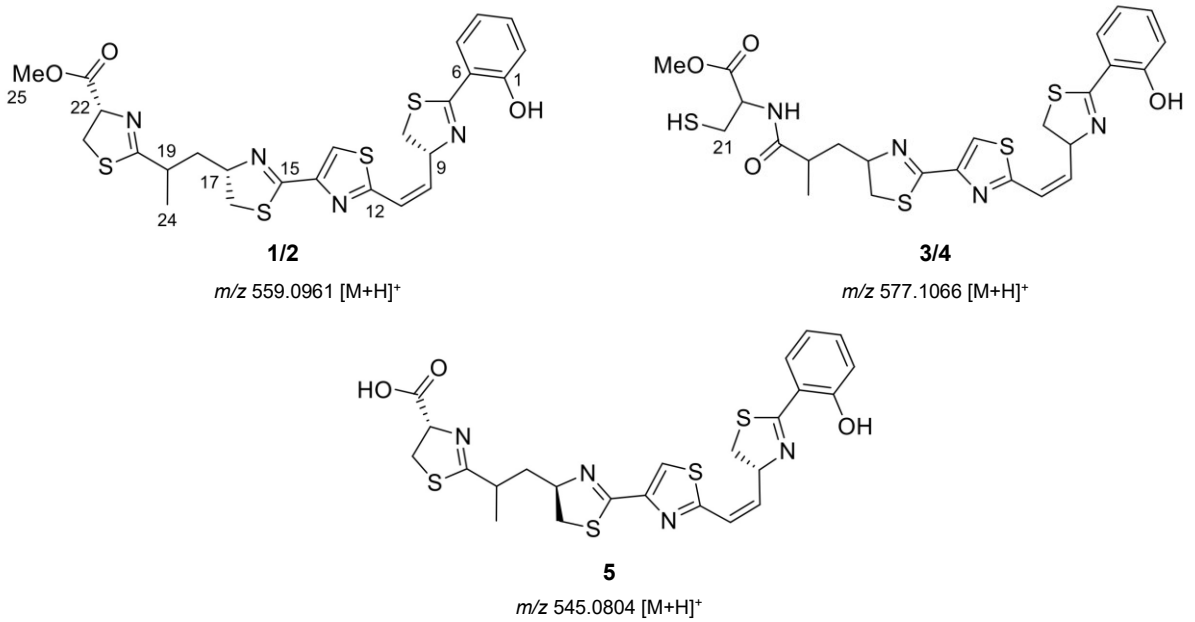

Figure 8. Chemical structures and exact mass of protonated molecules of lusichelins, a group of compounds isolated from *Lusitaniella coriacea* LEGE 07167.

1.5.2 *Leptothoe sp.* LEGE 181152

Leptothoe sp. LEGE 181152 is a marine cyanobacterium belonging to LEGE-CC, collected as an intertidal mat in Baía das Gatas (São Vicente Island, Cape Verde). In previous work of the group, phormidolide D (*m/z* 1061.593 $[M-H]^-$), a halogenated polyketide with cytotoxic activity, was isolated from this strain. This compound belongs the family of a phormidolide (*m/z* 1073.593 $[M-H]^-$) previously isolated in 2002 (Figure 9) (70). Leptochelins, another group of halogenated compounds, has also been isolated from this strain in previous work of the group. This group contains leptochelin A (*m/z* 895.078 $[M+H]^+$), leptochelin B (*m/z* 851.129 $[M+H]^+$) and leptochelin D (*m/z* 881.062 $[M+H]^+$) and all have strong cytotoxic activity.

The analysis of the assembly genome of *Leptothoe* sp. LEGE 181152 showed the existence of other BGCs besides the ones from phormidolides and leptochelins that can be cryptic or silent.

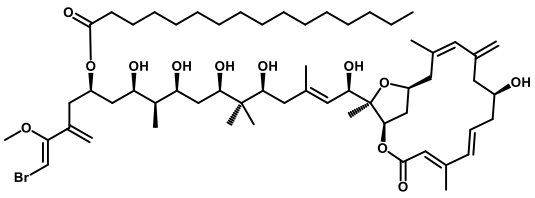

Figure 9. Chemical structure of phormidolide.

1.6 Goals

This dissertation was developed at the Blue Biotechnology and Ecotoxicology (BBE) research group at the Interdisciplinary Centre of Marine and Environmental Research (CIIMAR). This institution harbors a culture collection of over 2000 strains of cyanobacteria and microalgae - the Blue Biotechnology and Ecotoxicology Culture Collection (LEGE-CC).

At this group, one of the main research focuses is the exploration of these cyanobacteria for the discovery of NPs with pharmaceutical and biotechnological applications. However, only a small fraction of the biosynthetic potential of these microorganisms is known, as in standard culture conditions, many BGCs are silent or cryptic. Using OSMaC strategies, which imply the manipulation of the culture conditions, it is possible to unveil these silent/cryptic BGCs.

Thus, the main goal of this work was to employ OSMaC strategies – an innovative approach on cyanobacteria, with limited reports on it -, on two LEGE-CC strains. On *Lusitaniella coriacea* LEGE 07167, the objective was to study the effect of the different culture conditions on lusichelin production, while on *Leptothoe* sp. LEGE 181152, the objective was to modulate the metabolome and reveal silent/cryptic BGCs. To achieve this, the following workflow was followed:

1. **Genome mining:** BGCs of interest were identified in the assembly genomes of *Lusitaniella coriacea* LEGE 07167 and *Leptothoe* sp. LEGE 181152.
2. **Cultivation under different conditions:** *Lusitaniella coriacea* LEGE 07167 was grown in iron-limited and iron-depleted conditions, as well as with different copper concentrations. *Leptothoe* sp. LEGE 181152 was grown under different light conditions.
3. **Metabolomic analysis by mass spectrometry:** on *Lusitaniella coriacea* LEGE 07167, a targeted approach was used to comprehend the effect of the different culture conditions on lusichelin production. An untargeted approach was used on *Leptothoe* sp. LEGE 181152, to understand how the different light conditions modulated the metabolome.

2. Materials and methods

2.1 General experimental methods

2.1.1 Strain maintenance

The cyanobacterial strains were maintained in 40 mL culture flasks of Z8 medium (71) supplemented with 25 ‰ TM (Tropic Marin® Pro-Reef, Tropic Marin, Berlin, Germany) and 1 ‰ vitamin B12 (Z8-TM), at standard laboratory conditions: 25 °C with light/dark cycle of 14/10 h at a light intensity of 10–30 µmol photons m^{-2} s^{-1}. To obtain higher amounts of biomass, the cultures were scaled-up, by being progressively passed to 400 mL flasks and then 2 L glass flasks with aeration.

2.1.2 Genome mining

AntiSMASH version 6.1.1 and 7.0.0 was used to annotate BGCs on the assembly genomes of *Lusitaniella coriacea* LEGE 07167 and *Leptothoe* sp. LEGE 181152 (37,72). These were submitted to the platform as FASTA and GenBank files, respectively, a relaxed detection strictness was chosen and all the extra features were selected (KnownClusterBlast, MIBiG cluster comparison, Cluster Pfam analysis, Cluster Blast, ActiveSiteFinder, Pfam-based GO term annotation, SubClusterBlast, RREFinder, TIGRFam analysis and TFBS analysis). The identification of enzyme homologues and confirmation of annotations was done with Protein BLAST (BlastP) with default settings (73). CAGECAT clinker (with default settings) was used to compare BGCs of both strains (74).

2.1.3 Chemical extractions

The freeze-dried (LyoQuest, Telstar, Terrassa, Spain) biomass was macerated in MeOH and sonicated twice for 5 minutes, to exhaustively extract the compounds from the cells. The extracts were filtrated to trap residual biomass and concentrated in a rotary evaporator (Rotavapor® R-210, BUCHI, Flawil, Switzerland). The culture medium extracts were obtained through solid phase extraction (SPE) with a Strata® C18-E column (55 µm/70 Å; 1 g/6 mL; Phenomenex, Madrid, Spain). This column was activated with 100% MeOH and equilibrated with 95:5% water:MeOH. The samples were eluded with 95:5% water:MeOH to remove salts and then 100% MeOH. This last fraction was collected and concentrated in a rotary evaporator. Both biomass and culture medium extracts were dried overnight in high vacuum and weighed.

2.1.4 LC-HRESIMS/MS

All extracts were analyzed using liquid chromatography-high resolution electrospray ionization tandem mass spectrometry (LC-HRESIMS/MS). These analyses were performed on a Vanquish HPLC system coupled to Orbitrap Exploris 120 mass spectrometer and controlled by Q Exactive Focus Tune 2.9 and Xcalibur 4.1 (Thermo Fisher Scientific, Waltham, MA, USA). Full positive scan mode was used setting a capillary temperature of 262.5 °C, spray voltage of 3.5 kV, at the resolution of 70,000 FWHM (*m*/*z* range of 150–2000), and data dependent MS^2 ($ddMS^2$, Discovery mode) at the resolution of 17,500 FWHM (isolation window used was 3.0 amu and normalized collision energy was 35). The extracts (5 µl; 2 mg/ml in MS-grade MeOH) were separated on an ACE UltraCore 2.5 SuperC18 column (75 × 2.1

mm, ACE, Reading, UK), at 40 °C, using a gradient from 99.5 to 10% H_2O/MeOH/formic acid (95:5:0.1, v/v) to 0.5 to 90% isopropanol/MeOH/formic acid (95:5:0.1, v/v) for 9.5 min, maintaining the last mixture until 15.5 min before returning to the initial conditions, with a flow rate of 0.35 ml/min.

2.2 *Lusitaniella coriacea* LEGE 07167

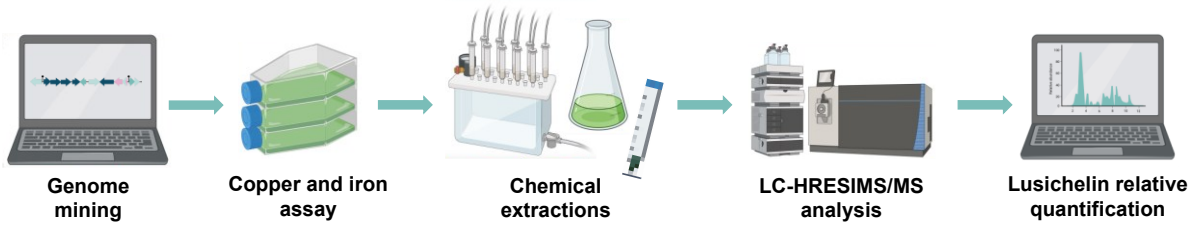

Figure 10. Workflow followed for the strain *Lusitaniella coriacea* LEGE 07167.

2.2.1 Copper and iron assay

2.2.1.1 Culture conditions

Lusitaniella coriacea LEGE 07167 was cultivated in 10 different conditions, varying the type of salt supplemented in the culture medium – TM (Z8-TM) or sodium chloride (Z8-NaCl) -, copper sulfate ($CuSO_4$) concentration, and presence/absence of iron chloride ($FeCl_3$) (Table 2). Because the main cyanobacterial culture was maintained in Z8-TM, the initial inoculum for the assays that used NaCl as a source of salt was adapted to complete Z8-NaCl one week before the beginning of the experiments. *Lusitaniella coriacea* LEGE 07167 is a filamentous cyanobacterium that forms biofilms. As such it is difficult to prepare initial inoculum based on cell density methods (e.g. optical density or cell counting). To overcome this, the initial inoculum of cyanobacterial cells (biofilm) were separated from the medium through a sieve, and circa of 0.5 mL of biomass were inoculated onto 40 mL culture flasks (in triplicate) with 12 mL of culture medium. The cultures were incubated for 30 days at standard laboratory conditions (25 °C with light/dark cycle of 14/10 h at a light intensity of 10–30 µmol photons m^{-2} s^{-1}). These were in continuous agitation on a shaker (100 rpm), where they were distributed horizontally, randomly in piles of three, with an empty flask on top, to avoid direct light. At the end of the incubation period, the biomass and culture medium were separated using a 0.41 µm sieve. After lyophilized, the dry weight of the biomass was measured.

Table 2. Different tested conditions: iron-repleted (TM $FeCl_3$(+)/NaCl $FeCl_3$(+)), iron-limited (TM $FeCl_3$(-)), iron-depleted (NaCl $FeCl_3$(-)) and various copper concentrations (0, 5, 200 and 450 nM $CuSO_4$). – (absence of $FeCl_3$); + (presence of $FeCl_3$).

Condition	Culture medium	Presence of $FeCl_3$	[$CuSO_4$]
TM $FeCl_3$ (+)	Z8-TM	+	5 nM
TM $FeCl_3$ (-)	Z8-TM	-	5 nM
NaCl $FeCl_3$ (+) 0 nM $CuSO_4$	Z8-NaCl	+	0 nM
NaCl $FeCl_3$ (+) 5 nM $CuSO_4$	Z8-NaCl	+	5 nM
NaCl $FeCl_3$ (+) 200 nM $CuSO_4$	Z8-NaCl	+	200 nM
NaCl $FeCl_3$ (+) 450 nM $CuSO_4$	Z8-NaCl	+	450 nM

NaCl $FeCl_3$ (-) 0 nM $CuSO_4$	Z8-NaCl	-	0 nM
NaCl $FeCl_3$ (-) 5 nM $CuSO_4$	Z8-NaCl	-	5 nM
NaCl $FeCl_3$ (-) 200 nM $CuSO_4$	Z8-NaCl	-	200 nM
NaCl $FeCl_3$ (-) 450 nM $CuSO_4$	Z8-NaCl	-	450 nM

2.2.1.2 Lusichelin quantification

The relative quantification of lusichelins **1-5** and lusichelin 5 coupled to iron (**5-Fe**) was achieved by LC-HRESIMS/MS analysis of the extracts in each condition. The raw data were viewed with XCalibur 4.1.31 program, where a relative quantification was done through the extracted ion chromatograms (EIC), for which the parameters are presented in Table 3. As triplicates of each condition were used, averages of *m/z*, retention time (RT) and the corresponding chromatogram peak areas were calculated.

Table 3. Reference values of the exact mass of the protonated molecules (*m/z*) and retention time (RT) of each lusichelin used for relative quantification.

	Lusichelin 1/2	**Lusichelin 3/4**	**Lusichelin 5**	**Lusichelin 5-Fe**
m/z	559.0961	577.1066	545.0804	597.9919
***m/z* tolerance**	5 ppm			
RT	9.90 min	9.32 min	9.05 min	4.15 min

The octanol-water partition coefficient (logP) of lusichelins **1-5** was calculated through Molinspiration calculator of molecular properties (75).

2.3 *Leptothoe* sp. LEGE 181152

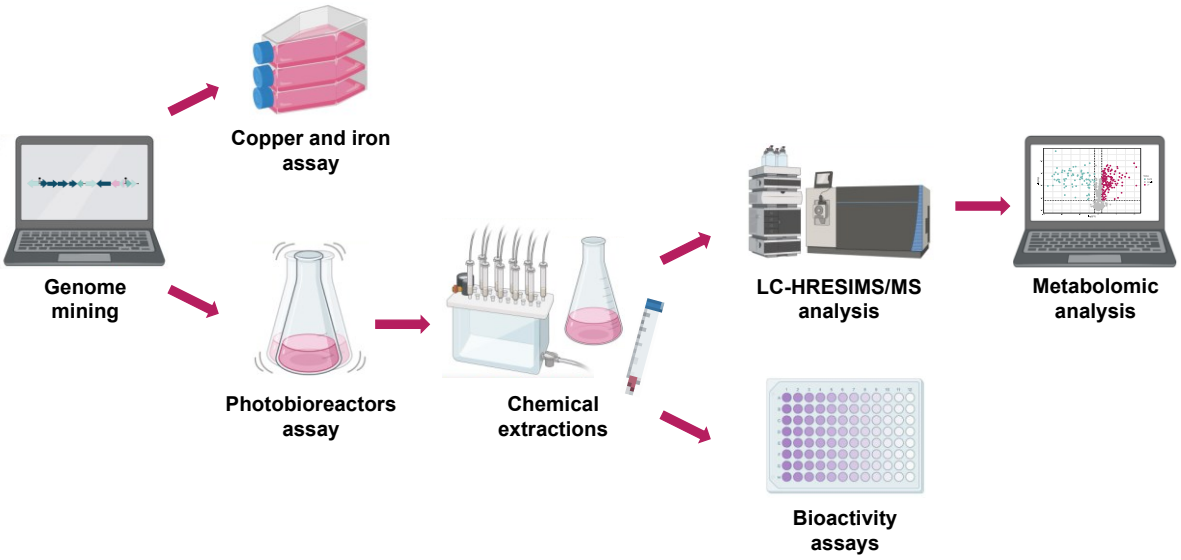

Figure 11. Workflow followed for the strain *Leptothoe* sp. LEGE 181152.

2.3.1 Copper and iron experiment

Leptothoe sp. LEGE 181152 was cultivated in the same procedure as described in 2.2.1.1., with only a slight modification in the tested conditions (Table 4).

Table 4. Different tested conditions: iron-repleted (TM $FeCl_3$(+)/NaCl $FeCl_3$(+)), iron-depleted (NaCl $FeCl_3$(-)) and various copper concentrations (0, 5, 200 and 450 nM $CuSO_4$).

Condition	Origin of inoculum	Culture medium	Presence of $FeCl_3$	[$CuSO_4$]
TM $FeCl_3$ (+)	Z8-TM	Z8-TM	+	5 nM
TM $FeCl_3$ (+)	Z8-NaCl	Z8-TM	+	5 nM
NaCl $FeCl_3$ (+) 0 nM $CuSO_4$	Z8-NaCl	Z8-NaCl	+	0 nM
NaCl $FeCl_3$ (+) 5 nM $CuSO_4$	Z8-NaCl	Z8-NaCl	+	5 nM
NaCl $FeCl_3$ (+) 200 nM $CuSO_4$	Z8-NaCl	Z8-NaCl	+	200 nM
NaCl $FeCl_3$ (+) 450 nM $CuSO_4$	Z8-NaCl	Z8-NaCl	+	450 nM
NaCl $FeCl_3$ (-) 0 nM $CuSO_4$	Z8-NaCl	Z8-NaCl	-	0 nM
NaCl $FeCl_3$ (-) 5 nM $CuSO_4$	Z8-NaCl	Z8-NaCl	-	5 nM
NaCl $FeCl_3$ (-) 200 nM $CuSO_4$	Z8-NaCl	Z8-NaCl	-	200 nM
NaCl $FeCl_3$ (-) 450 nM $CuSO_4$	Z8-NaCl	Z8-NaCl	-	450 nM

2.3.2 Photobioreactors experiment

2.3.2.1 Culture conditions

Leptothoe sp. LEGE 181152 was cultivated in Algem® Pro photobioreactors (Algenuity, Bedfordshire, UK). Six different conditions were tested: white (sunlight model), blue (465 nm), and red (660 nm) LED lights at an intensity of 200 µmol photons m^{-2} s^{-1} and two different photoperiods (24h of continuous light and 16/8h light/dark cycle). The cultures were in continuous shaking (100 rpm) at 22-25ºC, and the experiment lasted for 3 weeks. After this period, the biomass and culture medium were separated using a 0.20 µm sieve.

2.3.2.2 Bioactivity assays

a) Anticancer activity assays

The human cell line HCT-116 (colon adenocarcinoma) was obtained from Sigma-Aldrich (St. Louis, MO, USA) and cultured with McCoy′s 5A medium (Sigma-Aldrich, St. Louis, Missouri, EUA) supplemented with 10% of fetal bovine serum (Biochrom, Berlin, Germany), 1% of penicillin/streptomycin (Biochrom, Berlin, Germany), and 0.1% of amphotericin (GE Healthcare, Little Chafont, Buckinghamshire, UK). The cell line was incubated at 37ºC and 5% CO_2.

This cell line was seeded in 96-wells plates (Costar, Corning, New York, NY, USA), at a concentration of 3.3×10^4 cells/mL, for 24h. Then, the cells were incubated with the biomass extracts at a concentration of 50 and 25 µg/mL (0.2 and 0.1% of dimethyl sulfoxide (DMSO), respectively). Positive controls of staurosporin (1 µM), negative controls of DMSO (0.1 and 0.2%) and culture medium controls were also included. Triplicates of each extract and control were done. After 48h of exposure, the cell viability was determined through the MTT assay ((3-(4,5-dimethylthiazol-2-yl)-2,5-diphenyltetrazolium

bromide). Therefore, the cells were incubated for 4 hours with 20 µL of MTT reagent (1 mg/mL) and the formed formazan crystal dissolved in 100 µL of DMSO after this period. The absorbance was read at 550 nm on a multi-detection microplate reader (Cytation 5, Biotek, Winooski, Vermont, EUA) and cell viability was calculated with the formula below:

$$\%\ cell\ viability\ (to\ negative\ control) = \frac{\bar{x}\ (Absorbance_{sample})}{\bar{x}\ (Absorbance_{negative\ control})} \times 100$$

For the biomass, three independent assays were performed, while for the culture medium only one was done.

b) Anti-settlement activity assays

Mussel (*Mytilus galloprovincialis*) juveniles aggregates were collected at Memória Beach, North of Portugal (41◦13'59" N; 8◦43'28" W) during low tides. Competent mussel plantigrade larvae (0.5-2 mm) showing typical foot exploring behavior were selected for the bioassays among the aggregates using a binocular magnifier (Olympus SZX2-ILLT, Tokyo, Japan), and carefully washed with filtered seawater. 5 larvae per well of a 24-well plate (VWR, Radnor, PA, USA) were used, and 4 replicates of each condition were included. The tested biomass extracts were diluted in filtered seawater, to achieve a final concentration of 30 µg/mL and 2.5 mL of the solution was added to each well. A negative control of seawater and a positive control of $CuSO_4$ (5 µM) were also included. After 15 h at 18 ± 1 ◦C in the dark, the anti-settlement activity was assessed by the presence or absence of efficiently attached byssal threads produced by each larva. The assay was repeated for the extracts with observed activity.

c) Antibacterial activity assays

The inhibitory activity of the biomass extracts was tested against five biofilm-forming marine biofouling bacterial strains: *Cobetia marina* CECT 4278, *Vibrio harveyi* CECT 525, *Roseobacter litoralis* CECT 5395, *Halomonas aquamarina* CECT 5000, and *Pseudoalteromonas atlantica* CECT 570. Marine Broth (Difco, Detroit, MI, USA) was filtered with 0.45 µm filters and the strains were inoculated at an initial optical density (OD) of 0.100 - 0.150 at 600 nm. Extracts were tested at 30 µg/mL in 96-well flat-bottom plates (Costar®, Corning, New York, NY, USA), with four replicates per extract. A positive control of 1:100 penicilin-streptomycin-neomycin stabilized solution (P4083, Sigma-Aldrich, St. Louis, MO, USA), negative control of DMSO at 0.1%, and a blank (filtered Marine Broth) were also included. The OD was measured at the time of inoculation and after the incubation period (24h at 26ºC and 72h for *Roseobacter litoralis*) on a microplate reader (Synergy HT, Biotek, Bart Frederick Shahr, Germany) and the percentage of growth inhibition was calculated with the formula below.

$$\%\ Growth\ Inhibition = 100 - \left(\frac{Sample\ OD24h - Sample\ OD0h}{Ctr(DMSO)24h - Ctr(DMSO)0h}\right) \times 100$$

2.3.2.3 Metabolomic analysis

LC-MS/MS raw files were converted into mzML format using MSconvert and uploaded to MZmine 2 v.2.53 (76), with the parameters chosen for mass feature detection, chromatogram building, and alignment being presented in Table 5.

Table 5. Parameters defined for mass feature detection, chromatogram building and feature alignment on MZmine 2 v.2.53.

MZmine 2 workflow	Defined parameters	
Mass detection (mass detector centroid)	Noise level for MS1	1E6
	Noise level for MS2	1E5
ADAP chromatogram builder	Minimum group size in # of scans	5
	Group intensity threshold	3E5
	Minimum highest intensity	3E5
	m/z tolerance (ppm)	5
	Retention time (min)	3.50 - 14.00
Chromatogram resolving (local minimum search)	Chromatographic threshold	10%
	Search minimum in RT range	0.1
	Minimum relative height	10%
	Minimum absolute height	6E5
	Min ratio of peak/top edge	1
	Peak duration range (min)	0.05-3.00
	m/z range for MS2 scan pairing	0.01
	RT range for MS2 scan pairing (min)	0.2
Isotope grouping (isotope peak grouping)	m/z tolerance	5 ppm
	Retention time	0.1 min
	Maximum charge	2
	Representative isotope	Most intensive
Alignment (joint aligner)	m/z tolerance	5 ppm
	Weight for m/z	75
	Retention time tolerance	0.1 min
	Weight for RT	25
Filtering (feature list row filter)	Keep only peaks with MS2 scan	
Gap filling (peak finder)	Intensity tolerance	10%
	m/z tolerance	5 ppm
	Retention time tolerance	0.1 min

The data was exported as a Metaboanalyst file (.csv) and non-existent values were substituted by 1. The file was submitted to Metaboanalyst 5.0 (77) and a one-factor statistical analysis was performed with the default settings, except for the percentage to filter out, which was lowered to 0%. Various statistical analyses were done, including one-way ANOVA, principal component analysis (PCA) and volcano plots.

Molecular networks were created with the Feature-Based Molecular Networking (FBMN) workflow (78) on GNPS (https://gnps.ucsd.edu) (79). The mass spectrometry data were first processed with MZmine 2 (76), as described above, and the results were exported to GNPS for FBMN analysis. The data was filtered by removing all MS/MS fragment ions within +/- 17 Da of the precursor *m/z*. MS/MS spectra were window filtered by choosing only the top 6 fragment ions in the +/- 50 Da window throughout the

spectrum. The precursor ion mass tolerance was set to 0.02 Da and the MS/MS fragment ion tolerance to 0.02 Da. A molecular network was then created where edges were filtered to have a cosine score above 0.7 and more than 6 matched peaks. Further, edges between two nodes were kept in the network if and only if each of the nodes appeared in each other's respective top 10 most similar nodes. Finally, the maximum size of a molecular family was set to 100, and the lowest scoring edges were removed from molecular families until the molecular family size was below this threshold. The spectra in the network were then searched against GNPS spectral libraries (80). The library spectra were filtered in the same manner as the input data. All matches kept between network spectra and library spectra were required to have a score above 0.7 and at least 6 matched peaks. The DEREPLICATOR was used to annotate MS/MS spectra (81).

To enhance chemical structural information within the molecular networks, information from in silico structure annotations from GNPS Library Search, Network Annotation Propagation (82), Dereplicator (81), Varquest (83) and Ms2lda (84) were incorporated into the network using the GNPS MolNetEnhancer workflow (85) on the GNPS website (79). Chemical class annotations were performed using the ClassyFire chemical ontology (86). The molecular networks were visualized using Cytoscape software (87).

Additionally, another molecular network was created between bioactive and non-bioactive extracts (79). The precursor ion mass tolerance was set to 0.02 Da and a MS/MS fragment ion tolerance of 0.02 Da. All other conditions were set to default and the network was visualized with the Cytoscape software (87).

3. Results and Discussion

3.1 *Lusitaniella coriacea* LEGE 07167

3.1.1 Genome mining

Bioinformatics analysis with AntiSMASH 7.0 allowed to identify six secondary metabolite regions in the assembly genome of *Lusitaniella coriacea* LEGE 07167 (Table 1A of the Appendix A). The software predicted that region 2.1 contains putative genes to produce hybrid-NRP/PK metallophores (Figure 12). The BGC architecture and predicted function of the core biosynthetic genes matches the structure of lusichelins, compounds isolated from this cyanobacterium previously in the group.

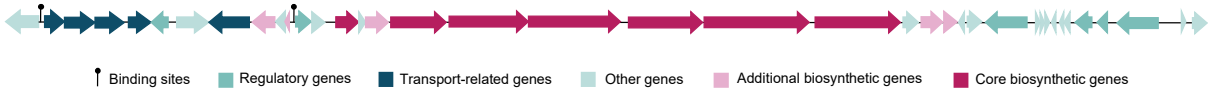

Figure 12. Putative lusichelins BGC.

In this BGC are present core and additional biosynthetic genes, regulatory genes, as well as transport genes, with the closest enzyme homologue for each of them (obtained with blastp) being displayed on Table 2A of the Appendix A. Among them, it is of interest to highlight the presence of putative genes encoding for typical iron-uptake systems proteins: ABC (ATP-binding cassette) and MFS (major facilitator superfamily) transporters, TonB-dependent receptor, and heavy metal translocating P-type ATPase. The latter is homologous to proteins ZosA/PfeT of *Bacillus subtilis*, which have been associated with transport of copper, zinc, and ferrous iron (88).

Additionally, various regulatory genes were identified, with one of them containing domains homologous to precorrin-8x methylmutase and MerR family transcription factors. Precorrin-8x methylmutase catalyzes a methyl rearrangement in the vitamin B12 biosynthesis (89). The MerR family of transcription factors includes a huge array of genes that can act as repressors or inducers in response to oxidative stress, antibiotics, or heavy metals, such as mercury, copper, lead, and others (90). In *Synechocystis* sp. PCC6803, a MerR-like regulator (Slr0701) was found to induce the expression of MerA, a mercury reductase, in the presence of mercury (90,91).

Moreover, through the Transcription Factor Binding Sites (TFBS) Finder, AntiSMASH identified three zinc-responsive repressor (ZurR) binding sites (one with strong and two with medium confidence). ZurR is a zinc-specific member of the Fur family of regulators and is responsible for maintaining zinc homeostasis (92).

Lusichelin **5** presents structural resemblances to known salicyl-thiazol(in)e siderophores like pyochelin, yersiniabactin and piscibactin (Figure 13). Just like the lusichelin BGC, the BGCs of these known siderophores all contain MFS and ABC transporters and TonB-dependent receptors (93–95). Moreover, lusichelin **5** has also been found complexed with iron. Due to all this, this compound is suspected of being a siderophore.

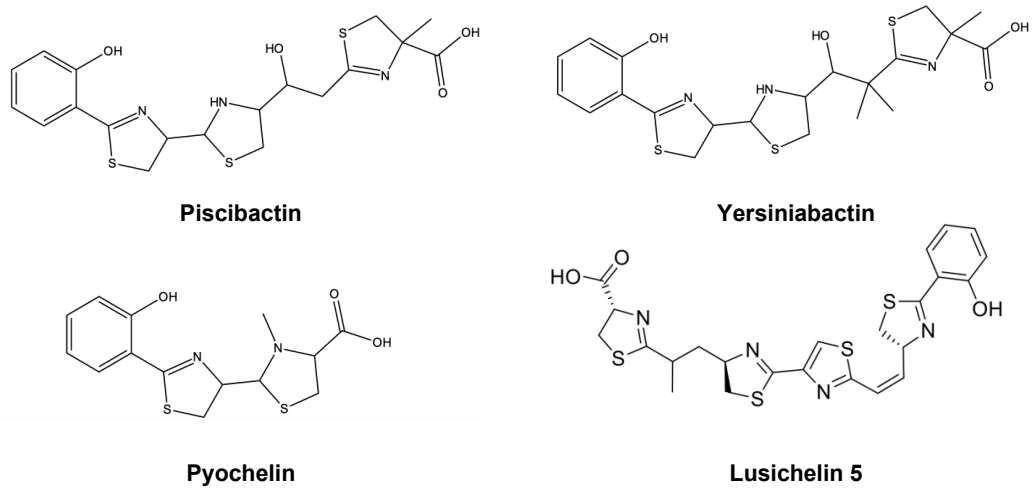

Figure 13. Chemical structures of lusichelin **5** and the known salicyl-thiazol(in)e siderophores piscibactin, yersiniabactin and pyochelin.

3.1.2 Copper and iron assays

Lusitaniella coriacea LEGE 07167 was cultivated for 30 days in iron-repleted (TM $FeCl_3$(+)/NaCl $FeCl_3$(+)), iron-limited (TM $FeCl_3$(-)) and iron-depleted conditions (NaCl $FeCl_3$(-)), as well as with different concentrations of copper (0, 5, 200 and 450 nM $CuSO_4$) to evaluate if these factors could be a trigger for lusichelin production. The formulation of the tropical marine salt (TM) contains multiple trace elements, including iron and copper. The only way of obtaining a culture medium with no iron, and the actual mentioned $CuSO_4$ concentrations, was to eliminate all traces of these metals. Therefore, for the iron-depleted conditions and the copper concentrations conditions, TM was substituted by NaCl.

After the experiment was concluded, differences were observed at macroscopic level in cultures of the different experimental conditions. In particular, the cultures supplemented with $CuSO_4$ at 200 nM and 450 nM showed different color as “light green” different from the “dark green” color usual in cultures grown in Z8-TM (the standard culture medium) (Figure 14). In these conditions, the dry weight of the lyophilized biomass was also lower than in all the other conditions, indicating that the cyanobacterium had its normal growth altered. As the standard concentration of $CuSO_4$ in Z8 medium is 5 nM, it is possible that 200 and 450 nM of $CuSO_4$ would be an excessive amount, presenting some toxicity for the strain. In the model cyanobacterium *Synechocystis* sp. PCC 6803, 3 µM of copper has been deemed toxic, while 0.3 µM (300 nM) is a non-inhibitory concentration (96). However, it has been shown that copper sensitivity varies greatly among photosynthetic microorganisms (97,98).

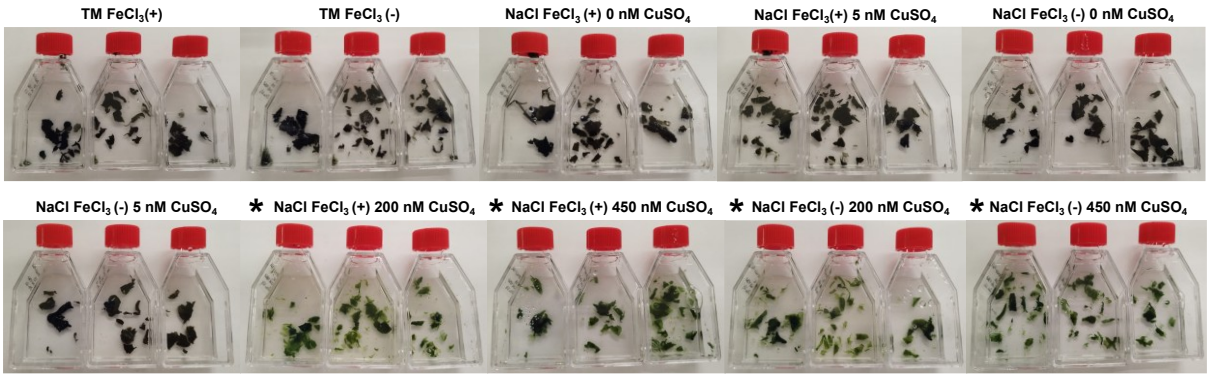

Figure 14. Cultures of *Lusitaniella coriacea* LEGE 07167 after 30 days of growth under different media (50 ml culture flasks; n=3). In the conditions marked with *, the cultures showed a "light green" appearance contrasting with the "dark green" usual in standard medium (Z8-TM).

To understand the effect of the different conditions on lusichelin production, a relative quantification of lusichelins **1-5** and 5 complexed with Fe (**5-Fe**) was conducted through the peak areas of the extracted ion chromatogram (EIC) (Figure 15 and Tables A1.3 and A1.4, appendix 1).

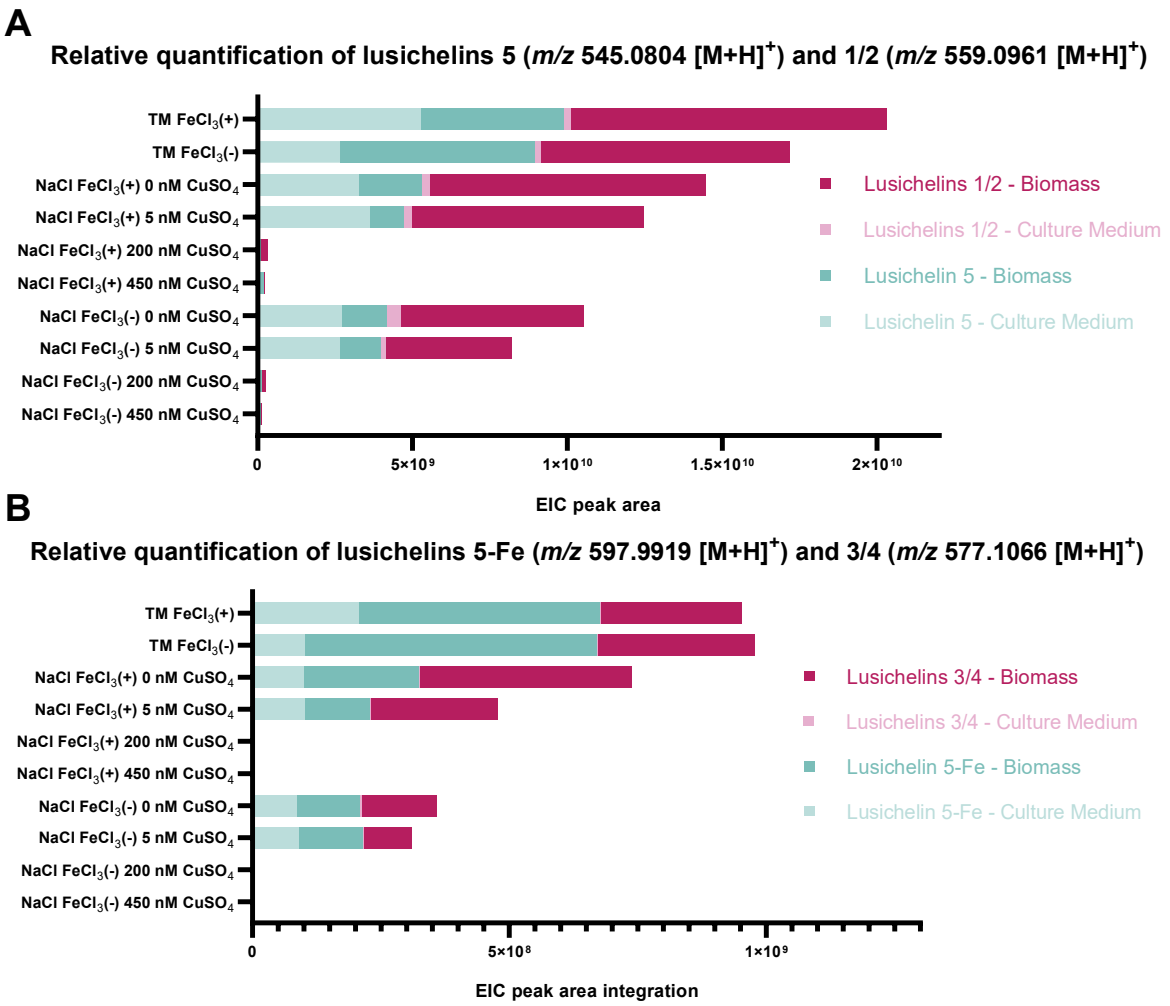

Figure 15. Relative quantification (EIC peak areas) of lusichelins **1/2** (*m/z* 559.0961 $[M+H]^+$) and **5** (*m/z* 545.0804 $[M+H]^+$) (**A**) and lusichelins **3/4** (*m/z* 577.1066 $[M+H]^+$) and **5-Fe** (*m/z* 597.9919 $[M+H]^+$) (**B**) in the different tested

conditions: iron-repleted (TM $FeCl_3$(+)/NaCl $FeCl_3$(+)), iron-limited (TM $FeCl_3$(-)), iron-depleted (NaCl $FeCl_3$(-)) and various copper concentrations (0, 5, 200 and 450 nM $CuSO_4$).

Starting with lusichelin **5** ($[M+H]^+$ ion at *m/z* 545.0804), the first major observation is that, in general, its production did not increase in iron-limited/iron-depleted conditions (Figure 15-A). Siderophores are usually synthesized in low iron conditions, to overcome this limitation. Lusichelin **5** is suspected of being a siderophore. Therefore, it was expected to detect larger amounts in the conditions without $FeCl_3$, which was not verified. In fact, there was even an almost two-fold decrease in the presence of lusichelin **5** in the culture medium extracts of Z8-TM without iron (iron-limited conditions). These findings possibly suggest that the primary biological function of this compound might not be iron chelation.

Curiously, the conditions in which the production of lusichelin **5** reached its peak were the standard Z8-TM and Z8-TM without iron (iron-limited condition). Once again, siderophores are not usually synthesized in standard conditions, so this was not expected. The decrease in the amount of lusichelin **5** between TM $FeCl_3$(-) and NaCl $FeCl_3$(-) 5 nM, where the only variable is the salt, was significative according to a t-test (p-value < 0.05). Therefore, it might be possible that one or more of the trace elements present in the formulation of the tropical marine salt (TM) are inducing the biosynthesis of this compound. A factor that could be attributed to this is the MerR-like transcription factor found in the BGC. This regulatory gene has been associated with the response to various heavy metals, including copper (90), so the influence of this heavy metal was assessed.

As observed in Figure 15-A, removing copper from the culture medium (0 nM $CuSO_4$) did not induce any major changes in relation to the standard copper concentration (5 nM $CuSO_4$). On the conditions in which 200 and 450 nM $CuSO_4$ were supplemented, the presence of *m/z* 545.0804 $[M+H]^+$ in biomass was negligible. Considering these concentrations of $CuSO_4$ might present some toxicity to the strain, this is not exactly surprising. Yet, there are several cases in which siderophores can also chelate other metals to diminish their toxicity: yersiniabactin (which presents structural resemblance to lusichelins) chelates iron in iron-limited conditions and copper in copper-overload situations (99).

To discover a putative complex between lusichelin **5** and copper, the mass data was screened to find an ion with more 61.9212 Da (Cu^{2+}) than the protonated mass of lusichelin **5** ($[M+H]^+$ ion at *m/z* 545.0804), but nothing was detected.

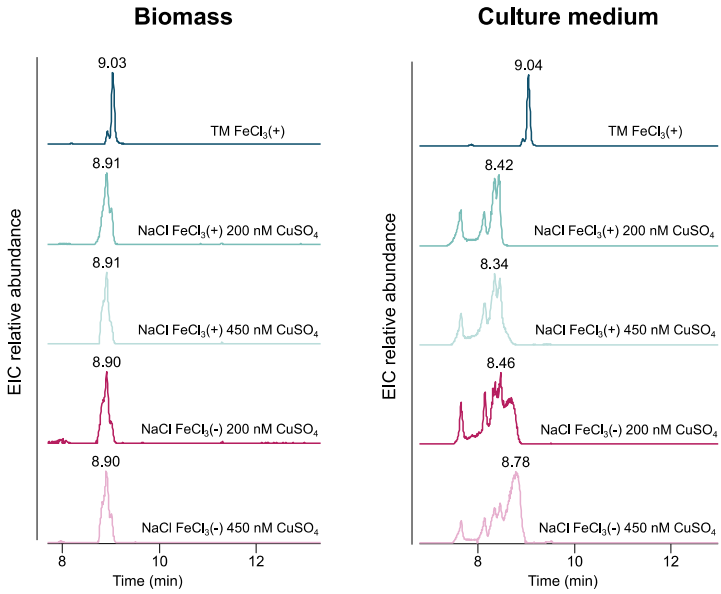

Figure 16. Extracted ion chromatograms (EIC) of *m/z* 545.0804 $[M+H]^+$ (lusichelin **5**) in biomass and culture medium in standard conditions (Z8-TM) and conditions supplemented with $CuSO_4$ (200 and 450 nM).

Also noteworthy is the fact that in the biomass, the RT of lusichelin **5** varied slightly in comparison to the standard culture conditions (Figure 16). However, it was still considered in the quantification, as the MS^2 fragmentation pattern coincided with the one from lusichelin **5** (Figure 17). In the culture medium, the RT variation was even larger (Figure 16) and the MS^2 fragmentation pattern was very different from the usual in standard conditions (Figure 17), so these values were not considered in the quantification. This also shows that a possible new compound, with the same mass as lusichelin **5** (($[M+H]^+$ ion at *m/z* 545.0804 with 5 ppm tolerance) is being produced in these conditions. To infer if this new compound is structurally related to lusichelins, a classic molecular network was constructed with GNPS (Table A1.5, appendix 1). The new compound was located in the same cluster as lusichelins **1/2** (*m/z* 545.0804 $[M+H]^+$), indicating a structural relation between both. However, the only way to confirm this would be to isolate the compounds in the future and elucidate their structure.

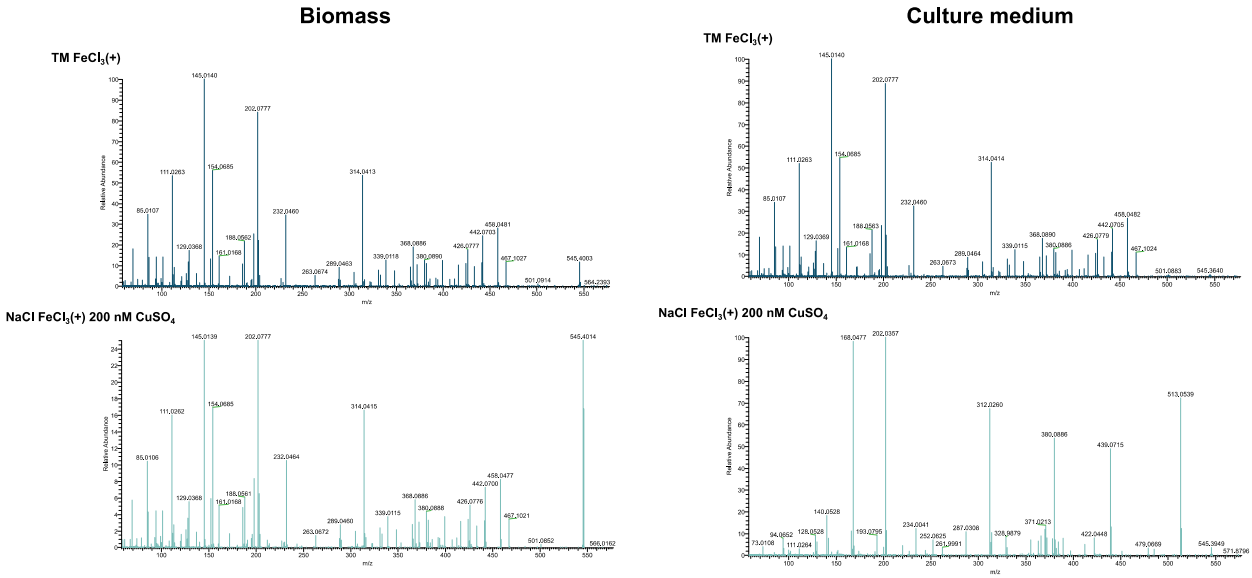

Figure 17. Comparison between MS/MS spectra of m/z 545.0804 $[M+H]^+$ (lusichelin **5**) of standard condition (Z8-TM) and NaCl (+Fe) 200 nM $CuSO_4$. In the biomass (left), the fragmentation patterns match, while in the culture medium (right) they do not.

Regarding lusichelins **1/2**, the results are quite alike the ones obtained for lusichelin **5**, and the decrease verified between TM $FeCl_3$(-) and NaCl $FeCl_3$(-) 5 nM was also significative for this compound, according to a t-test (p-value < 0.05). The main difference is that lusichelins **1/2** are present in very low amounts in the culture medium (Figure 15-A). While these compounds are structurally similar, lusichelins **1/2** contain a methoxycarbonyl group while compound **5** bears a carboxylic acid (Figure 8). To address this matter, their logP values were calculated using Molinspiration (75). Lusichelins **1/2** exhibited a logP of 4.66, whereas lusichelin **5** had a logP of 2.59. This showed that the methylation led to an approximately two-fold increase in the logP value and consequently, lusichelins **1/2** have lower polarity. As the culture medium is a polar environment, it is logical that these compounds are barely present in the culture medium extracts.

Lusichelins **3/4** (*m/z* 577.1066 $[M+H]^+$) and **5-Fe** (*m/z* 597.9919 $[M+H]^+$) were produced in much lower amounts than lusichelins **5** and **1/2** (Figure 15-B). Similarly to lusichelins **1/2** and **5**, the amount of lusichelins **3/4** and **5-Fe** did not increase in iron-limited/iron-depleted conditions. Also in accordance with the obtained for lusichelins **1/2** and **5**, *m/z* 597.9919 $[M+H]^+$ (lusichelin **5-Fe**) was more abundant in the TM conditions than in the NaCl conditions (2 to 4 times in the biomass). On the other hand, this was not verified for lusichelins **3/4**: their peak production was on NaCl $FeCl_3$(+) 0 nM $CuSO_4$, where it was 1.5 times higher than in the biomass of standard conditions (TM $FeCl_3$(+)). However, they were detected in residual amounts on the culture medium, possibly due to their low polarity (logP = 3.78).

3.2 *Leptothoe* sp. LEGE 181152

3.2.1 Genome mining

Analysis of the assembly genome of *Leptothoe* sp. LEGE 181152 with AntiSMASH 7.0.0 identified 19 BGCs (Table A2.1, appendix 2). Among these, a hybrid NRPS/PKS metallophore BGC was identified

(Figure 18), however in previous work of the group, in which the strain was grown in standard culture conditions, no NP was associated with this BGC.

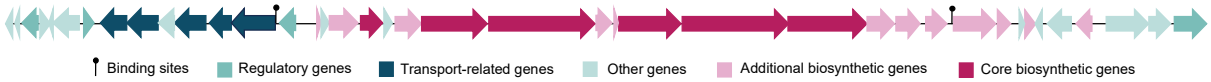

Figure 18. Secondary metabolite region 17.2 of *Leptothoe* sp. LEGE 181152, as proposed by AntiSMASH 7.0.0.

This hybrid NRPS/PKS BGC encodes 3 NRPS modules, intercalated by type I PKS genes. The NRPS modules contain adenylation domains, with predicted specificity to cysteine, and heterocyclization domains. This suggests the presence of thiazoline/thiazole moieties in the BGC products. Additionally, the BGC encodes for a salicylate synthase, various regulatory genes, and siderophore-associated genes: MSF transporters, ABC transporters and a TonB-dependent receptor (Table A2.2, appendix 2). Regarding regulatory genes, putative AraC family and Crp/Fnr family transcriptional regulators were detected. The AraC family members are globally distributed across bacteria, function mostly as activators of gene expression, and regulate various physiological processes (e.g. stress responses) (100,101). The Crp/Fnr (cyclic AMP (cAMP) receptor protein/ fumarate and nitrate reductase regulator protein) regulators also act as universal transcriptional activators in bacteria (102). They respond to stimuli like temperature and oxidative stress, regulating a wide range of metabolic pathways, including nitrogen fixation and photosynthesis (102). In cyanobacteria, there are various reports of light-induced increase of cAMP levels (103–106). As an example, blue light (450 nm) increased cAMP concentration, stimulating cell mobility in *Synechocystis* sp. PCC 6803 (103). Two putative ZurR binding sites were also identified with medium confidence, which, as previously explained, are involved in zinc homeostasis (107).

Noting various resemblances between this BGC and the lusichelin BGC (Figure 12), both were compared using CAGECAT clinker (Figure 19) (74). This confirmed that there are several similarities in the architecture of both BGCs, particularly in terms of biosynthetic and transport-related genes. Therefore, it is possible that the NP encoded in this cryptic/silent BGC could also constitute a salicyl-thiazol(in)e siderophore.

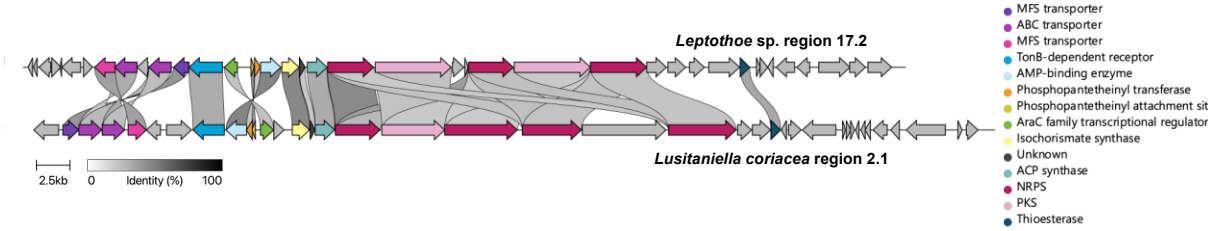

Figure 19. Comparison between region 17.2 of *Leptothoe* sp. LEGE 181152 and region 2.1 of *Lusitaniella coriacea* LEGE 07167 (putative lusichelins BGC), achieved with CAGECAT clinker.

3.2.2 Copper and iron experiment

Leptothoe sp. LEGE 181152 was cultivated in iron-limited and iron-depleted conditions, and under different concentrations of copper to try to induce the production of the putative metallophore predicted

by AntiSMASH. One week before the start of this experiment, part of the culture was passed from Z8-TM to Z8-NaCl to adapt. In standard Z8-TM, this strain usually has a red/dark pink color, however, when passed to Z8-NaCl, it turned green (Figure 20).

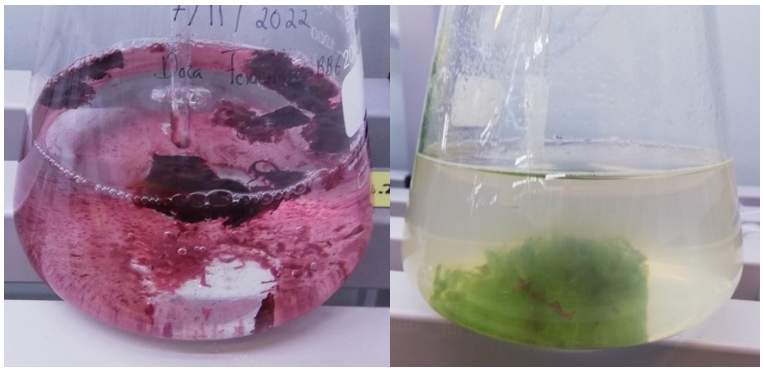

Figure 20. *Leptothoe* sp. LEGE 181152 in Z8-TM (standard culture medium) (left) and Z8-NaCl (right).

After 30 days of culture, the cultures grown in Z8-NaCl conditions were all colorless, meaning that the cells were dead. This led to the conclusion that one or more of the trace elements of TM is possibly essential to the strain's metabolism and the initial change of color to green was already a sign of stress. In this experiment, Z8-TM cultures were used to inoculate Z8-TM condition, while Z8-NaCl cultures were used to inoculate its respective Z8-NaCl conditions. However, to evaluate if the strain regained its original color when reinoculated in Z8-TM, the Z8-NaCl cultures were also used to inoculate an additional Z8-TM condition. It was confirmed that the strain regained its original red/pink color, proving that the state of stress induced by the change to Z8-NaCl was reversible.

3.2.3 Photobioreactors experiment

Leptothoe sp. LEGE 181152 was cultivated for three weeks under controlled different light qualities (white, blue, and red) and regimes (16/8h light/dark cycle and 24h of continuous light) on Algem® Pro photobioreactors. At the end of the experiment, an untargeted metabolomics analysis approach was applied to study the differences on the chemical constituents of the biomass and culture media among the different experimental groups. Moreover, these extracts were screened for potential bioactivity in anticancer, anti-settlement and antibacterial activity assays.

3.2.3.1 Bioactivity assays

a) Anticancer activity assays

Biomass and culture media extracts of *Leptothoe* sp. LEGE 181152 were tested for anticancer activity through the MTT assay on a human colon adenocarcinoma cell line (HCT-116) at 25 and 50 µg/mL (Figure 21). None of the extracts diminished the cell viability below the 50% threshold. This was unexpected, as in previous work of the group, two groups of cytotoxic compounds (leptochelins and phormidolides) were isolated from this strain. Biomass extracts (25 µg/mL) containing these compounds resulted in 25.69% cell viability, while fractions (25 µg/mL) containing leptochelins and phormidolides yielded 18.56% and 29.98% of cell viability, respectively (108). However, their bioactivity-guided

discovery process used cultures grown under standard conditions: 25 °C with light/dark cycle of 14/10 h at a light intensity of 10–30 µmol photons m^{-2} s^{-1}. In this assay, the closest to this standard condition is the 16/8h light/dark cycle of white light. Yet, there are still many variations between the two, namely the photoperiod, light intensity, agitation, vessel type, and time of culture. All these factors can affect metabolite production, and so, leptochelins and phormidolides might not be produced or be present in low amounts in these conditions, justifying the lack of activity.

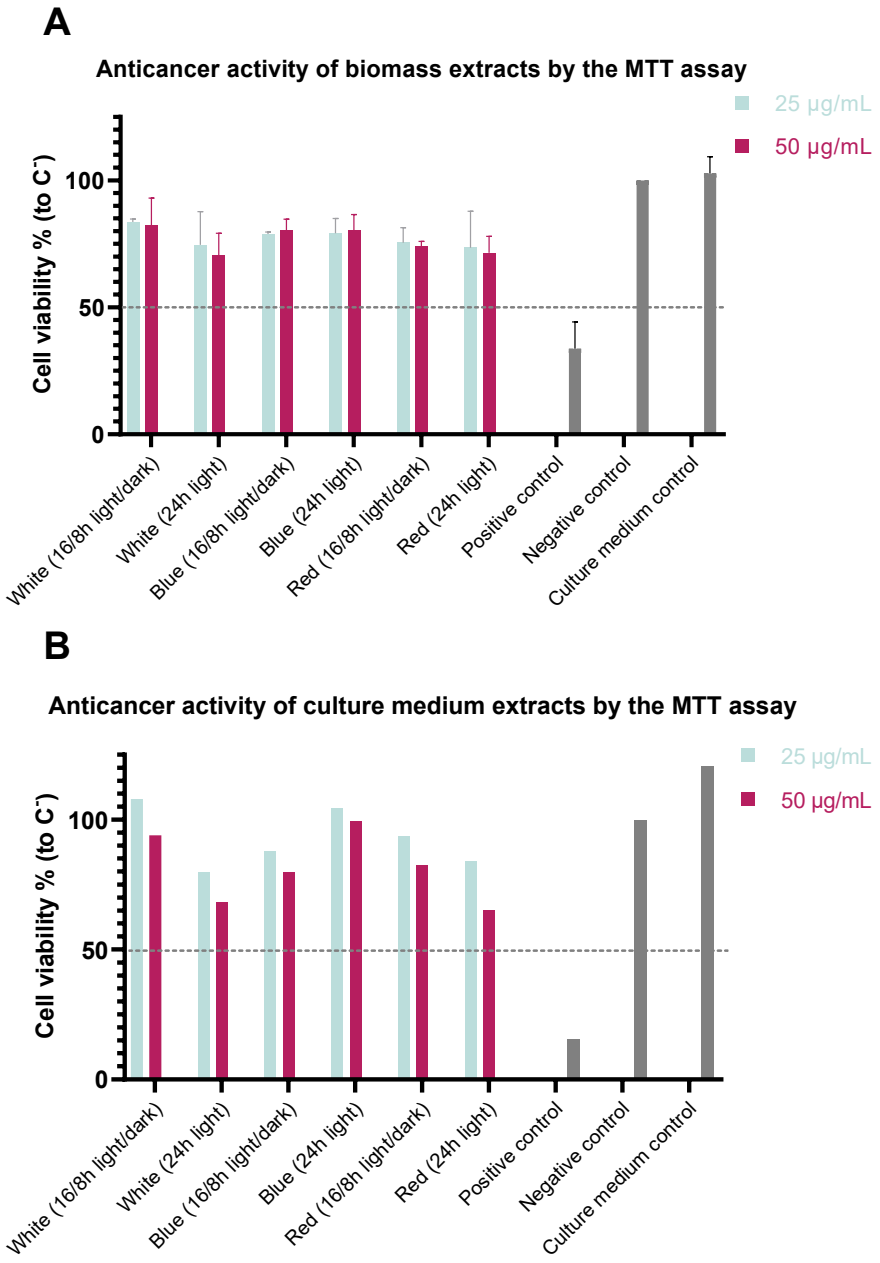

Figure 21. Anticancer activity of biomass (n=3) (**A**) and culture medium (n=1) (**B**) extracts of *Leptothoe* sp. LEGE 181152 grown under different light conditions, evaluated by the MTT assay on human cell line HCT-116. Activity was considered when cell viability was below the threshold of 50%.

b) Anti-settlement activity assays

The anti-settlement activity of the biomass extracts of *Leptothoe* sp. LEGE 181152 grown under different light conditions was assessed on *Mytilus galloprovincialis* larvae (Figure 22). On the first assay, four extracts presented reduced settlement activity: 24h of continuous white, blue, and red light and the red light with a 16/8h light/dark cycle. However, in the second assay for results validation, the only extracts that retained activity, considering *in vivo* natural variability of larvae individual responses, were the ones from the red light conditions, which showed consistent anti-settlement activity in both assay trials with a percentage of inhibition of 80%.

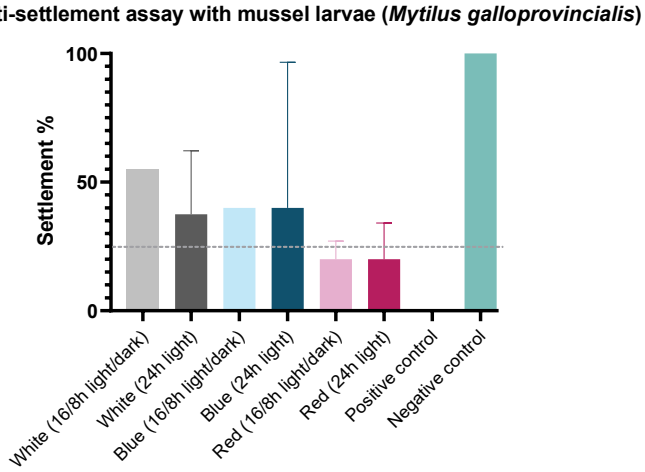

Figure 22. Anti-settlement activity of biomass extracts of *Leptothoe* sp. LEGE 181152 grown under different light conditions against mussel larvae (*Mytilus galloprovincialis*). Activity was considered when settlement percentage was below the threshold of 25%. The positive control was $CuSO_4$ at 5 µM and the negative control was filtrated seawater.

c) Antibacterial activity assays

The antibacterial activity of the biomass extracts of *Leptothoe* sp. LEGE 181152 grown under different light conditions was tested against five marine biofouling bacterial strains (Figure 23). Considering a threshold of 30%, none of the extracts presented activity. In fact, some extracts even resulted in a negative growth inhibition, meaning they slightly promoted the growth of the strains.

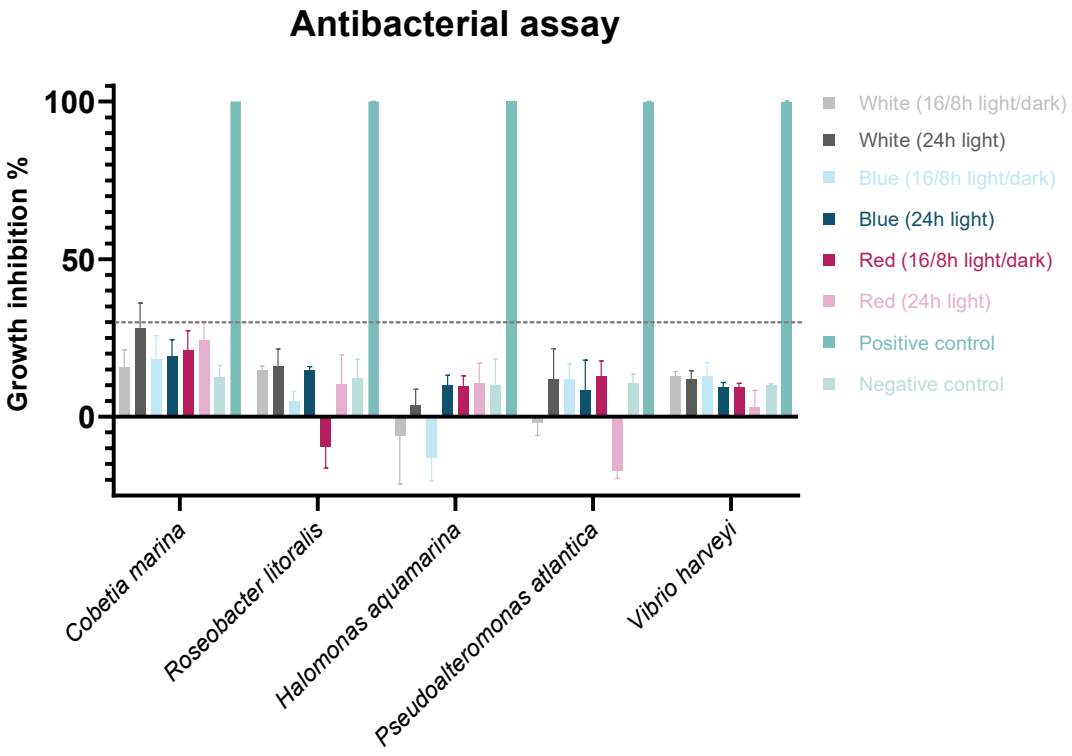

Figure 23. Antibacterial activity of biomass extracts of *Leptothoe* sp. LEGE 181152 grown under different light conditions against several biofilm-forming bacteria (*Cobetia marina*, *Vibrio harveyi*, *Roseobacter litoralis*, *Halomonas aquamarina*, and *Pseudoalteromonas atlantica*). Activity was considered when growth inhibition was above the threshold of 30%. The positive control was a 1:100 penicilin-streptomycin-neomycin stabilized solution and the negative control was DMSO at 0.1%.

3.2.3.2 Metabolomic analysis

To understand how the different light conditions modulated the metabolome, LC-MS/MS data were processed with MZmine 2.53 and submitted to Metaboanalyst 5.0, where various statistical analysis were carried out. Classic and feature-based molecular networks were also assembled on GNPS to identify putative new compounds and infer on the relation between metabolome and bioactivity.

Metabolomic analysis with Metaboanalyst: culture medium extracts

A one-way ANOVA analysis (p-value < 0.01) between the culture medium of the 6 different conditions revealed 1249 significant features and only 315 unsignificant, proving that the light quality and regime has a major impact on the metabolomic content.

A principal component analysis (PCA) was done, to understand in which experimental conditions the metabolomes are more similar and to detect striking differences (Figure 24). This analysis revealed three major clusters: white with a 16/8h light/dark cycle, blue with a 16/8h light/dark cycle and the four other conditions.

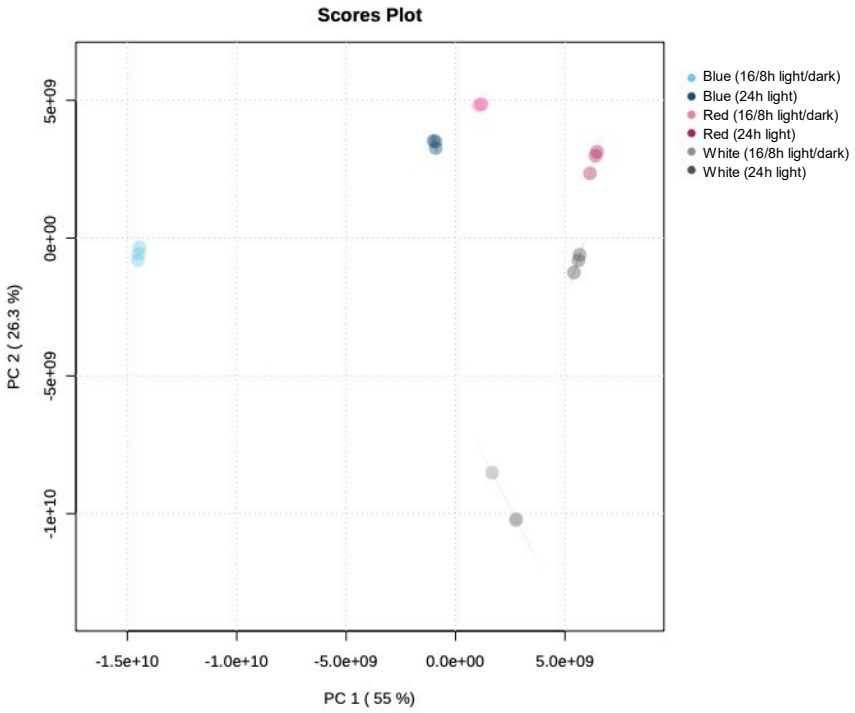

Figure 24. Two-dimensional principal component analysis of the metabolomic profile of the culture medium in the six different light conditions (n=3). Three major clusters can be observed: white with a 16/8h light/dark cycle, blue with a 16/8h light/dark cycle and the four other conditions.

To study the effect of the quality of the light, two distinct one-way ANOVA analysis were done, one compared the white, blue, and red at 16/8h light/dark cycle and the second compared the white, blue, and red at 24h light photoperiod.

Starting with the first analysis, 153 significant mass features were identified, against 1038 unsignificant (p-value < 0.01). Of these, the 20 most significant (lowest p-value) are displayed on Table 6. All of these belong to the red light condition, showing that the metabolome is especially different under this wavelength.

Table 6. Features with the lowest raw p-value from the comparison between the white, blue, and red 16/8h light/dark cycle conditions in the culture medium, obtained through ANOVA post-hoc Fisher's LSD analysis (p-value < 0.01).

m/z	RT	p-value	Prevalent condition
1042.0977	13.32 min	9.42E-13	Red (16/8h light/dark)
311.1617	8.23 min	1.89E-12	Red (16/8h light/dark)
903.0698	6.27 min	2.21E-12	Red (16/8h light/dark)
665.5827	11.87 min	3.24E-12	Red (16/8h light/dark)
587.2500	7.73 min	6.21E-12	Red (16/8h light/dark)
317.1496	5.20 min	6.55E-12	Red (16/8h light/dark)
287.1390	6.95 min	7.62E-12	Red (16/8h light/dark)
534.5607	13.36 min	2.84E-11	Red (16/8h light/dark)
571.2550	6.92 min	6.81E-11	Red (16/8h light/dark)
276.1230	5.63 min	7.03E-11	Red (16/8h light/dark)

1012.0509	13.10 min	8.89E-11	Red (16/8h light/dark)
543.364	6.56 min	1.63E-10	Red (16/8h light/dark)
817.168	7.21 min	2.63E-10	Red (16/8h light/dark)
536.5764	13.60 min	3.71E-10	Red (16/8h light/dark)
289.1798	8.23 min	4.22E-10	Red (16/8h light/dark)
1068.1139	13.36 min	5.72E-10	Red (16/8h light/dark)
601.4609	12.35 min	5.95E-10	Red (16/8h light/dark)
508.5451	13.30 min	8.51E-10	Red (16/8h light/dark)
819.1663	7.21 min	8.79E-10	Red (16/8h light/dark)
721.5775	13.86 min	1.16E-09	Red (16/8h light/dark)

Regarding the one-way ANOVA analysis between the different light colors with 24h of light, 915 significant features were detected and only 65 were unsignificant (p-value < 0.01). This result is drastically different from the one obtained for the comparison above, hinting that continuous light induces more metabolomic changes than the 16/8h light/dark cycle. The 20 most significant features were prevalent in the 24h of blue light (Table 7), contrarily to the observed above, in which they were mainly present in the red light.

Table 7. Features with the lowest raw p-value from the comparison between the white, blue, and red 24h light conditions in the culture medium, obtained through ANOVA post-hoc Fisher's LSD analysis (p-value < 0.01).

m/z	RT	p-value	Prevalent condition
711.5013	4.43 min	4.05E-16	Blue (24h light)
795.4576	10.20 min	5.87E-16	Blue (24h light)
888.6402	12.26 min	6.28E-15	White (24h light)
725.2421	5.74 min	4.72E-14	Blue (24h light)
598.4173	4.17 min	5.45E-14	Blue (24h light)
875.0852	8.70 min	6.22E-14	Blue (24h light)
340.3938	10.11 min	7.61E-14	Blue (24h light)
589.4283	10.59 min	8.57E-14	Blue (24h light)
857.0928	6.88 min	1.13E-13	Blue (24h light)
938.6534	5.01 min	1.47E-13	Blue (24h light)
899.075	7.88 min	1.62E-13	White (24h light)
501.3762	10.79 min	1.68E-13	Blue (24h light)
599.4014	4.43 min	2.10E-13	Blue (24h light)
806.6147	11.21 min	2.30E-13	Red (24h light)
369.384	9.62 min	2.31E-13	Blue (24h light)
859.0719	8.46 min	2.49E-13	Blue (24h light)
895.0784	7.88 min	2.71E-13	White (24h light)
271.188	6.81 min	3.07E-13	Blue (24h light)
873.0876	8.70 min	3.35E-13	Blue (24h light)
429.3186	10.04 min	3.67E-13	Blue (24h light)

These results show that, in general, the blue and red light seem to cause more modulation in the metabolome than the white light. To explore the impact of the photoperiod, volcano plots were elaborated between the 16/8h light/dark cycle and the 24h of light, in each color.

Starting with this comparison on the white light, 201 features were upregulated on the 24h of white light, only 5 were downregulated and 771 were unsignificant (Figure 25). Once again, this points to the continuous light changing more the metabolome than the light/dark cycle.

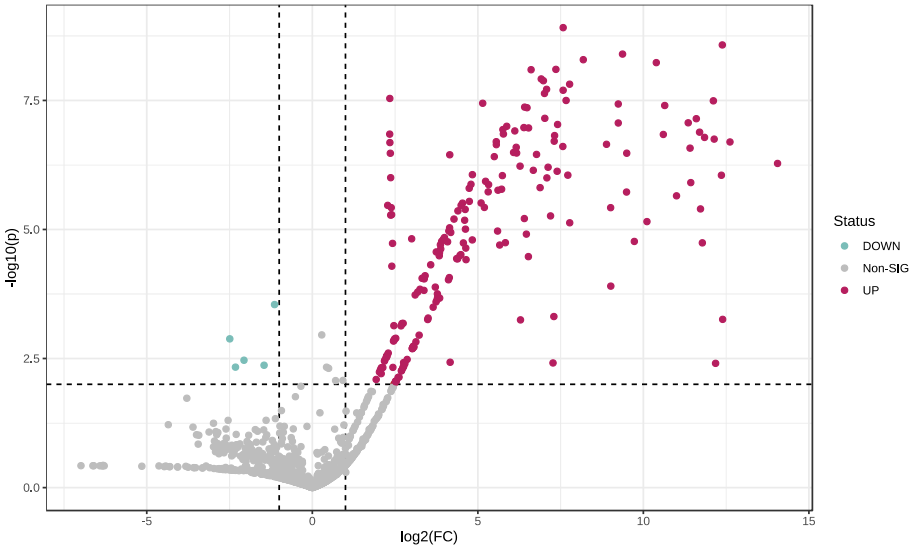

Figure 25. Volcano plot of white 16/8h light/dark cycle against white 24h light (p-value < 0.01). 201 features were upregulated and 5 were downregulated on the 24h of white light condition, while 771 were unsignificant.

The table constructed with the 20 features with highest p-value also confirmed this, as all of them were present in the 24h of white light (Table 8). Curiously, one of the features present on this table corresponds to the exact mass of leptochelin A (895.0784 $[M+H]^+$). As this compound was previously isolated from cultures maintained in standard conditions, its absence on white 16/8h light/dark cycle condition was not expected. However, as previously discussed, although this condition is the closest to the standard, there are still too many variables that might be affecting the metabolome, and particularly leptochelin production.

Table 8. Features with the lowest raw p-value from the comparison between white 16/8h light/dark cycle against white 24h light in the culture medium.

m/z	RT	FC	p-value	Prevalent condition
888.6398	12.25 min	190.94	1.23E-09	White (24h light)
901.5490	12.19 min	5348.5	2.66E-09	White (24h light)
821.5400	11.85 min	662.35	4.00E-09	White (24h light)
759.2029	6.81 min	291.23	5.14E-09	White (24h light)
823.5565	12.57 min	1342.5	5.86E-09	White (24h light)
500.4825	12.76 min	163.99	7.91E-09	White (24h light)
895.0784	7.89 min	97.591	8.03E-09	White (24h light)
839.1113	7.54 min	120.64	1.21E-08	White (24h light)

534.5605	13.39 min	126.18	1.31E-08	White (24h light)
536.5763	13.63 min	218.73	1.53E-08	White (24h light)
899.0748	7.89 min	134.97	1.92E-08	White (24h light)
837.1133	7.54 min	190.81	2.01E-08	White (24h light)
897.0765	7.89 min	129.21	2.32E-08	White (24h light)
418.2337	4.97 min	5.0676	2.89E-08	White (24h light)
839.5512	11.75 min	203.16	3.17E-08	White (24h light)
788.6034	11.78 min	4436.5	3.22E-08	White (24h light)
721.5773	13.91 min	35.436	3.59E-08	White (24h light)
520.5451	13.24 min	605.32	3.71E-08	White (24h light)
307.2267	8.64 min	1601.7	3.97E-08	White (24h light)
893.4993	13.54 min	85.236	4.26E-08	White (24h light)

The results obtained for the comparison between the blue light photoperiods agree with the obtained for the white light: 121 features were upregulated in the 24h of blue light and only 4 were downregulated (Figure 26). The 20 most significant features were also all found in the 24h of continuous blue light (Table 9).

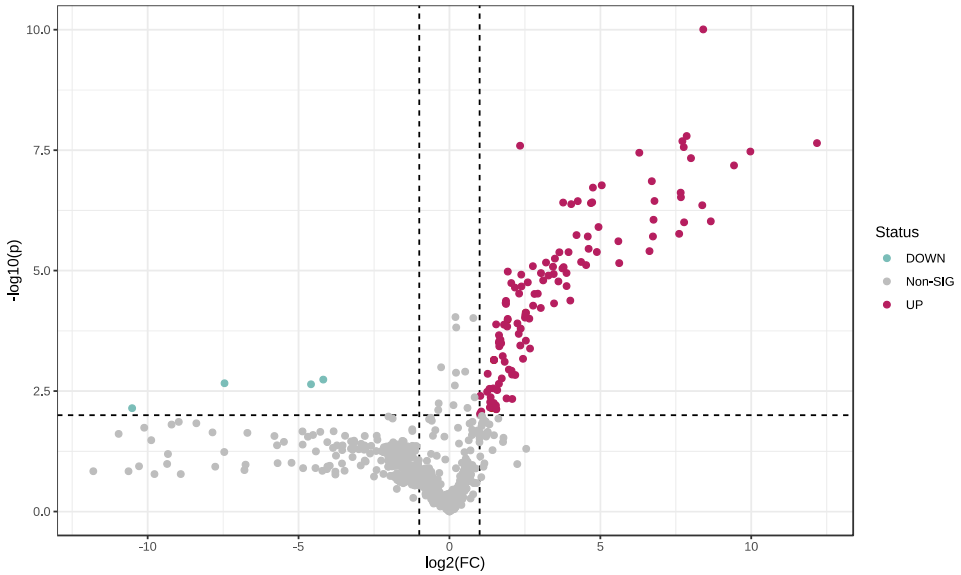

Figure 26. Volcano plot of blue 16/8h light/dark cycle against blue 24h light in the culture medium (p-value < 0.01). 121 features were upregulated and 4 were downregulated on the 24h of blue light condition, while 701 were unsignificant.

Table 9. Features with the lowest raw p-value from the comparison between blue 16/8h light/dark cycle against blue 24h light in the culture medium.

m/z	RT	FC	p-value	Prevalent condition
795.4578	10.20 min	339.8	9.85E-11	Blue (24h light)
522.5972	11.72 min	232.22	1.61E-08	Blue (24h light)
550.6284	11.87 min	210.5	2.06E-08	Blue (24h light)
960.0202	13.03 min	4629.3	2.25E-08	Blue (24h light)

1016.0816	13.30 min	5.0631	2.56E-08	Blue (24h light)
508.5452	13.31 min	217.35	2.74E-08	Blue (24h light)
1019.773	12.43 min	1003.1	3.37E-08	Blue (24h light)
1012.0509	13.10 min	78.251	3.58E-08	Blue (24h light)
581.598	13.30 min	256.37	4.64E-08	Blue (24h light)
386.3994	10.89 min	688.78	6.56E-08	Blue (24h light)
534.5606	13.36 min	104.3	1.39E-07	Blue (24h light)
368.4251	10.73 min	33.051	1.70E-07	Blue (24h light)
398.2326	10.21 min	26.959	1.89E-07	Blue (24h light)
986.0359	13.06 min	202.4	2.41E-07	Blue (24h light)
494.5658	11.59 min	203.5	3.00E-07	Blue (24h light)
564.6079	13.96 min	110.97	3.59E-07	Blue (24h light)
521.3812	12.43 min	19.059	3.61E-07	Blue (24h light)
493.3498	12.21 min	26.542	3.82E-07	Blue (24h light)
699.5956	13.88 min	13.616	3.87E-07	Blue (24h light)
480.5139	13.04 min	25.791	3.97E-07	Blue (24h light)

The results for the comparison between the photoperiod in the red light conditions were quite different from the ones obtained for the white and blue light. Unlike those, the tendency for the 24h of continuous light was not as pronounced: 117 were upregulated on the 24h of red light but 83 were downregulated (Figure 27). In the table of the 20 most significant features, there is also an even distribution between the two photoperiods (Table 10). The second most significant feature, upregulated on the 24h of red light, corresponds to the exact mass of leptochelin D (881.0626 $[M+H]^+$).

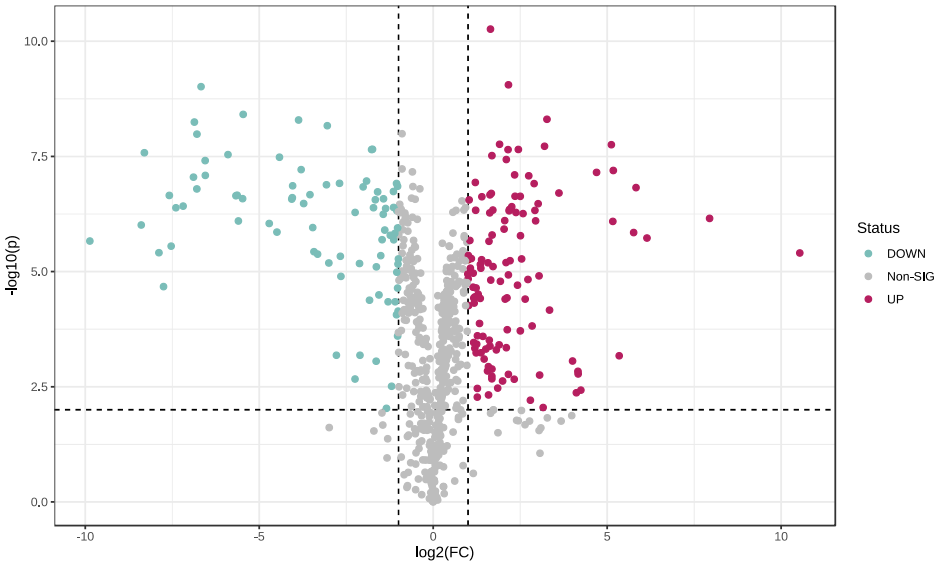

Figure 27. Volcano plot of red 16/8h light/dark cycle against red 24h light in the culture medium (p-value < 0.01). 117 features were upregulated and 83 were downregulated on the 24h of red light condition, while 504 were non-significant.

Table 10. Features with the lowest raw p-value from the comparison between red 16/8h light/dark cycle against red 24h light in the culture medium.

m/z	RT	FC	p-value	Prevalent condition
861.0695	8.45 min	3.1275	5.47E-11	Red (24h light)
881.0626	7.64 min	4.4754	8.85E-10	Red (24h light)
598.4173	4.17 min	0.0098041	9.70E-10	Red (16/8h light/dark)
905.6797	4.96 min	0.022701	3.88E-09	Red (16/8h light/dark)
763.4621	6.27 min	9.6366	4.95E-09	Red (24h light)
566.4275	4.07 min	0.068431	5.14E-09	Red (16/8h light/dark)
825.5692	4.80 min	0.0085845	5.69E-09	Red (16/8h light/dark)
453.3434	3.99 min	0.12132	6.83E-09	Red (16/8h light/dark)
469.8305	5.00 min	0.0090366	1.04E-08	Red (16/8h light/dark)
788.6032	11.63 min	3.75	1.73E-08	Red (24h light)
625.2656	11.02 min	34.775	1.77E-08	Red (24h light)
710.5929	12.39 min	9.1818	1.91E-08	Red (24h light)
536.3711	10.66 min	0.2983	2.22E-08	Red (16/8h light/dark)
761.4469	6.25 min	5.4503	2.24E-08	Red (24h light)
514.4103	10.65 min	0.29317	2.25E-08	Red (16/8h light/dark)
885.0593	7.64 min	4.4413	2.26E-08	Red (24h light)
711.5013	4.42 min	0.0031705	2.64E-08	Red (16/8h light/dark)
599.4014	4.43 min	0.01677	2.90E-08	Red (16/8h light/dark)
239.1642	5.49 min	3.2198	3.05E-08	Red (24h light)
695.5064	4.19 min	0.046788	3.30E-08	Red (16/8h light/dark)

This metabolomic analysis of the culture medium extracts in the different light conditions resulted in two major conclusions. The first is that blue and red light seem to cause higher modulation of the cyanobacterial metabolome than the white light, as they resulted in more significantly different mass features. The second is that continuous light provokes more changes in the metabolome than the 16/8h light/dark cycle. Reports on the effect of light on the metabolome of cyanobacteria are limited, and mostly focused on primary metabolites (109–112). Moreover, light response is very strain specific, so no major comparisons can be drawn from the literature.

b) Metabolomic analysis with Metaboanalyst: biomass extracts

A similar analysis was also performed for the biomass extracts. A one-way ANOVA analysis (p-value < 0.01) between the 6 different conditions exposed 696 significant features and 169 unsignificant. Once again, this demonstrated that the changes in the light conditions modulated the metabolome.

A PCA was also done, revealing three major clusters: white with 24h of light, blue with a 16/8h light/dark cycle and the four other conditions (Figure 28). This pattern of variation of the data differs from the one obtained for the culture medium. This shows that there are differences in the way the light conditions affect the metabolome in the biomass and culture medium.

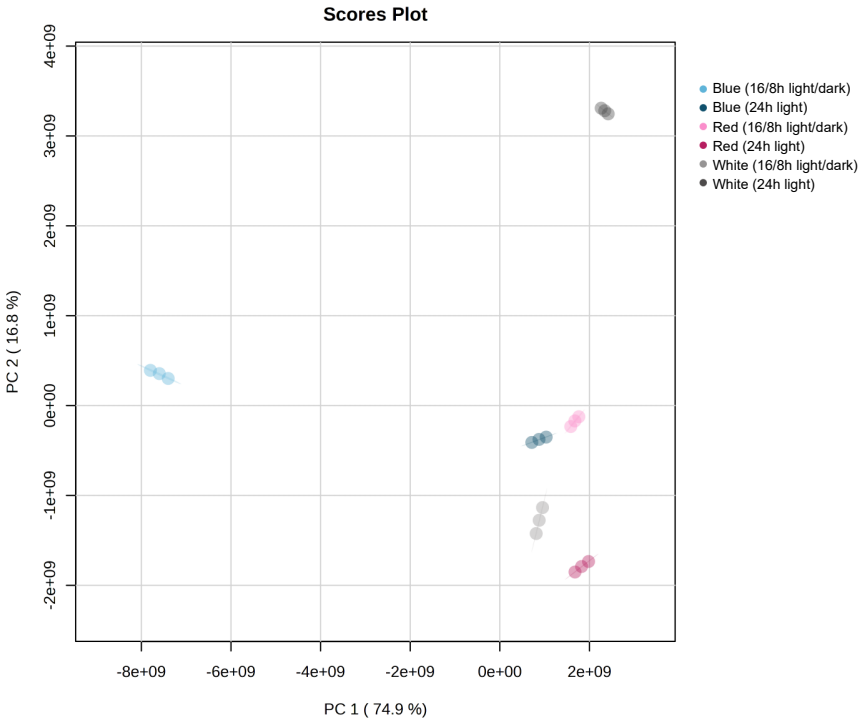

Figure 28. Two-dimensional principal component analysis of the metabolomic profile of the biomass in the six different light conditions (n=3). Three major clusters can be observed: 24h of white light, blue with a 16/8h light/dark cycle and the four other conditions.

The one-way ANOVA analysis of the white, blue, and red 16/8h light dark cycle revealed 402 significant and 207 unsignificant features (p-value < 0.01). The number of significant features is quite high in comparison to the obtained for the same analysis done in the culture medium (153). The 20 most significant are evenly distributed between the red and blue photoperiod (Table 11).

Table 11. Features with the lowest raw p-value from the comparison between the white, blue, and red 16/8h light/dark cycle conditions in the biomass, obtained through ANOVA post-hoc Fisher's LSD analysis (p-value < 0.01).

m/z	RT	p-value	Condition
457.2796	8.29 min	7.18E-14	White (16/8h light/dark)
735.3737	7.67 min	7.58E-13	Blue (16/8h light/dark)
945.452	3.78 min	1.16E-12	Red (16/8h light/dark)
762.4211	6.30 min	1.54E-12	Blue (16/8h light/dark)
441.1885	6.55 min	3.04E-12	Red (16/8h light/dark)
344.2545	3.95 min	5.19E-12	Red (16/8h light/dark)
734.3898	6.39 min	5.66E-12	Blue (16/8h light/dark)
952.9958	9.54 min	8.81E-12	Blue (16/8h light/dark)
1557.8534	9.15 min	1.10E-11	Blue (16/8h light/dark)
1120.5991	6.97 min	1.26E-11	Blue (16/8h light/dark)
946.4872	4.05 min	1.27E-11	Red (16/8h light/dark)
954.9934	9.54 min	1.47E-11	Blue (16/8h light/dark)

950.9982	9.54 min	2.48E-11	Blue (16/8h light/dark)
479.2614	8.29 min	2.49E-11	White (16/8h light/dark)
940.978	9.29 min	3.08E-11	Blue (16/8h light/dark)
710.5925	12.39 min	3.90E-11	Blue (16/8h light/dark)
907.0486	9.33 min	6.79E-11	Blue (16/8h light/dark)
726.403	4.13 min	7.22E-11	Red (16/8h light/dark)
790.4133	5.64 min	8.27E-11	Red (16/8h light/dark)
394.2225	5.96 min	9.25E-11	Blue (16/8h light/dark)

Regarding the comparison between the 24h of continuous light conditions, the one-way ANOVA analysis revealed 498 significant and 249 unsignificant features. Unlike in the culture medium, the effect of the 24h does not seem as pronounced. The majority of the 20 features with lowest p-value are present in the 24h of blue light (Table 12).

Table 12. Features with the lowest raw p-value from the comparison between the white, blue, and red 24h light conditions in the biomass, obtained through ANOVA post-hoc Fisher's LSD analysis (p-value < 0.01).

m/z	RT	p-value	Prevalent condition
575.2824	3.99 min	3.90E-18	Blue (24h light)
587.2863	5.49 min	1.43E-15	Blue (24h light)
473.297	4.27 min	1.48E-15	Blue (24h light)
945.4523	3.77 min	7.63E-15	Blue (24h light)
344.2545	3.95 min	2.66E-14	Blue (24h light)
518.2822	3.95 min	7.05E-14	Blue (24h light)
457.2792	8.29 min	9.16E-14	Red (24h light)
824.4035	4.01 min	1.74E-13	Blue (24h light)
654.4938	10.88 min	2.07E-13	Red (24h light)
436.2332	6.54 min	4.34E-13	White (24h light)
1003.6172	10.03 min	5.00E-13	Red (24h light)
474.3058	8.27 min	5.93E-13	Red (24h light)
596.2962	6.64 min	6.03E-13	White (24h light)
663.3715	5.39 min	6.38E-13	Blue (24h light)
735.3736	7.67 min	7.55E-13	White (24h light)
377.3163	6.77 min	8.54E-13	Blue (24h light)
910.4844	7.71 min	8.92E-13	White (24h light)
902.5792	13.55 min	8.94E-13	Blue (24h light)
479.2614	8.29 min	1.12E-12	Red (24h light)
954.9934	9.53 min	1.40E-12	Blue (24h light)

To further infer on the role of the photoperiod on modulating the metabolome, volcano plots were constructed for the comparison between photoperiods in each light quality.

135 features were upregulated and 52 were downregulated on the 24h of white light, in comparison to the 16/8h light/dark cycle (Figure 29). Once again, it is clear that the effect of the 24h, although stronger

than the light/dark cycle, is not as pronounced on the biomass as it on the culture medium (where 201 were upregulated and only 5 downregulated). Even though there are 53 downregulated features on the 24h (meaning they are upregulated on the 16/8h light/dark cycle), only 4 features of the photoperiod were on the 20 most significant features, with the majority being present on the 24h (Table 13).

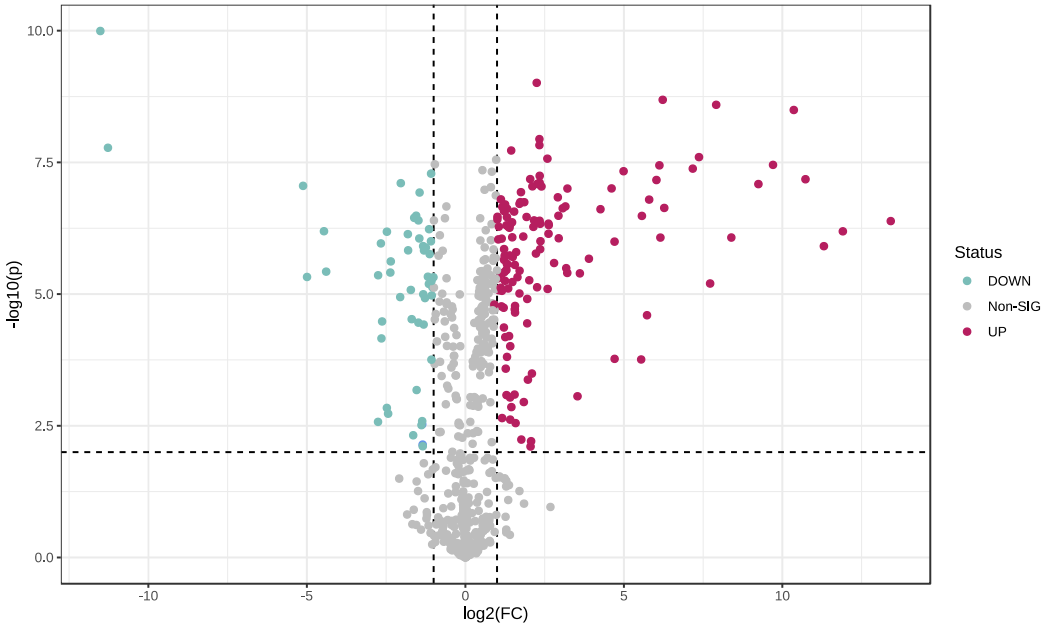

Figure 29. Volcano plot of white 16/8h light/dark cycle against white 24h light in the biomass (p-value < 0.01). 135 features were upregulated and 52 were downregulated on the 24h of white light condition, while 433 were non-significant.

Table 13. Features with the lowest raw p-value from the comparison between white 16/8h light/dark cycle against white 24h light in the biomass.

m/z	RT	FC	p-value	Prevalent condition
457.2794	8.29 min	0.00034177	1.01E-10	White (16/8h light/dark)
368.4251	10.72 min	4.7591	9.77E-10	White (24h light)
760.3689	7.27 min	74.795	2.05E-09	White (24h light)
735.3736	7.67 min	240.82	2.55E-09	White (24h light)
436.2332	6.55 min	1314.4	3.20E-09	White (24h light)
596.2962	6.63 min	5.0463	1.14E-08	White (24h light)
910.4844	7.72 min	5.0495	1.49E-08	White (24h light)
479.2616	8.29 min	0.00040341	1.67E-08	White (16/8h light/dark)
396.4201	12.34 min	2.7241	1.88E-08	White (24h light)
1120.5992	6.96 min	165.36	2.51E-08	White (24h light)
851.1291	7.77 min	6.0082	2.69E-08	White (24h light)
441.1884	6.55 min	833.96	3.53E-08	White (24h light)
661.3368	8.36 min	69.607	3.60E-08	White (24h light)
1092.5678	7.17 min	144.22	4.15E-08	White (24h light)
399.1778	5.97 min	31.794	4.66E-08	White (24h light)

512.4157	9.89 min	0.47244	5.17E-08	White (16/8h light/dark)
685.337	8.72 min	5.0803	5.69E-08	White (24h light)
510.9498	8.91 min	4.1265	6.57E-08	White (24h light)
423.1781	7.53 min	1695.9	6.60E-08	White (24h light)
734.3897	6.39 min	65.186	6.83E-08	White (24h light)

Surprisingly, the comparison between photoperiods on the blue light revealed 64 upregulated and 90 downregulated features on the 24h (Figure 30). This is also confirmed by the 20 most significant features, which are mainly present in the light/dark cycle (Table 14).

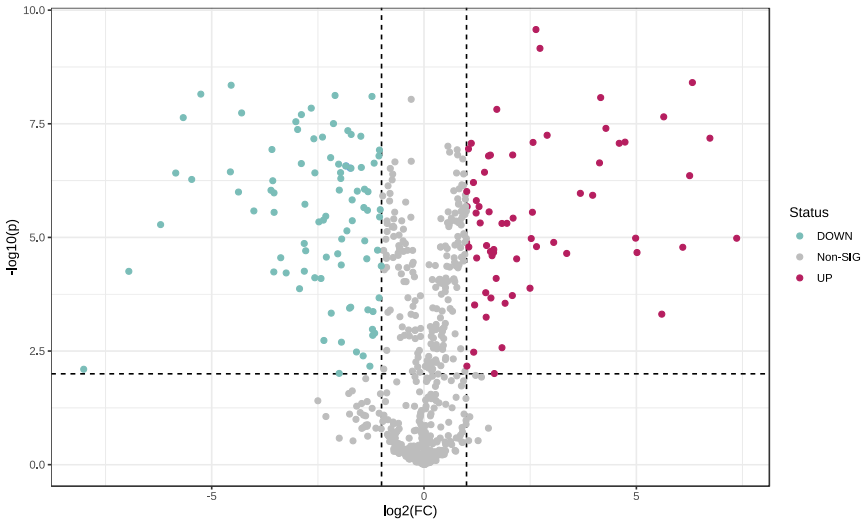

Figure 30. Volcano plot of blue 16/8h light/dark cycle against blue 24h light in the biomass (p-value < 0.01). 64 features were upregulated and 90 were downregulated on the 24h of white light condition, while 478 were non-significant.

Table 14. Features with the lowest raw p-value from the comparison between blue 16/8h light/dark cycle against blue 24h light in the biomass.

m/z	RT	FC	p-value	Prevalent condition
587.2862	5.50 min	6.2181	2.67E-10	Blue (24h light)
945.452	3.78 min	6.6355	6.92E-10	Blue (24h light)
575.2816	3.99 min	79.907	3.92E-09	Blue (24h light)
762.421	6.30 min	0.042919	4.49E-09	Blue (16/8h light/dark)
735.3736	7.67 min	0.026154	7.03E-09	Blue (16/8h light/dark)
475.3254	3.99 min	0.234	7.53E-09	Blue (16/8h light/dark)
710.5925	12.39 min	0.42775	7.90E-09	Blue (16/8h light/dark)
824.4035	4.01 min	17.872	8.38E-09	Blue (24h light)
674.3722	4.13 min	0.15869	1.43E-08	Blue (16/8h light/dark)
344.2544	3.95 min	3.2795	1.52E-08	Blue (24h light)
436.2332	6.55 min	0.050928	1.82E-08	Blue (16/8h light/dark)
394.2225	5.97 min	0.13515	1.99E-08	Blue (16/8h light/dark)

546.7628	3.95 min	50.045	2.22E-08	Blue (24h light)
1120.5993	6.97 min	0.019629	2.31E-08	Blue (16/8h light/dark)
399.1778	5.97 min	0.12343	2.84E-08	Blue (16/8h light/dark)
579.2809	10.75 min	0.22809	3.13E-08	Blue (16/8h light/dark)
895.4404	4.23 min	19.472	3.98E-08	Blue (24h light)
760.3689	7.27 min	0.12701	4.22E-08	Blue (16/8h light/dark)
619.7969	4.58 min	0.2885	4.48E-08	Blue (16/8h light/dark)
788.6034	12.29 min	0.30455	5.44E-08	Blue (16/8h light/dark)

The final comparison done, between photoperiods in the red light, disclosed 155 upregulated and 82 downregulated features in the 24h of red light (Figure 31). In the 20 most significant, there was also a predominance of features in the 24h of red light (Table 15).

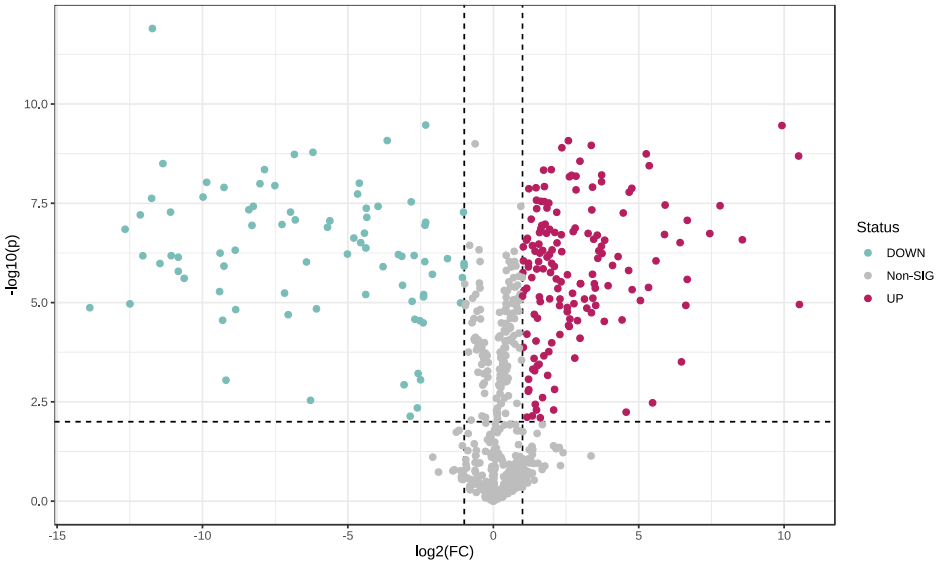

Figure 31. Volcano plot of red 16/8h light/dark cycle against red 24h light in the biomass (p-value < 0.01). 155 features were upregulated and 82 were downregulated on the 24h of white light condition, while 417 were non-significant.

Table 15. Features with the lowest raw p-value from the comparison between red 16/8h light/dark cycle against red 24h light in the biomass.

m/z	RT	FC	p-value	Prevalent condition
726.4034	4.12 min	0.00029579	1.26E-12	Red (16/8h light/dark)
890.579	13.38 min	0.19956	3.38E-10	Red (16/8h light/dark)
481.3098	11.14 min	971.53	3.48E-10	Red (24h light)
906.5374	11.31 min	0.079733	8.33E-10	Red (16/8h light/dark)
788.6031	11.76 min	5.9817	8.40E-10	Red (24h light)
654.4938	10.88 min	10.331	1.10E-09	Red (24h light)
653.5825	11.88 min	5.1247	1.26E-09	Red (24h light)
735.3736	7.67 min	0.013603	1.65E-09	Red (16/8h light/dark)
329.2687	10.02 min	38.291	1.80E-09	Red (24h light)

441.1885	6.54 min	0.0087191	1.86E-09	Red (16/8h light/dark)
1003.6171	10.02 min	1446.2	2.04E-09	Red (24h light)
579.2809	10.74 min	7.8851	2.75E-09	Red (24h light)
945.4525	3.77 min	0.00037984	3.17E-09	Red (16/8h light/dark)
534.3638	10.31 min	41.104	3.58E-09	Red (24h light)
344.2545	3.95 min	0.004282	4.48E-09	Red (16/8h light/dark)
457.2795	8.28 min	3.9804	4.51E-09	Red (24h light)
897.0765	7.87 min	3.3177	4.63E-09	Red (24h light)
313.2738	10.42 min	13.225	6.13E-09	Red (24h light)
762.6244	12.50 min	6.4527	6.24E-09	Red (24h light)
656.5092	10.75 min	7.1706	6.56E-09	Red (24h light)

This metabolomic analysis of biomass extracts of *Leptothoe* sp. LEGE 181152 was mainly in agreement with the observed for the culture medium in extracts. Once again, blue, and red light seem to have a more pronounced effect on the modulation of the metabolome of the strain. The continuous light also has a larger effect than the light/dark cycle. However, this effect was not as noticeable in the biomass as in the culture medium, and there was a more balanced distribution of the significant features.

c) Metabolomic analysis of culture medium and biomass extracts with GNPS

Feature-based molecular networks for the culture medium and biomass were constructed on GNPS (78). These rely on processed spectral information (obtained, per example, with MZmine), allowing spectral annotation, isomers characterization and quantitative analysis (78). These can be further enhanced with MolNetEnhancer (85), by joining tools such as the DEREPLICATOR (annotation of peptidic NPs) (81), MS2LDA (unsupervised substructure discovery) (84), NAP (propagation of structural annotations) (82) and CLASSYFIRE (automated chemical classification) (86). The visualization of the enhanced feature-based molecular networks was done through Cytoscape 3.9.1 (87).

In the culture medium, clusters belonging to multiple superclasses were detected: benzenoids, organic nitrogen compounds, organic oxygen compounds, organic acids and derivatives, organoheterocyclic compounds, phenylpropanoids and polyketides and lipids and lipid-like molecules (Figure 32).

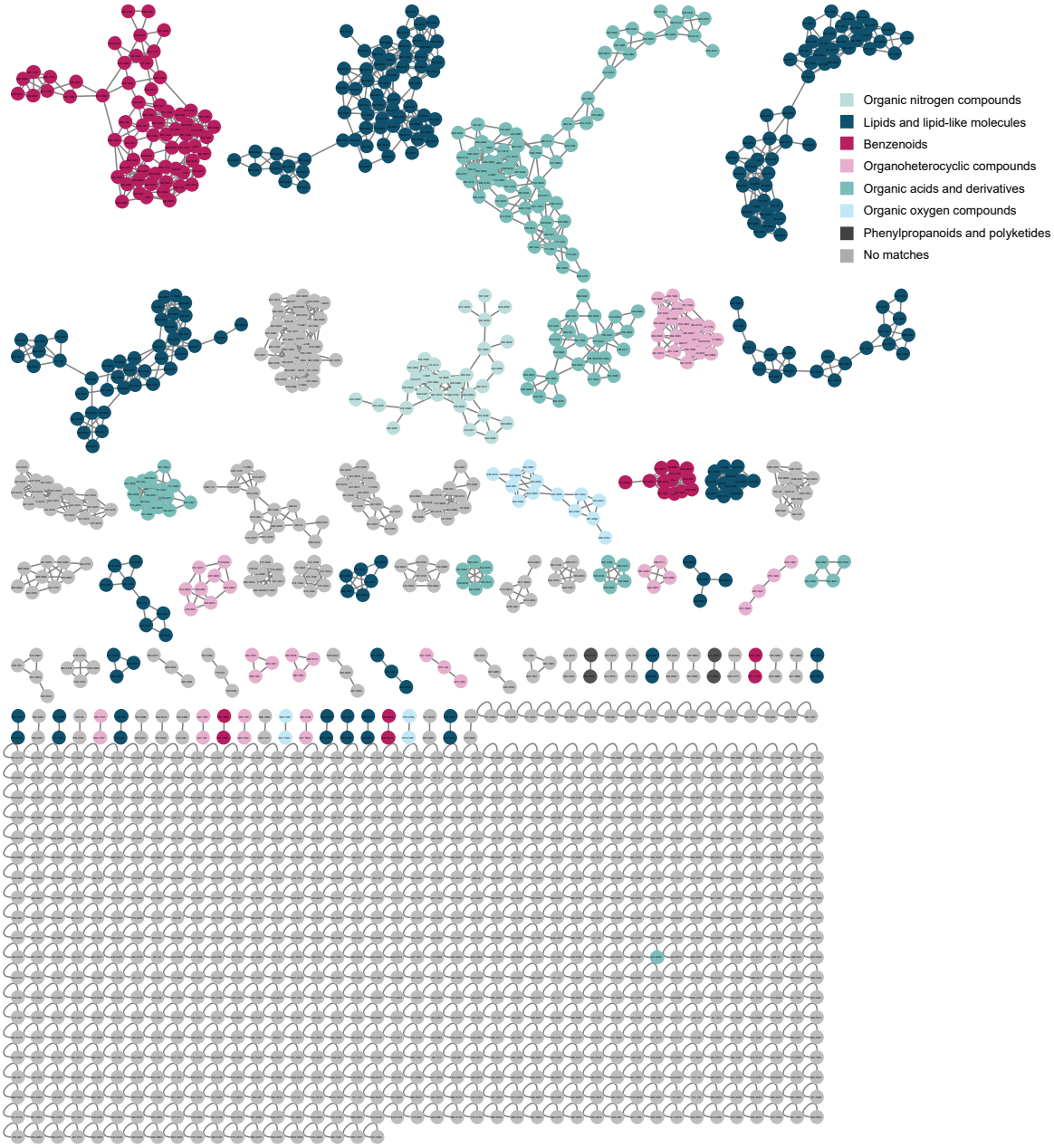

Figure 32. Feature-based molecular network of the culture medium of *Leptothoe* sp. LEGE 181152 enhanced with MolNetEnhancer (including NAP, DEREPLICATOR and MS2LDA MotifDB).

During this analysis, and examination of the LC-MS/MS data, a potential new group of halogenated compounds captured attention. This is especially interesting as two groups of halogenated compounds (leptochelins and phormidolides) have already been isolated from this strain. These compounds seem to be predominant in the blue light conditions, as demonstrated by the color distribution of the molecular network cluster (Figure 33). Moreover, in the one-way ANOVA analysis done between the different continuous light conditions, *m/z* 875.0852 was upregulated in the 24h of blue light condition (Table 7). No superclass was attributed to this cluster and no hits were obtained in GNPS for any of its features. Manual annotation of the features of this cluster with The Natural Products Altas and the Dictionary of Natural Products also did not produce any hits, pointing to this representing a new group of compounds.

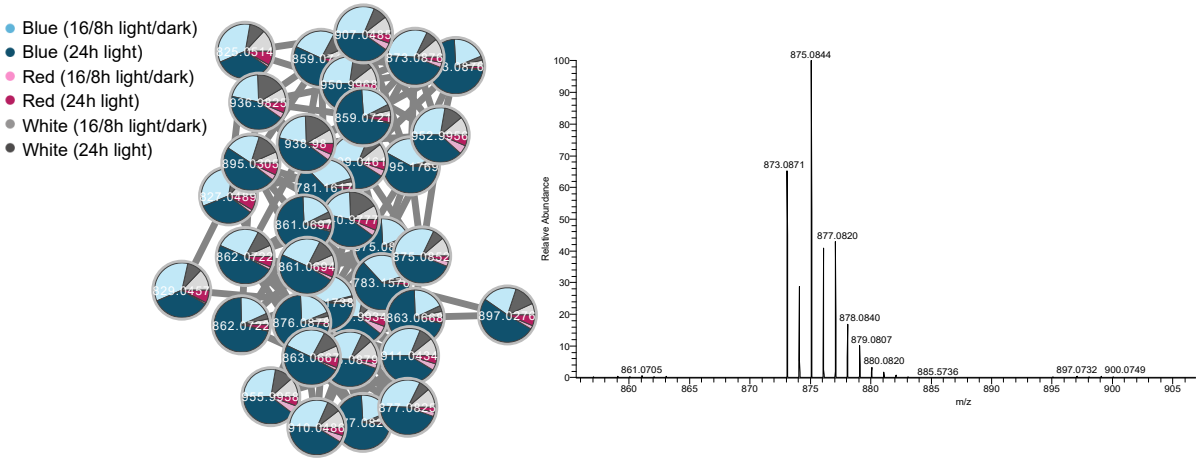

Figure 33. On the left, cluster obtained with GNPS feature-based molecular networking enhanced with MolNetEnhancer, representing a possibly new group of halogenated compounds. On the right, MS spectrum of *m/z* 875.0852, displaying a typical isotopic pattern (M+2, M+4) of compounds bearing multiple Br or Cl atoms.

In the biomass, all the previously mentioned superclasses were detected (organic nitrogen compounds, organic oxygen compounds, organic acids and derivatives, organoheterocyclic compounds, phenylpropanoids and polyketides and lipids and lipid-like molecules), with the exception of benzenoids (Figure 34).

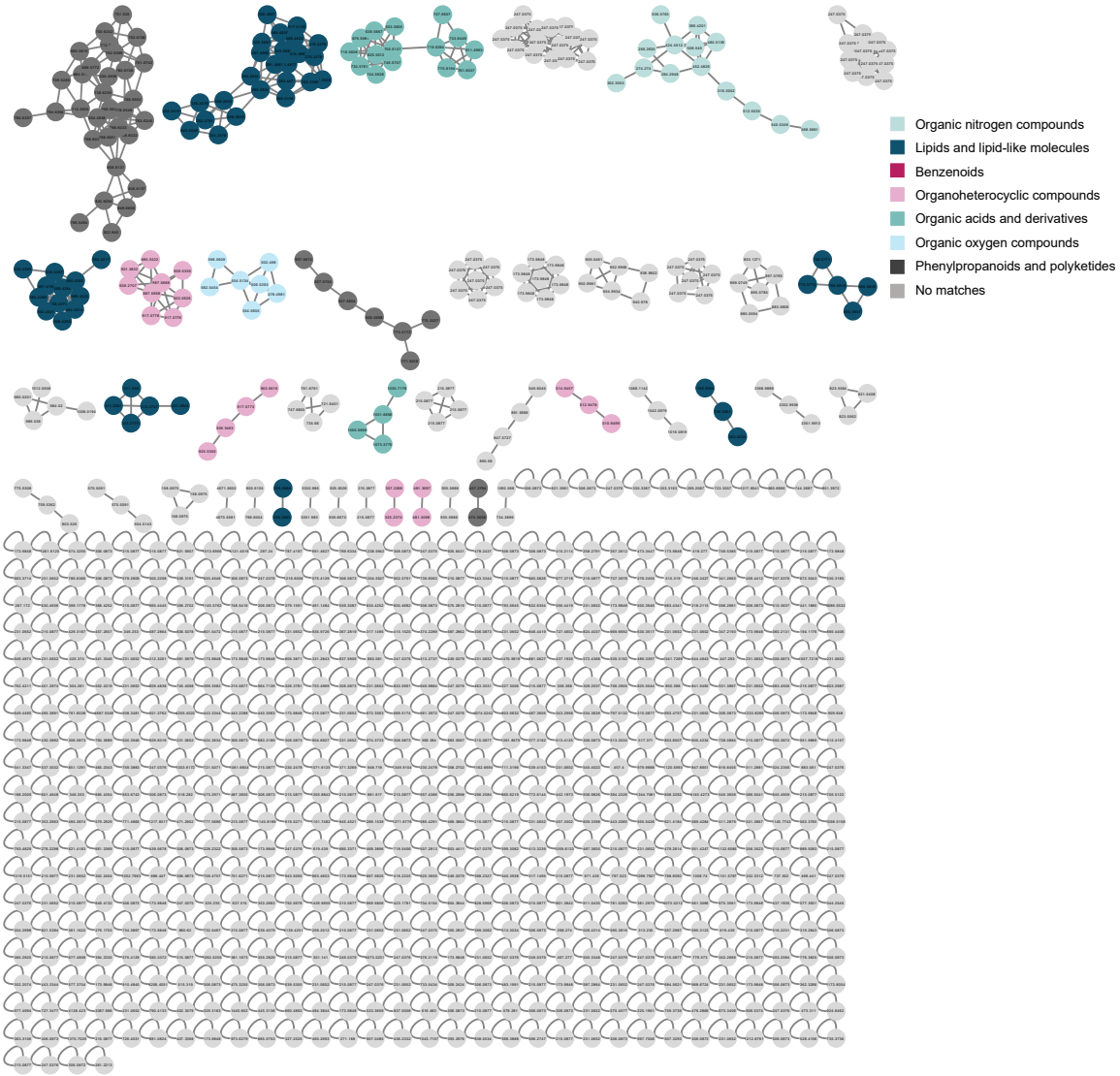

Figure 34. Feature-based molecular network of the biomass of *Leptothoe* sp. LEGE 181152 enhanced with MolNetEnhancer (including NAP, DEREPLICATOR and MS2LDA MotifDB).

As shown before, neither the biomass, nor the culture medium extracts presented the expected cytotoxic activity (Figure 21). Leptochelins are present in both biomass and culture medium, with lusichelin A being especially upregulated in the culture medium of the white continuous light condition and lusichelin D on the 24h of red light condition. Phormidolides are also present in the biomass extracts. Still, the lack of cytotoxicity could be due to these compounds being in concentrations that are too low to exert activity.

To discover a possible cause for the bioactivity detected in the anti-settlement assays, a classic molecular network was created between the bioactive conditions (red 16/8h light/dark cycle and 24h) and all the other conditions, which were not bioactive (Table A2.3, appendix 2). This molecular network did not reveal any cluster exclusive of the bioactive conditions, so no apparent cause for the bioactivity could be determined. It is possible that it a matter of concentration, where the active compounds could be in higher concentration in these conditions, but still present in the others, or a joint effect of the

mixture of molecules present in the extracts. To fully understand this, though, a bioactivity-guided fractionation of the extracts would be necessary.

4. Conclusion

In this work, OSMaC strategies were employed to (1) understand how variating iron and copper concentrations alter lusichelin production on *Lusitaniella coriacea* LEGE 01767 and (2) modulate the metabolome and possibly induce expression of cryptic/silent BGCs in *Leptothoe* sp. LEGE 181152.

Lusitaniella coriacea LEGE 01767 was cultivated for 30 days under iron-limited and iron-depleted conditions, as well as with different concentrations of copper. LC-MS/MS data from the culture medium and biomass extracts were analyzed to relatively quantify lusichelins. The first observation from this assay was that cultures from the 200 and 450 nM of $CuSO_4$ conditions were visibly different from what is usual in standard culture conditions and grew less. This seems to indicate that these concentrations present some toxicity for the strain.

Regarding lusichelin production, unexpectedly, it did not increase in iron-limited and iron-depleted conditions. In fact, the *m/z* of these compounds was detected in higher amounts on standard culture conditions (Z8-TM). These results show that even though lusichelin **5** was thought to be a siderophore, its biological purpose is probably not iron chelation. It is possible that one of the many trace elements present in the TM is inducing this production, probably through the MerR-like transcription factor. Further experiments will be designed to reveal its true biological role and address the regulation of its biosynthesis. Additionally, a potentially new compound with the same exact mass as lusichelin **5** was identified in the culture medium of the 200 and 450 nM of $CuSO_4$ conditions.

To modulate its metabolome and induce expression of silent/cryptic BGCs, *Leptothoe* sp. LEGE 181152 was grown under different culture conditions. Firstly, it was cultivated for 30 days under presence/absence of iron and various copper concentrations. However, none of the cultures from Z8-NaCl conditions survived the 30 day-period, indicating that one or more of the trace elements present in TM is essential to the strain's metabolism.

Then, *Leptothoe* sp. LEGE 181152 was cultivated under white, red, and blue light, and two photoperiods: 16/8h light/dark cycle and 24h of continuous light. Metabolomic analysis demonstrated major modulation of the metabolome in the different conditions. The blue and red light seemed to cause more changes in the metabolome than the white light and continuous light also induced the production of more metabolites than the 16/8h light/dark cycle.

Extracts prevenient from this photobioreactors assay were also tested for anticancer, anti-settlement and antibacterial activity. No activity was detected in anticancer and antibacterial activity assays, but biomass extracts of red light conditions presented anti-settlement activity. No apparent cause for this bioactivity has been detected yet.

Finally, a potential new group of halogenated compounds was identified, mainly in the blue light conditions. No compound could yet be linked to the putative cryptic/silent BGC identified during the bioinformatic analysis. However, it is possible that in the large array of significant features present in the various light conditions more novel compounds are present. In the future, efforts will be made to identify, isolate them, and possibly attribute a NP to the cryptic/silent BGC. Ultimately, employing OSMaC strategies on both strains showed that their biosynthetic potential can be modulated through manipulation of culture conditions. This altered the levels of expression of various metabolites and induced the production of different ones, with some of them possibly representing new natural products.

5. Future work

The findings presented in this study raised noteworthy questions that will be addressed in future experiments. In *Lusitaniella coriacea* LEGE 07167, it would be interesting to test a larger array of copper concentrations and perform additional tests, such as quantification of chlorophyl levels, that could enlighten the potential toxicity of $CuSO_4$. As the actual biological purpose of lusichelin production still has not been unveiled, it would be useful to test the effect of other heavy metals. Zinc would be particularly interesting, given the ZurR binding domain present in the BGC. To uncover the role of the MerR-like transcription factor, also present in the BGC, measurement of its expression (through qRT-PCR) in the different conditions will be carried out. As the metabolomic analysis done for this strain was focused only on lusichelins, it would be interesting to also perform an untargeted metabolomic analysis, evaluating the effect of iron and copper in the whole metabolome.

In *Leptothoe* sp. LEGE 181152, the most urgent work will be the isolation of the putative new group of halogenated compounds. The identification, and posterior isolation and elucidation of chemical structure, of other possible new compounds present in the extracts is also imperative. This can potentially lead to the linking of one of these compounds to the cryptic/silent BGC identified in this study. Moreover, it would be of interest to perform a bioactivity-guided fractionation of the biomass extracts of the red light conditions, to uncover the cause of the bioactivity in the anti-settlement assays. Finally, understanding why the continuous light provoked more modulation of the metabolome can also constitute a future endeavor.

Appendix 1

Table A1.1. Secondary metabolites regions identified by AntiSMASH 7.0 in the assembly genome of *Lusitaniella coriacea* LEGE 07167.

Region	Type	From	To	Most similar known cluster	Similarity
1.1	RRE-containing	2,331,835	2,352,119	-	-
1.2	terpene	3,110,536	3,129,925	-	-
1.3	terpene	3,290,594	3,308,539	-	-
1.4	terpene	3,923,163	3,943,984	-	-
1.5	NRPS,NRPS-like	4,324,068	4,378,211	-	-
2.1	NRP-metallophore, NRPS,T1PKS	16,772	91,061	anachelin	NRP + Polyketide (35%)

Table A1.2. Putative function of genes present in the putative lusichelin BGC, through AntiSMASH 7.0 and BlastP.

AntiSMASH 7.0		BlastP		
Identifier	**Function**	**Best hit description**	**Identity %**	**Query cover %**
ctg2_16	Other	heavy metal translocating P-type ATPase [*Calothrix parasitica*]	67%	99%
ctg2_17	Transport	MFS transporter [*Roseofilum* sp. BLCC_M143]	86.91%	98%
ctg2_18	Transport	ABC transporter ATP-binding protein [*Roseofilum* sp. SID3]	83.16%	99%
ctg2_19	Transport	ABC transporter ATP-binding protein [*Roseofilum* sp. BLCC_M143]	90.14%	100%
ctg2_20	Transport	nickel resistance protein [*Rivularia* sp. IAM M-261]	61.41%	100%
ctg2_21	Regulatory	precorrin-8X methylmutase [*Roseofilum* sp. BLCC_M143]	83%	99%
ctg2_22	Other	heavy metal translocating P-type ATPase [*Roseofilum* sp. BLCC_M143]	89.24%	100%
ctg2_23	Transport	TonB-dependent receptor [*Roseofilum* sp. SID2]	78.34%	100%
ctg2_24	Biosynthetic (additional)	benzoate-CoA ligase family protein [*Roseofilum* sp. BLCC_M143]	85.58%	100%
ctg2_25	Other	4'-phosphopantetheinyl transferase superfamily protein [*Roseofilum* sp. SID3]	84.21%	100%
ctg2_26	Biosynthetic (additional)	phosphopantetheine-binding protein [*Roseofilum* sp. BLCC_M143]	88.10%	100%
ctg2_27	Regulatory	AraC family transcriptional regulator [*Roseofilum* sp. BLCC_M143]	87.28%	99%
ctg2_28	Other	class I SAM-dependent methyltransferase [*Roseofilum* sp. Belize Diploria]	74.62%	99%
ctg2_29	Biosynthetic	chorismate-binding protein [*Roseofilum* sp. SID3]	84.81%	99%
ctg2_30	Other	hypothetical protein [*Roseofilum* sp. Belize Diploria]	81.30%	97%
ctg2_31	Biosynthetic (additional)	3-oxoacyl-ACP synthase [*Roseofilum* sp. SID3]	82.66%	98%
ctg2_32	Biosynthetic	amino acid adenylation domain-containing protein [*Roseofilum* sp. BLCC_M143]	85.32%	100%
ctg2_33	Biosynthetic	SDR family NAD(P)-dependent oxidoreductase [*Roseofilum* sp. SID3]	81.17%	99%
ctg2_34	Biosynthetic	amino acid adenylation domain-containing protein [*Roseofilum* sp. BLCC_M143]	84.05%	99%
ctg2_35	Biosynthetic	amino acid adenylation domain-containing protein [*Roseofilum* sp. SID3]	87.75%	99%
ctg2_36	Biosynthetic	SDR family NAD(P)-dependent oxidoreductase [*Roseofilum* sp. Belize Diploria]	86.03%	100%
ctg2_37	Biosynthetic	amino acid adenylation domain-containing protein [*Roseofilum* sp. Belize Diploria]	84.60%	99%
ctg2_38	Other	PEP-CTERM sorting domain-containing protein [*Roseofilum* sp. BLCC_M143]	79.55%	97%
ctg2_39	Biosynthetic (additional)	cytochrome P450 [*Microcoleus* sp. PH2017_10_PVI_O_A]	94.22%	100%
ctg2_40	Biosynthetic (additional)	thioesterase [*Microcoleus* sp. PH2017_10_PVI_O_A]	91.94%	98%
ctg2_41	Other	MULTISPECIES: hypothetical protein [*Kamptonema*]	70.37%	83%
ctg2_42	Other	tyrosine-type recombinase/integrase [*Symplocastrum torsivum* CPER-KK1]	75.08%	100%
ctg2_43	Regulatory	Tetratricopeptide [*Lyngbya* sp. PCC 8106]	57.84%	95%
ctg2_44	Other	type II toxin-antitoxin system HicB family antitoxin [*Lusitaniella coriacea*]	97.14%	100%
ctg2_45	Other	type II toxin-antitoxin system RelE/ParE family toxin [*Lusitaniella coriacea*]	100%	100%
ctg2_46	Other	XRE family transcriptional regulator [*Lusitaniella coriacea*]	97.06%	100%
ctg2_47	Other	hypothetical protein [*Lusitaniella coriacea*]	97.53%	100%
ctg2_48	Other	XisI protein [*Symploca* sp. SIO2D2]	85.59%	100%
ctg2_49	Other	fatty-acid oxidation protein subunit alpha [*Symploca* sp. SIO2D2]	83.94%	98%
ctg2_50	Regulatory	hybrid sensor histidine kinase/response regulator [*Limnospira fusiformis*]	53.61%	97%
ctg2_51	Regulatory	response regulator transcription factor [*Gloeobacter violaceus*]	50%	99%
ctg2_52	Regulatory	response regulator [*Phormidium*] sp. ETS-05]	42.70%	51%
ctg2_53	Other	hypothetical protein [*Laspinema* sp. D3a]	77%	73.56%
ctg2_54	Other	hypothetical protein [*Symploca* sp. SIO2D2]	57.85%	79%

Table A1.3. Data used for the relative quantification of lusichelins 1-5 and 5-Fe in the biomass of the different tested conditions: EIC area, retention time and *m/z* $[M+H]^+$.

Condition	Compound	Replicates	*m/z* $[M+H]^+$	Average m/z	Retention time	Average retention time	EIC area	Average EIC area	Standard deviation
TM $FeCl_3$(+) 5 nM $CuSO_4$	1/2	A	559.0946	559.0945	9.85	9.85	8.67E+09	1.02E+10	1.54E+09
		B	559.0945		9.85		1.17E+10		
		C	559.0945		9.86		1.01E+10		
	3/4	A	577.1057	577.1058	9.26	9.26	3.81E+08	2.76E+08	1.93E+08
		B	577.1058		9.26		5.29E+07		
		C	577.1058		9.26		3.95E+08		
	5	A	545.0790	545.0790	9.03	9.04	5.45E+09	4.62E+09	1.20E+09
		B	545.0791		9.04		3.24E+09		
		C	545.079		9.04		5.17E+09		
	5-Fe	A	597.9906	597.9906	4.23	4.23	4.68E+08	4.68E+08	8.67E+07
		B	597.9906		4.24		3.81E+08		
		C	597.9905		4.23		5.54E+08		
NaCl $FeCl_3$(-) 0 nM $CuSO_4$	1/2	A	559.0945	559.0946	9.85	9.85	7.38E+09	5.92E+09	1.74E+09
		B	559.0947		9.85		4.00E+09		
		C	559.0946		9.85		6.39E+09		
	3/4	A	577.1061	577.1063	9.27	9.26	2.29E+08	1.47E+08	7.75E+07
		B	577.1066		9.26		7.57E+07		
		C	577.1062		9.26		1.35E+08		
	5	A	545.0791	545.0792	9.03	9.04	2.28E+09	1.46E+09	1.15E+09
		B	545.0793		9.04		6.51E+08		
		C	545.0792		9.04		9.34E+08		
	5-Fe	A	597.9908	597.9908	4.22	4.23	1.87E+08	1.24E+08	5.98E+07
		B	597.9908		4.23		6.74E+07		
		C	597.9908		4.23		1.18E+08		
NaCl $FeCl_3$(-) 5 nM $CuSO_4$	1/2	A	559.0947	559.0947	9.86	9.86	3.25E+09	4.08E+09	7.48E+08
		B	559.0947		9.87		4.28E+09		
		C	559.0947		9.85		4.70E+09		
	3/4	A	577.1064	577.1063	9.26	9.26	7.29E+07	9.15E+07	1.74E+07
		B	577.1063		9.26		9.41E+07		
		C	577.1063		9.26		1.07E+08		
	5	A	545.079	545.0792	9.05	9.04	1.89E+09	1.31E+09	7.74E+08
		B	545.0794		9.04		4.33E+08		
		C	545.0792		9.03		1.62E+09		
	5-Fe	A	597.9909	597.9908	4.24	4.23	1.31E+08	1.27E+08	5.63E+07
		B	597.9909		4.23		6.86E+07		
		C	597.9907		4.23		1.81E+08		
NaCl $FeCl_3$(-) 200 nM $CuSO_4$	1/2	A	559.0956	559.0956	9.84	9.84	1.03E+08	1.33E+08	9.53E+07
		B	559.0954		9.84		2.40E+08		
		C	559.0957		9.84		5.63E+07		
	3/4	A	577.107	577.1068	9.24	9.24	5.01E+05	5.65E+05	3.49E+05
		B	577.1065		9.24		9.41E+05		
		C	577.1069		9.24		2.53E+05		
	5	A	545.0798	545.0800	8.91	8.91	1.83E+08	1.33E+08	6.72E+07
		B	545.08		8.9		1.59E+08		
		C	545.0801		8.91		5.66E+07		
	5-Fe	A	597.9919	597.9918	4.15	4.16	2.06E+06	1.75E+06	4.38E+05
		B	597.9916		4.14		1.94E+06		
		C	597.9918		4.18		1.25E+06		
NaCl $FeCl_3$(-) 450 nM $CuSO_4$	1/2	A	559.0958	559.0960	9.84	9.84	2.18E+07	1.33E+07	7.71E+06
		B	559.0959		9.84		1.14E+07		
		C	559.0963		9.84		6.73E+06		
	3/4	A	-	-	-	-	0.00E+00	0.00E+00	0.00E+00
		B	-		-		0.00E+00		
		C	-		-		0.00E+00		
	5	A	545.0802	545.0802	8.91	8.90	1.10E+08	1.06E+08	7.52E+06
		B	545.0803		8.9		1.11E+08		
		C	545.0802		8.89		9.73E+07		
	5-Fe	A	597.9917	597.9914	4.15	4.13	9.66E+05	8.19E+05	3.38E+05
		B	597.9912		4.12		4.33E+05		
		C	597.9913		4.13		1.06E+06		
NaCl $FeCl_3$(+) 0 nM $CuSO_4$	1/2	A	559.0947	559.0946	9.85	9.86	1.45E+10	8.90E+09	4.91E+09
		B	559.0947		9.86		6.98E+09		
		C	559.0945		9.86		5.25E+09		
	3/4	A	577.1058	577.1061	9.27	9.27	8.97E+08	4.14E+08	4.22E+08
		B	577.106		9.27		2.29E+08		
		C	577.1065		9.27		1.16E+08		
	5	A	545.0790	545.0791	9.04	9.04	2.93E+09	2.02E+09	1.07E+09
		B	545.0793		9.05		8.44E+08		
		C	545.0791		9.04		2.29E+09		
	5-Fe	A	597.9907	597.9908	4.22	4.23	3.01E+08	2.25E+08	1.17E+08
		B	597.9910		4.24		9.01E+07		
		C	597.9907		4.24		2.84E+08		
NaCl $FeCl_3$(+) 5 nM $CuSO_4$	1/2	A	559.0947	559.0947	9.86	9.86	7.22E+09	7.49E+09	3.73E+09
		B	559.0947		9.86		3.91E+09		

		C	559.0947		9.85		1.13E+10		
	3/4	A	577.1062	577.1062	9.26	9.27	1.91E+08	2.49E+08	2.13E+08
		B	577.1066		9.27		7.19E+07		
		C	577.1059		9.27		4.86E+08		
	5	A	545.0792	545.0792	9.04	9.04	1.03E+09	1.10E+09	2.43E+08
		B	545.0793		9.04		9.08E+08		
		C	545.0792		9.05		1.37E+09		
	5-Fe	A	597.9908	597.9909	4.24	4.24	1.45E+08	1.25E+08	4.47E+07
		B	597.9909		4.24		7.40E+07		
		C	597.9909		4.24		1.57E+08		
NaCl $FeCl_3$(+) 200 nM $CuSO_4$	1/2	A	559.0954	559.0954	9.85	9.84	1.65E+08	2.27E+08	1.82E+08
		B	559.0956		9.84		8.39E+07		
		C	559.0952		9.83		4.31E+08		
	3/4	A	577.1069	577.1068	9.23	9.24	9.99E+05	1.62E+06	1.27E+06
		B	577.106		9.25		7.71E+05		
		C	577.1075		9.24		3.08E+06		
	5	A	545.0798	545.0801	8.9	8.90	1.10E+08	9.77E+07	3.80E+07
		B	545.0804		8.9		5.52E+07		
		C	545.08		8.91		1.28E+08		
	5-Fe	A	597.9916	597.9917	4.16	4.16	2.80E+06	2.22E+06	1.14E+06
		B	597.9918		4.15		8.98E+05		
		C	597.9916		4.16		2.95E+06		
NaCl $FeCl_3$(+) 450 nM $CuSO_4$	1/2	A	559.0957	559.0957	9.83	9.83	3.25E+07	6.54E+07	5.66E+07
		B	559.0958		9.84		3.30E+07		
		C	559.0956		9.83		1.31E+08		
	3/4	A	577.1065	577.1065	9.25	9.24	1.48E+05	1.77E+05	1.94E+05
		B	-		-		0.00E+00		
		C	577.1064		9.23		3.84E+05		
	5	A	545.0802	545.0800	8.9	8.90	1.48E+08	1.79E+08	1.78E+08
		B	545.0799		8.9		1.87E+07		
		C	545.0798		8.9		3.70E+08		
	5-Fe	A	597.9915	597.9917	4.15	4.14	8.67E+05	5.26E+05	3.04E+05
		B	597.991		4.15		4.33E+05		
		C	597.9927		4.13		2.80E+05		
TM $FeCl_3$(-)	1/2	A	559.0947	559.0947	9.86	9.86	9.54E+09	8.05E+09	2.00E+09
		B	559.0945		9.86		8.82E+09		
		C	559.0948		9.86		5.77E+09		
	3/4	A	577.1057	577.1058	9.26	9.26	3.69E+08	3.05E+08	1.08E+08
		B	577.1057		9.27		3.66E+08		
		C	577.106		9.26		1.79E+08		
	5	A	545.0791	545.0790	9.04	9.05	6.36E+09	6.29E+09	1.11E+09
		B	545.079		9.05		7.37E+09		
		C	545.079		9.05		5.15E+09		
	5-Fe	A	597.9907	597.9907	4.23	4.23	6.00E+08	5.68E+08	8.58E+07
		B	597.9907		4.24		6.34E+08		
		C	597.9907		4.23		4.71E+08		

Table A1.4 Data used for the relative quantification of lusichelins 1-5 and 5-Fe in the biomass of the different tested conditions: EIC area, retention time and *m/z* $[M+H]^+$.

Condition	Compound	Replicates	*m/z* $[M+H]^+$	Average m/z	Retention time	Average retention time	Peak area integration	Average area	Standard deviation
TM $FeCl_3$(+) 5 nM $CuSO_4$	1/2	A	559.0953	559.0955	9.87	9.87	2.31E+08	2.31E+08	1.78E+08
		B	559.0957		9.87		5.74E+07		
		C	559.0955		9.86		4.04E+08		
	3/4	A	577.1067	577.1061	9.25	9.26	1.94E+06	2.06E+06	2.13E+06
		B	-		-		0.00E+00		
		C	577.1054		9.26		4.25E+06		
	5	A	545.0792	545.0793	9.04	9.05	5.24E+09	5.26E+09	3.74E+09
		B	545.0795		9.05		1.53E+09		
		C	545.0793		9.05		9.01E+09		
	5-Fe	A	597.9908	597.9910	4.26	4.27	2.20E+08	2.07E+08	1.57E+08
		B	597.9913		4.27		4.41E+07		
		C	597.9910		4.27		3.57E+08		
NaCl $FeCl_3$(-) 0 nM $CuSO_4$	1/2	A	559.0954	559.0953	9.87	9.87	1.24E+08	4.47E+08	2.82E+08
		B	559.0952		9.87		5.78E+08		
		C	559.0953		9.87		6.40E+08		
	3/4	A	577.1063	577.1065	9.24	9.25	7.18E+05	2.51E+06	3.23E+06
		B	577.1062		9.25		6.24E+06		
		C	577.1069		9.26		5.87E+05		
	5	A	545.0794	545.0794	9.04	9.05	1.94E+09	2.70E+09	1.08E+09
		B	545.0794		9.05		3.47E+09		
		C	545.0794		9.05		4.95E+09		
	5-Fe	A	597.9912	597.9913	4.27	4.28	6.05E+07	8.54E+07	4.54E+07
		B	597.9914		4.28		5.78E+07		
		C	597.9912		4.28		1.38E+08		

NaCl $FeCl_3$(-) 5 nM $CuSO_4$	1/2	A	559.0958	559.0957	9.76	9.76	8.99E+07	1.51E+08	1.02E+08
		B	559.0953		9.76		2.69E+08		
		C	559.0961		9.75		9.55E+07		
	3/4	A	577.1069	577.1063	9.28	9.27	7.23E+05	9.77E+05	1.13E+06
		B	577.1056		9.25		2.21E+06		
		C					0.00E+00		
	5	A	545.0794	545.0794	9.04	9.04	1.93E+09	2.66E+09	8.24E+08
		B	545.0794		9.04		2.50E+09		
		C	545.0793		9.05		3.56E+09		
	5-Fe	A	597.9915	597.9915	4.28	4.28	5.72E+07	8.93E+07	9.50E+07
		B	597.9919		4.28		1.45E+07		
		C	597.9911		4.27		1.96E+08		
NaCl $FeCl_3$(-) 200 nM $CuSO_4$	1/2	A	-	-	-	-	0.00E+00	0.00E+00	0.00E+00
		B	-		-		0.00E+00		
		C	-		-		0.00E+00		
	3/4	A	-	-	-	-	0.00E+00	0.00E+00	0.00E+00
		B	-		-		0.00E+00		
		C	-		-		0.00E+00		
	5	A	-	-	-	-	0.00E+00	0.00E+00	0.00E+00
		B	-		-		0.00E+00		
		C	-		-		0.00E+00		
	5-Fe	A	-	-	-	-	0.00E+00	0.00E+00	0.00E+00
		B	-		-		0.00E+00		
		C	-		-		0.00E+00		
NaCl $FeCl_3$(-) 450 nM $CuSO_4$	1/2	A	-	-	-	-	0.00E+00	0.00E+00	0.00E+00
		B	-		-		0.00E+00		
		C	-		-		0.00E+00		
	3/4	A	-	-	-	-	0.00E+00	0.00E+00	0.00E+00
		B	-		-		0.00E+00		
		C	-		-		0.00E+00		
	5	A	-	-	-	-	0.00E+00	0.00E+00	0.00E+00
		B	-		-		0.00E+00		
		C	-		-		0.00E+00		
	5-Fe	A	-	-	-	-	0.00E+00	0.00E+00	0.00E+00
		B	-		-		0.00E+00		
		C	-		-		0.00E+00		
NaCl $FeCl_3$(+) 0 nM $CuSO_4$	1/2	A	559.0953	559.0957	9.87	9.86	6.77E+08	2.77E+08	3.46E+08
		B	559.0958		9.86		8.42E+07		
		C	559.0960		9.86		7.06E+07		
	3/4	A	577.1079	577.1077	9.27	9.26	3.80E+06	1.33E+06	2.14E+06
		B	577.1074		9.25		1.92E+05		
		C	-		-		0.00E+00		
	5	A	545.0794	545.0796	9.04	9.03	4.07E+09	3.27E+09	2.82E+09
		B	545.0800		9.01		1.32E+08		
		C	545.0793		9.04		5.60E+09		
	5-Fe	A	597.9916	597.9914	4.29	4.29	4.98E+07	9.92E+07	1.31E+08
		B	-		-		0.00E+00		
		C	597.9911		4.28		2.48E+08		
NaCl $FeCl_3$(+) 5 nM $CuSO_4$	1/2	A	559.0953	559.0955	9.86	9.87	4.20E+08	2.29E+08	1.65E+08
		B	559.0955		9.87		1.37E+08		
		C	559.0958		9.87		1.30E+08		
	3/4	A	577.1075	577.1069	9.25	9.27	3.82E+06	1.70E+06	1.85E+06
		B	577.1057		9.29		9.08E+05		
		C	577.1074		9.28		3.80E+05		
	5	A	545.0794	545.0794	9.05	9.05	3.03E+09	3.63E+09	1.41E+09
		B	545.0794		9.04		2.61E+09		
		C	545.0795		9.05		5.24E+09		
	5-Fe	A	597.9915	597.9914	4.28	4.28	7.12E+07	1.03E+08	3.86E+07
		B	597.9914		4.28		9.25E+07		
		C	597.9912		4.29		1.46E+08		
NaCl $FeCl_3$(+) 200 nM $CuSO_4$	1/2	A	-	-	-	-	0.00E+00	0.00E+00	0.00E+00
		B	-		-		0.00E+00		
		C	-		-		0.00E+00		
	3/4	A	-	-	-	-	0.00E+00	0.00E+00	0.00E+00
		B	-		-		0.00E+00		
		C	-		-		0.00E+00		
	5	A	-	-	-	-	0.00E+00	0.00E+00	0.00E+00
		B	-		-		0.00E+00		
		C	-		-		0.00E+00		
	5-Fe	A	-	-	-	-	0.00E+00	0.00E+00	0.00E+00
		B	-		-		0.00E+00		
		C	-		-		0.00E+00		
NaCl $FeCl_3$(+) 450 nM $CuSO_4$	1/2	A	-	-	-	-	0.00E+00	0.00E+00	0.00E+00
		B	-		-		0.00E+00		
		C	-		-		0.00E+00		
	3/4	A	-	-	-	-	0.00E+00	0.00E+00	0.00E+00
		B	-		-		0.00E+00		
		C	-		-		0.00E+00		
	5	A	-	-	-	-	0.00E+00	0.00E+00	0.00E+00
		B	-		-		0.00E+00		
		C	-		-		0.00E+00		

	5-Fe	A	-	-	-	-	0.00E+00	0.00E+00	0.00E+00
		B	-		-		0.00E+00		
		C	-		-		0.00E+00		
TM $FeCl_3$(-)	1/2	A	559.0953	559.0956	9.86	9.87	4.42E+08	1.79E+08	2.28E+08
		B	559.0958		9.87		4.52E+07		
		C	559.0956		9.88		5.01E+07		
	3/4	A	577.1058	577.1058	9.27	9.27	5.09E+06	1.70E+06	2.94E+06
		B	-		-		0.00E+00		
		C	-		-		0.00E+00		
	5	A	545.0793	545.0794	9.04	9.04	4.04E+09	2.66E+09	1.53E+09
		B	545.0795		9.03		1.02E+09		
		C	545.0793		9.04		2.92E+09		
	5-Fe	A	597.9911	597.9913	4.27	4.27	1.58E+08	1.03E+08	7.57E+07
		B	597.9917		4.27		1.66E+07		
		C	597.9911		4.27		1.35E+08		

Table A1.5 Link for the GNPS Molecular Network done between the conditions TM $FeCl_3$ (+) and NaCl $FeCl_3$ (-) 0 nM $CuSO_4$.

GNPS tool	Link of the job
Molecular Network	https://gnps.ucsd.edu/ProteoSAFe/status.jsp?task=0819c5b05d9b4143bc4d524de34767ea

Appendix 2

Table A2.1. Secondary metabolites regions identified by AntiSMASH 7.0 in the assembly genome of *Leptothoe* sp. LEGE 181152.

Region	Type	From	To	Most similar known cluster	Similarity
3.1	NRP-metallophore, NRPS,T1PKS,NRPS-like	13,093	193,772	anachelin	NRP + Polyketide (40%)
3.2	NRPS-like,T1PKS	194,016	269,031	vatiamide A/ vatiamide B/ vatiamide C/ vatiamide D/ vatiamide E/ vatiamide F	NRP + Polyketide (16%)
6.1	cyanobactin	127,163	149,271	-	-
9.1	lassopeptide	165,442	194,085	-	-
10.1	transAT-PKS,PKS-like	1,436	98,974	leptolyngbyalide	Polyketide (51%)
12.1	T1PKS,NRPS	61,044	131,299	nodularin	NRP + Polyketide (33%)
12.2	T3PKS	139,8	167,458	phormidolide	Polyketide (52%)
16.1	lanthipeptide-class-v	41,857	84,184	-	-
17.1	NRPS-like	346,988	389,067	gobichelin A / gobichelin B	NRP (11%)
17.2	NRP-metallophore, NRPS,T1PKS	603,690	671,880	anachelin	NRP + Polyketide (20%)
17.3	terpene	822,457	839,842	-	-
19.1	RiPP-like	3,287	16,379	-	-
30.1	NRPS	11,760	60,062	-	-
47.1	T3PKS	171,214	212,317	-	-
47.2	terpene	346,675	367,604	-	-
62.1	arylpolyene	111,761	152,876	-	-
66.1	lassopeptide, RPE-containing	330,151	352,901	-	-
67.1	NRPS,cyanobactin	216,336	280,335	tenuecyclamide A / tenuecyclamide C	RiPP:Cyanobactin (71%)
68.1	LAP	293,955	316,319	-	-

Table A2.2. Putative function of genes present in secondary metabolite region 17.2 of *Leptothoe* sp. LEGE 181152, through AntiSMASH 7.0 and BlastP.

AntiSMASH 7.0		BlastP		
Locus tag	**Gene type**	**Best hit description**	**Identity %**	**Query cover**
ctg17_509	Other	hypothetical protein [*Adonisia turfae*]	99.15%	100%
ctg17_510	Other	antibiotic biosynthesis monooxygenase [*Adonisia turfae*]	98.96%	100%
ctg17_511	Regulatory	AraC family transcriptional regulator [*Adonisia turfae*]	98.34%	100%
ctg17_512	Other	aspartate racemase [*Leptolyngbya* sp. PCC 7375]	97.87%	100%
ctg17_513	Other	No hit	-	-
ctg17_514	Other	NB-ARC domain-containing protein [*Adonisia turfae*]	98.77%	100%
ctg17_515	Regulatory	Crp/Fnr family transcriptional regulator [*Adonisia turfae*]	98.72%	100%
ctg17_516	Transport	MFS transporter [*Adonisia turfae*]	99.56%	85%
ctg17_517	Transport	ABC transporter ATP-binding protein [*Adonisia turfae*]	100%	100%
ctg17_518	Other	class I SAM-dependent methyltransferase [*Adonisia turfae*]	100%	100%
ctg17_519	Transport	ABC transporter ATP-binding protein [*Adonisia turfae*]	99.83%	100%
ctg17_520	Transport	MFS transporter [*Adonisia turfae*]	99.75%	100%
ctg17_521	Transport	TonB-dependent receptor [*Adonisia turfae* CCMR0081]	99.65%	100%
ctg17_522	Regulatory	AraC family transcriptional regulator [*Adonisia turfae*]	99.70%	100%
ctg17_523	Biosynthetic (additional)	phosphopantetheine-binding protein [*Adonisia turfae*]	100%	100%
ctg17_524	Other	holo-ACP synthase [*Adonisia turfae* CCMR0081]	98.66%	100%
ctg17_525	Biosynthetic (additional)	benzoate-CoA ligase family protein [*Adonisia turfae*]	99.62%	100%
ctg17_526	Biosynthetic	salicylate synthase [*Adonisia turfae*]	99.32%	100%
ctg17_527	Other	holo-ACP synthase [*Adonisia turfae*]	99.32%	100%
ctg17_528	Biosynthetic (additional)	3-oxoacyl-[acyl-carrier-protein] synthase III C-terminal domain-containing protein [*Adonisia turfae*]	99.02%	100%
ctg17_529	Biosynthetic	non-ribosomal peptide synthetase [*Adonisia turfae*]	97.54%	99%
ctg17_530	Biosynthetic	type I polyketide synthase [*Adonisia turfae*]	97.54%	99%
ctg17_531	Biosynthetic (additional)	3-hydroxyacyl-CoA dehydrogenase NAD-binding domain-containing protein [*Adonisia turfae*]	96.60%	100%
ctg17_532	Biosynthetic (additional)	phosphopantetheine-binding protein [*Adonisia turfae*]	98.80%	100%
ctg17_533	Biosynthetic	non-ribosomal peptide synthetase [*Adonisia turfae*]	97.31%	100%
ctg17_534	Biosynthetic	type I polyketide synthase [*Adonisia turfae*]	98.42%	100%
ctg17_535	Biosynthetic	non-ribosomal peptide synthetase [*Adonisia turfae*]	98.97%	99%
ctg17_536	Biosynthetic (additional)	thioester reductase domain-containing protein [*Adonisia turfae*]	99.01%	100%
ctg17_537	Biosynthetic (additional)	aspartate aminotransferase family protein [*Adonisia turfae*]	100%	100%
ctg17_538	Biosynthetic (additional)	acyl-CoA dehydrogenase family protein [*Adonisia turfae*]	100%	100%
ctg17_539	Biosynthetic (additional)	amino acid adenylation domain-containing protein [*Adonisia turfae*]	99.87%	100%
ctg17_540	Biosynthetic (additional)	alpha/beta fold hydrolase [*Adonisia turfae*]	99.59%	100%
ctg17_541	Other	DUF3493 domain-containing protein [*Adonisia turfae*]	100%	100%
ctg17_542	Biosynthetic (additional)	alpha/beta fold hydrolase [*Adonisia turfae* CCMR0081]	99.49%	100%
ctg17_543	Other	VOC family protein [*Adonisia turfae*]	100%	100%
ctg17_544	Other	pyruvate kinase [*Adonisia turfae*]	100%	100%

ctg17_545	Biosynthetic (additional)	2-hydroxyacid dehydrogenase [*Adonisia turfae*]	100%	100%
ctg17_546	Other	phosphoketolase family protein [*Adonisia turfae*]	99.63%	99%
ctg17_547	Other	acetate kinase [*Adonisia turfae*]	99.75%	98%
ctg17_548	Regulatory	cyclic nucleotide-binding domain-containing protein [*Adonisia turfae*]	99.51%	100%

Table A2.3 Link for the GNPS Molecular Network done between the bioactive (red 16/8h light/dark cycle and 24h) and the other non-bioactive conditions in the anti-settlement assay.

GNPS tool	Link of the job
Molecular Network	https://gnps.ucsd.edu/ProteoSAFe/status.jsp?task=05db69cae1824ac3811763ae014dff05

References

1. Hoiczyk E, Hansel A. Cyanobacterial Cell Walls: News from an Unusual Prokaryotic Envelope. J Bacteriol [Internet]. 2000 Mar [cited 2023 Jul 2];182(5):1191. Available from: /pmc/articles/PMC94402/
2. Mazard S, Penesyan A, Ostrowski M, Paulsen IT, Egan S. Tiny Microbes with a Big Impact: The Role of Cyanobacteria and Their Metabolites in Shaping Our Future. Mar Drugs [Internet]. 2016 May 1 [cited 2023 Jul 2];14(5). Available from: /pmc/articles/PMC4882571/
3. Montoya JP, Holl CM, Zehr JP, Hansen A, Villareal TA, Capone DG. High rates of N2 fixation by unicellular diazotrophs in the oligotrophic Pacific Ocean. Nature [Internet]. 2004 Aug 26 [cited 2023 Jul 2];430(7003):1027–31. Available from: https://pubmed.ncbi.nlm.nih.gov/15329721/
4. Sánchez-Baracaldo P, Bianchini G, Wilson JD, Knoll AH. Cyanobacteria and biogeochemical cycles through Earth history. Trends Microbiol. 2022 Feb 1;30(2):143–57.
5. Kumar K, Mella-Herrera RA, Golden JW. Cyanobacterial Heterocysts. Cold Spring Harb Perspect Biol [Internet]. 2010 Apr 1 [cited 2023 Jul 2];2(4). Available from: /pmc/articles/PMC2845205/
6. Kaplan-Levy RN, Hadas O, Summers ML, Rücker J, Sukenik A. Akinetes: Dormant cells of cyanobacteria. Top Curr Genet [Internet]. 2010 [cited 2023 Jul 2];21:5–27. Available from: https://link.springer.com/chapter/10.1007/978-3-642-12422-8_2
7. Meeks JC, Elhai J. Regulation of cellular differentiation in filamentous cyanobacteria in free-living and plant-associated symbiotic growth states. Microbiol Mol Biol Rev [Internet]. 2002 Mar [cited 2023 Jul 2];66(1):94–121. Available from: https://pubmed.ncbi.nlm.nih.gov/11875129/
8. Castenholz RW. General Characteristics of the Cyanobacteria. Bergey's Manual of Systematics of Archaea and Bacteria [Internet]. 2015 Sep 14 [cited 2023 Jul 2];1–23. Available from: https://onlinelibrary.wiley.com/doi/full/10.1002/9781118960608.cbm00019
9. Kaebernick M, Neilan BA. Ecological and molecular investigations of cyanotoxin production. FEMS Microbiol Ecol [Internet]. 2001 Jan 5 [cited 2023 Jul 2];35(1):1–9. Available from: https://pubmed.ncbi.nlm.nih.gov/11248384/
10. Johansen JR, Casamatta DA. Recognizing cyanobacterial diversity through adoption of a new species paradigm. Algological Studies/Archiv für Hydrobiologie, Supplement Volumes. 2005 Oct 1;117:71–93.
11. Strunecký O, Ivanova AP, Mareš J. An updated classification of cyanobacterial orders and families based on phylogenomic and polyphasic analysis. J Phycol [Internet]. 2023 Feb 1 [cited 2023 Jul 2];59(1):12–51. Available from: https://onlinelibrary.wiley.com/doi/full/10.1111/jpy.13304
12. Sánchez-Baracaldo P, Hayes PK, Blank CE. Morphological and habitat evolution in the Cyanobacteria using a compartmentalization approach. Geobiology [Internet]. 2005 Jul 1 [cited 2023 Jul 2];3(3):145–65. Available from: https://onlinelibrary.wiley.com/doi/full/10.1111/j.1472-4669.2005.00050.x
13. Mutalipassi M, Riccio G, Mazzella V, Galasso C, Somma E, Chiarore A, et al. Symbioses of Cyanobacteria in Marine Environments: Ecological Insights and Biotechnological Perspectives. Mar Drugs [Internet]. 2021 Apr 1 [cited 2023 Jul 2];19(4). Available from: /pmc/articles/PMC8074062/
14. Buratti FM, Manganelli M, Vichi S, Stefanelli M, Scardala S, Testai E, et al. Cyanotoxins: producing organisms, occurrence, toxicity, mechanism of action and human health toxicological risk evaluation. Arch Toxicol [Internet]. 2017 Mar 1 [cited 2023 Jul 2];91(3):1049–130. Available from: https://pubmed.ncbi.nlm.nih.gov/28110405/

15. Demay J, Bernard C, Reinhardt A, Marie B. Natural Products from Cyanobacteria: Focus on Beneficial Activities. Mar Drugs [Internet]. 2019 May 30 [cited 2023 Jul 2];17(6). Available from: /pmc/articles/PMC6627551/
16. Twaij BM, Hasan MN. Bioactive Secondary Metabolites from Plant Sources: Types, Synthesis, and Their Therapeutic Uses. International Journal of Plant Biology 2022, Vol 13, Pages 4-14 [Internet]. 2022 Feb 21 [cited 2023 Jul 2];13(1):4–14. Available from: https://www.mdpi.com/2037-0164/13/1/3/htm
17. Dias DA, Urban S, Roessner U. A Historical Overview of Natural Products in Drug Discovery. Metabolites [Internet]. 2012 Apr 16 [cited 2023 Jul 2];2(2):303. Available from: /pmc/articles/PMC3901206/
18. Hong J. Natural product diversity and its role in chemical biology and drug discovery. Curr Opin Chem Biol [Internet]. 2011 Jun [cited 2023 Jul 2];15(3):350. Available from: /pmc/articles/PMC3110584/
19. Dixon N, Wong LS, Geerlings TH, Micklefield J. Cellular targets of natural products. Nat Prod Rep [Internet]. 2007 Nov 21 [cited 2023 Jul 2];24(6):1288–310. Available from: https://pubs.rsc.org/en/content/articlehtml/2007/np/b616808f
20. Gerwick WH, Moore BS. Lessons from the past and charting the future of marine natural products drug discovery and chemical biology. Chem Biol [Internet]. 2012 Jan 27 [cited 2023 Jul 2];19(1):85–98. Available from: https://pubmed.ncbi.nlm.nih.gov/22284357/
21. Piel J. Metabolites from symbiotic bacteria. Nat Prod Rep [Internet]. 2009 Feb 25 [cited 2023 Jul 2];26(3):338–62. Available from: https://pubs.rsc.org/en/content/articlehtml/2009/np/b703499g
22. Fu Z, Li S, Han S, Shi C, Zhang Y. Antibody drug conjugate: the “biological missile” for targeted cancer therapy. Signal Transduction and Targeted Therapy 2022 7:1 [Internet]. 2022 Mar 22 [cited 2023 Jul 2];7(1):1–25. Available from: https://www.nature.com/articles/s41392-022-00947-7
23. Luesch H, Moore RE, Paul VJ, Mooberry SL, Corbett TH. Isolation of dolastatin 10 from the marine cyanobacterium Symploca species VP642 and total stereochemistry and biological evaluation of its analogue symplostatin 1. J Nat Prod [Internet]. 2001 [cited 2023 Jul 2];64(7):907–10. Available from: https://pubmed.ncbi.nlm.nih.gov/11473421/
24. Ali Shah SA, Akhter N, Auckloo BN, Khan I, Lu Y, Wang K, et al. Structural Diversity, Biological Properties and Applications of Natural Products from Cyanobacteria. A Review. Mar Drugs [Internet]. 2017 Nov 1 [cited 2023 Jul 2];15(11). Available from: https://pubmed.ncbi.nlm.nih.gov/29125580/
25. Leão PN, Engene N, Antunes A, Gerwick WH, Vasconcelos V. The chemical ecology of cyanobacteria. Nat Prod Rep [Internet]. 2012 Mar [cited 2023 Jul 2];29(3):372–91. Available from: https://pubmed.ncbi.nlm.nih.gov/22237837/
26. Bushley KE, Turgeon BG. Phylogenomics reveals subfamilies of fungal nonribosomal peptide synthetases and their evolutionary relationships. BMC Evol Biol [Internet]. 2010 Jan 26 [cited 2023 Jul 2];10(1):1–23. Available from: https://bmcecolevol.biomedcentral.com/articles/10.1186/1471-2148-10-26
27. Duban M, Cociancich S, Leclère V. Nonribosomal Peptide Synthesis Definitely Working Out of the Rules. Microorganisms 2022, Vol 10, Page 577 [Internet]. 2022 Mar 7 [cited 2023 Jul 2];10(3):577. Available from: https://www.mdpi.com/2076-2607/10/3/577/htm

28. Korman TP, Ames B, Tsai SC. Structural Enzymology of Polyketide Synthase: The Structure–Sequence–Function Correlation. Comprehensive Natural Products II: Chemistry and Biology. 2010 Jan 1;1:305–45.
29. Reimer JM, Haque AS, Tarry MJ, Schmeing TM. Piecing together nonribosomal peptide synthesis. Curr Opin Struct Biol [Internet]. 2018 Apr 1 [cited 2023 Jul 2];49:104–13. Available from: https://pubmed.ncbi.nlm.nih.gov/29444491/
30. Courtial J, Helesbeux JJ, Oudart H, Aligon S, Bahut M, Hamon B, et al. Characterization of NRPS and PKS genes involved in the biosynthesis of SMs in Alternaria dauci including the phytotoxic polyketide aldaulactone. Scientific Reports 2022 12:1 [Internet]. 2022 May 17 [cited 2023 Jul 2];12(1):1–20. Available from: https://www.nature.com/articles/s41598-022-11896-0
31. Robbins T, Liu YC, Cane DE, Khosla C. Structure and Mechanism of Assembly Line Polyketide Synthases. Curr Opin Struct Biol [Internet]. 2016 Dec 1 [cited 2023 Jul 2];41:10. Available from: /pmc/articles/PMC5136517/
32. Kehr JC, Picchi DG, Dittmann E. Natural product biosyntheses in cyanobacteria: A treasure trove of unique enzymes. Beilstein Journal of Organic Chemistry 7:191 [Internet]. 2011 Dec 5 [cited 2023 Jul 2];7(1):1622–35. Available from: https://www.beilstein-journals.org/bjoc/articles/7/191
33. Moretto L, Heylen R, Holroyd N, Vance S, Broadhurst RW. Modular type I polyketide synthase acyl carrier protein domains share a common N-terminally extended fold. Scientific Reports 2019 9:1 [Internet]. 2019 Feb 20 [cited 2023 Jul 2];9(1):1–16. Available from: https://www.nature.com/articles/s41598-019-38747-9
34. Romano S, Jackson SA, Patry S, Dobson ADW. Extending the “One Strain Many Compounds” (OSMAC) Principle to Marine Microorganisms. Mar Drugs [Internet]. 2018 Jul 1 [cited 2023 Jul 2];16(7). Available from: /pmc/articles/PMC6070831/
35. Singh G, Dal Grande F, Schmitt I. Genome mining as a biotechnological tool for the discovery of novel biosynthetic genes in lichens. Frontiers in Fungal Biology. 2022 Oct 3;3:993171.
36. Rajwani R, Ohlemacher SI, Zhao G, Liu HB, Bewley CA. Genome-Guided Discovery of Natural Products through Multiplexed Low-Coverage Whole-Genome Sequencing of Soil Actinomycetes on Oxford Nanopore Flongle. mSystems [Internet]. 2021 Dec 21 [cited 2023 Jul 2];6(6). Available from: https://journals.asm.org/doi/10.1128/mSystems.01020-21
37. Blin K, Shaw S, Augustijn HE, Reitz ZL, Biermann F, Alanjary M, et al. antiSMASH 7.0: new and improved predictions for detection, regulation, chemical structures and visualisation. Nucleic Acids Res [Internet]. 2023 May 4 [cited 2023 Jul 2]; Available from: https://dx.doi.org/10.1093/nar/gkad344
38. Ziemert N, Alanjary M, Weber T. The evolution of genome mining in microbes - a review. Nat Prod Rep [Internet]. 2016 Aug 1 [cited 2023 Jul 2];33(8):988–1005. Available from: https://pubmed.ncbi.nlm.nih.gov/27272205/
39. Scott TA, Piel J. The hidden enzymology of bacterial natural product biosynthesis. Nat Rev Chem [Internet]. 2019 Jul 1 [cited 2023 Jul 2];3(7):404–25. Available from: https://pubmed.ncbi.nlm.nih.gov/32232178/

40. Bode HB, Bethe B, Hˆfs R, Zeeck A. Big Effects from Small Changes: Possible Ways to Explore Nature's Chemical Diversity [Internet]. Vol. 3, ChemBioChem. WILEY; 2002. Available from: http://www.sanger.ac.uk/Projects/S
41. Fdhila F, Vazquez V, Sánchez JL, Riguera R. dd-diketopiperazines: antibiotics active against Vibrio anguillarum isolated from marine bacteria associated with cultures of Pecten maximus. J Nat Prod [Internet]. 2003 Oct [cited 2023 Jul 2];66(10):1299–301. Available from: https://pubmed.ncbi.nlm.nih.gov/14575426/
42. Tangerina MMP, Furtado LC, Leite VMB, Bauermeister A, Velasco-Alzate K, Jimenez PC, et al. Metabolomic study of marine Streptomyces sp.: Secondary metabolites and the production of potential anticancer compounds. PLoS One [Internet]. 2020 Dec 1 [cited 2023 Jul 2];15(12):e0244385. Available from: https://journals.plos.org/plosone/article?id=10.1371/journal.pone.0244385
43. Si Y, Tang M, Lin S, Chen G, Feng Q, Wang Y, et al. Cytotoxic cytochalasans from Aspergillus flavipes PJ03-11 by OSMAC method. Tetrahedron Lett. 2018 May 2;59(18):1767–71.
44. Burja AM, Abou-Mansour E, Banaigs B, Payri C, Burgess JG, Wright PC. Culture of the marine cyanobacterium, Lyngbya majuscula (Oscillatoriaceae), for bioprocess intensified production of cyclic and linear lipopeptides. J Microbiol Methods [Internet]. 2002 [cited 2023 Jul 2];48(2–3):207–19. Available from: https://pubmed.ncbi.nlm.nih.gov/11777570/
45. Veerabadhran M, Chakraborty S, Mitra S, Karmakar S, Mukherjee J. Effects of flask configuration on biofilm growth and metabolites of intertidal Cyanobacteria isolated from a mangrove forest. J Appl Microbiol [Internet]. 2018 Jul 1 [cited 2023 Jul 2];125(1):190–202. Available from: https://pubmed.ncbi.nlm.nih.gov/29573511/
46. Pasqua M, Visaggio D, Lo Sciuto A, Genah S, Banin E, Visca P, et al. Ferric Uptake Regulator Fur Is Conditionally Essential in Pseudomonas aeruginosa. J Bacteriol [Internet]. 2017 Nov 11 [cited 2023 Jul 2];199(22). Available from: /pmc/articles/PMC5648857/
47. Riediger M, Hernández-Prieto MA, Song K, Hess WR, Futschik ME. Genome-wide identification and characterization of Fur-binding sites in the cyanobacteria Synechocystis sp. PCC 6803 and PCC 6714. DNA Res [Internet]. 2021 Dec 1 [cited 2023 Jul 2];28(6). Available from: /pmc/articles/PMC8634477/
48. Årstøl E, Hohmann-Marriott MF. Cyanobacterial Siderophores—Physiology, Structure, Biosynthesis, and Applications. Mar Drugs [Internet]. 2019 [cited 2023 Jul 2];17(5). Available from: /pmc/articles/PMC6562677/
49. Chakraborty S, Verma E, Singh SS. Cyanobacterial Siderophores: Ecological and Biotechnological Significance. Cyanobacteria: From Basic Science to Applications. 2019 Jan 1;383–97.
50. Liu X, Millero FJ. The solubility of iron in seawater. Mar Chem. 2002 Jan 1;77(1):43–54.
51. Kranzler C, Lis H, Finkel OM, Schmetterer G, Shaked Y, Keren N. Coordinated transporter activity shapes high-affinity iron acquisition in cyanobacteria. The ISME Journal 2014 8:2 [Internet]. 2013 Oct 3 [cited 2023 Jul 2];8(2):409–17. Available from: https://www.nature.com/articles/ismej2013161
52. Qiu GW, Koedooder C, Qiu BS, Shaked Y, Keren N. Iron transport in cyanobacteria - from molecules to communities. Trends Microbiol [Internet]. 2022 Mar 1 [cited 2023 Jul 2];30(3):229–40. Available from: https://pubmed.ncbi.nlm.nih.gov/34175176/

53. Fresenborg LS, Graf J, Schätzle H, Schleiff E. Iron homeostasis of cyanobacteria: advancements in siderophores and metal transporters. Advances in Cyanobacterial Biology. 2020 Jan 1;85–117.
54. Kranzler C, Lis H, Finkel OM, Schmetterer G, Shaked Y, Keren N. Coordinated transporter activity shapes high-affinity iron acquisition in cyanobacteria. ISME J [Internet]. 2014 Feb 26 [cited 2023 Jul 2];8(2):409–17. Available from: https://pubmed.ncbi.nlm.nih.gov/24088625/
55. Jiang HB, Lu XH, Deng B, Liu LM, Qiu BS. Adaptive Mechanisms of the Model Photosynthetic Organisms, Cyanobacteria, to Iron Deficiency. Microbial Photosynthesis [Internet]. 2020 [cited 2023 Jul 2];197–244. Available from: https://link.springer.com/chapter/10.1007/978-981-15-3110-1_11
56. Khan A, Singh P, Srivastava A. Synthesis, nature and utility of universal iron chelator - Siderophore: A review. Microbiol Res [Internet]. 2018 Jul 1 [cited 2023 Jul 2];212–213:103–11. Available from: https://pubmed.ncbi.nlm.nih.gov/29103733/
57. Kramer J, Özkaya Ö, Kümmerli R. Bacterial siderophores in community and host interactions. Nature Reviews Microbiology 2019 18:3 [Internet]. 2019 Nov 20 [cited 2023 Jul 2];18(3):152–63. Available from: https://www.nature.com/articles/s41579-019-0284-4
58. Saha M, Sarkar S, Sarkar B, Sharma BK, Bhattacharjee S, Tribedi P. Microbial siderophores and their potential applications: a review. Environ Sci Pollut Res Int [Internet]. 2016 Mar 1 [cited 2023 Jul 2];23(5):3984–99. Available from: https://pubmed.ncbi.nlm.nih.gov/25758420/
59. Beiderbeck H, Taraz K, Budzikiewicz H, Walsby AE. Anachelin, the siderophore of the cyanobacterium Anabaena cylindrica CCAP 1403/2A. Z Naturforsch C J Biosci [Internet]. 2000 [cited 2023 Jul 2];55(9–10):681–7. Available from: https://pubmed.ncbi.nlm.nih.gov/11098815/
60. Katumba GL, Tran H, Henderson JP. The Yersinia High-Pathogenicity Island Encodes a Siderophore-Dependent Copper Response System in Uropathogenic Escherichia coli. mBio [Internet]. 2022 Feb 1 [cited 2023 Jul 2];13(1). Available from: https://journals.asm.org/doi/10.1128/mBio.02391-21
61. Lee JW, Helmann JD. Functional specialization within the Fur family of metalloregulators. Biometals [Internet]. 2007 Jun [cited 2023 Jul 2];20(3–4):485–99. Available from: https://pubmed.ncbi.nlm.nih.gov/17216355/
62. Clarke SE, Stuart J, Sanders-Loehr J. Induction of siderophore activity in Anabaena spp. and its moderation of copper toxicity. Appl Environ Microbiol [Internet]. 1987 [cited 2023 Jul 2];53(5):917. Available from: /pmc/articles/PMC203786/?report=abstract
63. Singh A, Kaushik MS, Srivastava M, Tiwari DN, Mishra AK. Siderophore mediated attenuation of cadmium toxicity by paddy field cyanobacterium Anabaena oryzae. Algal Res [Internet]. 2016 Jun 1 [cited 2023 Jul 2];C(16):63–8. Available from: https://www.infona.pl//resource/bwmeta1.element.elsevier-2b6b9125-e67f-31c3-8db5-24cdab0deab7
64. Miethke M, Marahiel MA. Siderophore-Based Iron Acquisition and Pathogen Control. Microbiology and Molecular Biology Reviews [Internet]. 2007 Sep [cited 2023 Jul 2];71(3):413–51. Available from: https://journals.asm.org/doi/10.1128/mmbr.00012-07
65. Zheng T, Nolan EM. Enterobactin-mediated delivery of ß-lactam antibiotics enhances antibacterial activity against pathogenic escherichia coli. J Am Chem Soc [Internet]. 2014 Jul 9 [cited 2023 Jul 2];136(27):9677–91. Available from: https://pubs.acs.org/doi/full/10.1021/ja503911p

66. Saha P, Yeoh BS, Xiao X, Golonka RM, Kumarasamy S, Vijay-Kumar M. Enterobactin, an iron chelating bacterial siderophore, arrests cancer cell proliferation. Biochem Pharmacol [Internet]. 2019 Oct 1 [cited 2023 Jul 2];168:71–81. Available from: https://pubmed.ncbi.nlm.nih.gov/31228465/
67. Breidbach T, Scory S, Krauth-Siegel RL, Steverding D. Growth inhibition of bloodstream forms of Trypanosoma brucei by the iron chelator deferoxamine. Int J Parasitol [Internet]. 2002 [cited 2023 Jul 2];32(4):473–9. Available from: https://pubmed.ncbi.nlm.nih.gov/11849643/
68. Miller MJ, Walz AJ, Zhu H, Wu C, Moraski G, Möllmann U, et al. Design, synthesis, and study of a mycobactin-artemisinin conjugate that has selective and potent activity against tuberculosis and malaria. J Am Chem Soc [Internet]. 2011 Feb 23 [cited 2023 Jul 2];133(7):2076–9. Available from: https://pubs.acs.org/doi/abs/10.1021/ja109665t
69. Gademann K, Kobylinska J, Wach JY, Woods TM. Surface modifications based on the cyanobacterial siderophore anachelin: from structure to functional biomaterials design. Biometals [Internet]. 2009 Aug [cited 2023 Jul 2];22(4):595–604. Available from: https://pubmed.ncbi.nlm.nih.gov/19350397/
70. Williamson RT, Boulanger A, Vulpanovici A, Roberts MA, Gerwick WH. Structure and absolute stereochemistry of phormidolide, a new toxic metabolite from the marine cyanobacterium Phormidium sp. J Org Chem [Internet]. 2002 Nov 15 [cited 2023 Jul 3];67(23):7927–36. Available from: https://pubmed.ncbi.nlm.nih.gov/12423120/
71. Kotai J. Instructions for preparation of modified nutrient solution Z8 for algae. Norwegian Institute for Water Research, Oslo . 1972;
72. Blin K, Shaw S, Kloosterman AM, Charlop-Powers Z, Van Wezel GP, Medema MH, et al. antiSMASH 6.0: improving cluster detection and comparison capabilities. Nucleic Acids Res [Internet]. 2021 Jul 2 [cited 2023 Jul 2];49(W1):W29–35. Available from: https://pubmed.ncbi.nlm.nih.gov/33978755/
73. Altschul SF, Gish W, Miller W, Myers EW, Lipman DJ. Basic local alignment search tool. J Mol Biol [Internet]. 1990 [cited 2023 Jul 2];215(3):403–10. Available from: https://pubmed.ncbi.nlm.nih.gov/2231712/
74. Gilchrist CLM, Chooi YH. clinker & clustermap.js: automatic generation of gene cluster comparison figures. Bioinformatics [Internet]. 2021 Aug 25 [cited 2023 Jul 2];37(16):2473–5. Available from: https://dx.doi.org/10.1093/bioinformatics/btab007
75. Molinspiration Cheminformatics [Internet]. [cited 2023 Jul 2]. Available from: https://www.molinspiration.com/
76. Pluskal T, Castillo S, Villar-Briones A, Orešič M. MZmine 2: Modular framework for processing, visualizing, and analyzing mass spectrometry-based molecular profile data. BMC Bioinformatics [Internet]. 2010 Jul 23 [cited 2023 Jul 4];11(1):1–11. Available from: https://bmcbioinformatics.biomedcentral.com/articles/10.1186/1471-2105-11-395
77. Pang Z, Chong J, Zhou G, De Lima Morais DA, Chang L, Barrette M, et al. MetaboAnalyst 5.0: narrowing the gap between raw spectra and functional insights. Nucleic Acids Res [Internet]. 2021 Jul 2 [cited 2023 Jul 4];49(W1):W388–96. Available from: https://dx.doi.org/10.1093/nar/gkab382
78. Nothias LF, Petras D, Schmid R, Dührkop K, Rainer J, Sarvepalli A, et al. Feature-based molecular networking in the GNPS analysis environment. Nature Methods 2020 17:9 [Internet]. 2020 Aug 24 [cited 2023 Jul 4];17(9):905–8. Available from: https://www.nature.com/articles/s41592-020-0933-6

79. Wang M, Carver JJ, Phelan V V., Sanchez LM, Garg N, Peng Y, et al. Sharing and community curation of mass spectrometry data with Global Natural Products Social Molecular Networking. Nat Biotechnol. 2016 Sep 8;34(8):828–37.
80. Wang M, Carver JJ, Phelan V V., Sanchez LM, Garg N, Peng Y, et al. Sharing and community curation of mass spectrometry data with Global Natural Products Social Molecular Networking. Nat Biotechnol. 2016 Sep 8;34(8):828–37.
81. Mohimani H, Gurevich A, Mikheenko A, Garg N, Nothias LF, Ninomiya A, et al. Dereplication of peptidic natural products through database search of mass spectra. Nat Chem Biol. 2017 Jan 1;13(1):30–7.
82. da Silva RR, Wang M, Nothias LF, van der Hooft JJJ, Caraballo-Rodríguez AM, Fox E, et al. Propagating annotations of molecular networks using in silico fragmentation. PLoS Comput Biol. 2018 Apr 1;14(4).
83. Gurevich A, Mikheenko A, Shlemov A, Korobeynikov A, Mohimani H, Pevzner PA. Increased diversity of peptidic natural products revealed by modification-tolerant database search of mass spectra. Nat Microbiol [Internet]. 2018 Mar 1 [cited 2023 Jul 6];3(3):319–27. Available from: https://pubmed.ncbi.nlm.nih.gov/29358742/
84. Wandy J, Zhu Y, Van Der Hooft JJJ, Daly R, Barrett MP, Rogers S. Ms2lda.org: Web-based topic modelling for substructure discovery in mass spectrometry. Bioinformatics. 2018 Jan 15;34(2):317–8.
85. Ernst M, Kang K Bin, Caraballo-Rodríguez AM, Nothias LF, Wandy J, Chen C, et al. MolNetEnhancer: Enhanced Molecular Networks by Integrating Metabolome Mining and Annotation Tools. Metabolites [Internet]. 2019 Jul 16 [cited 2023 Jul 4];9(7). Available from: http://www.ncbi.nlm.nih.gov/pubmed/31315242
86. Djoumbou Feunang Y, Eisner R, Knox C, Chepelev L, Hastings J, Owen G, et al. ClassyFire: automated chemical classification with a comprehensive, computable taxonomy. J Cheminform. 2016 Nov 4;8(1):1–20.
87. Shannon P, Markiel A, Ozier O, Baliga NS, Wang JT, Ramage D, et al. Cytoscape: A Software Environment for Integrated Models of Biomolecular Interaction Networks. Genome Res [Internet]. 2003 Nov [cited 2023 Jul 4];13(11):2498. Available from: /pmc/articles/PMC403769/
88. CDD Conserved Protein Domain Family: P-type_ATPase_HM_ZosA_PfeT-like [Internet]. [cited 2023 Jul 4]. Available from: https://www.ncbi.nlm.nih.gov/Structure/cdd/cddsrv.cgi?ascbin=8&maxaln=10&seltype=2&uid=319849&query=MIRSSASLGKLRYWLTTYPEAIAALTCALLTLMGWFALNQSWLGWGIWILMAAYIIGGRDSCWEGLKTLWQERELDVDLLMIVAALGAAILGFWQQQYYLLVDGAVLILIFAASGALESIAMHRTERNIRSLMQLTPDTARILQDKQERTIATE
89. Thibaut D, Couder M, Famechon A, Debussche L, Cameron B, Crouzet J, et al. The final step in the biosynthesis of hydrogenobyrinic acid is catalyzed by the cobH gene product with precorrin-8x as the substrate. J Bacteriol [Internet]. 1992 [cited 2023 Jul 4];174(3):1043–9. Available from: https://pubmed.ncbi.nlm.nih.gov/1732194/
90. Brown NL, Stoyanov J V., Kidd SP, Hobman JL. The MerR family of transcriptional regulators. FEMS Microbiol Rev [Internet]. 2003 Jun 1 [cited 2023 Jul 4];27(2–3):145–63. Available from: https://dx.doi.org/10.1016/S0168-6445(03)00051-2

91. Singh DK, Lingaswamy B, Koduru TN, Nagu PP, Jogadhenu PSS. A putative merR family transcription factor Slr0701 regulates mercury inducible expression of MerA in the cyanobacterium Synechocystis sp. PCC6803. Microbiologyopen [Internet]. 2019 Sep 1 [cited 2023 Jul 4];8(9). Available from: /pmc/articles/PMC6741143/
92. Shin JH, Oh SY, Kim SJ, Roe JH. The Zinc-Responsive Regulator Zur Controls a Zinc Uptake System and Some Ribosomal Proteins in Streptomyces coelicolor A3(2). J Bacteriol [Internet]. 2007 Jun [cited 2023 Jul 4];189(11):4070. Available from: /pmc/articles/PMC1913400/
93. BGC0002715 [Internet]. [cited 2023 Jul 6]. Available from: https://mibig.secondarymetabolites.org/repository/BGC0002715/index.html#r1c1
94. BGC0002678 [Internet]. [cited 2023 Jul 6]. Available from: https://mibig.secondarymetabolites.org/repository/BGC0002678/index.html#r1c1
95. BGC0001055 [Internet]. [cited 2023 Jul 6]. Available from: https://mibig.secondarymetabolites.org/repository/BGC0001055/index.html#r1c1
96. Giner-Lamia J, López-Maury L, Florencio FJ. Global transcriptional profiles of the copper responses in the cyanobacterium Synechocystis sp. PCC 6803. PLoS One [Internet]. 2014 Sep 30 [cited 2023 Jul 4];9(9). Available from: https://pubmed.ncbi.nlm.nih.gov/25268225/
97. Rojíčková-Padrtová R, Maršálek B. Selection and sensitivity comparisons of algal species for toxicity testing. Chemosphere. 1999 Jun 1;38(14):3329–38.
98. Wu H, Wei G, Tan X, Li L, Li M. Species-dependent variation in sensitivity of Microcystis species to copper sulfate: implication in algal toxicity of copper and controls of blooms. Sci Rep [Internet]. 2017 Jan 12 [cited 2023 Jul 4];7. Available from: /pmc/articles/PMC5227962/
99. Katumba GL, Tran H, Henderson JP. The Yersinia High-Pathogenicity Island Encodes a Siderophore-Dependent Copper Response System in Uropathogenic Escherichia coli. mBio [Internet]. 2022 Feb 1 [cited 2023 Jul 5];13(1). Available from: https://journals.asm.org/doi/10.1128/mBio.02391-21
100. Mari´ M, Gallegos MT, Schleif † Robert, Bairoch A, Hofmann K, Ramos JL. Arac/XylS family of transcriptional regulators. Microbiology and Molecular Biology Reviews [Internet]. 1997 Dec [cited 2023 Jul 3];61(4):393–410. Available from: https://journals.asm.org/doi/10.1128/mmbr.61.4.393-410.1997
101. Kotecka K, Kawalek A, Kobylecki K, Bartosik AA. The arac-type transcriptional regulator glir (Pa3027) activates genes of glycerolipid metabolism in pseudomonas aeruginosa. Int J Mol Sci [Internet]. 2021 May 2 [cited 2023 Jul 3];22(10). Available from: /pmc/articles/PMC8151288/
102. Zhou A, Chen YI, Zane GM, He Z, Hemme CL, Joachimiak MP, et al. Functional Characterization of Crp/Fnr-Type Global Transcriptional Regulators in Desulfovibrio vulgaris Hildenborough. Appl Environ Microbiol [Internet]. 2012 Feb [cited 2023 Jul 3];78(4):1168. Available from: /pmc/articles/PMC3273024/
103. Terauchi K, Ohmori M. Blue light stimulates cyanobacterial motility via a cAMP signal transduction system. Mol Microbiol [Internet]. 2004 Apr [cited 2023 Jul 3];52(1):303–9. Available from: https://pubmed.ncbi.nlm.nih.gov/15049828/
104. Ohmori M, Ohmori K, Hasunuma K. Rapid change in cyclic 3′,5′-AMP concentration triggered by a light-off or light-on signal in Anabaena cylindrica. Arch Microbiol [Internet]. 1988 Jun [cited 2023 Jul 3];150(2):203–4. Available from: https://link.springer.com/article/10.1007/BF00425163

105. Okamoto S, Kasahara M, Kamiya A, Nakahira Y, Ohmori M. A Phytochrome-like Protein AphC Triggers the cAMP Signaling Induced by Far-red Light in the Cyanobacterium Anabaena sp. Strain PCC7120¶. Photochem Photobiol [Internet]. 2004 Nov 1 [cited 2023 Jul 3];80(3):429–33. Available from: https://onlinelibrary.wiley.com/doi/full/10.1111/j.1751-1097.2004.tb00109.x
106. Ohmori M, Okamoto S. Photoresponsive cAMP signal transduction in cyanobacteria. Photochem Photobiol Sci [Internet]. 2004 Jun 1 [cited 2023 Jul 3];3(6):503–11. Available from: https://pubmed.ncbi.nlm.nih.gov/15170478/
107. Shin JH, Oh SY, Kim SJ, Roe JH. The Zinc-Responsive Regulator Zur Controls a Zinc Uptake System and Some Ribosomal Proteins in Streptomyces coelicolor A3(2). J Bacteriol [Internet]. 2007 Jun [cited 2023 Jul 3];189(11):4070. Available from: /pmc/articles/PMC1913400/
108. Ferreira L, Sousa ML, Ribeiro T, Morais J, Forero A, Castelo-Branco R, et al. Uncovering the Cyanobacterial Chemical Diversity: The Search for Novel Anticancer Compounds. Biology and Life Sciences Forum 2022, Vol 14, Page 49 [Internet]. 2022 Sep 15 [cited 2023 Jul 6];14(1):49. Available from: https://www.mdpi.com/2673-9976/14/1/49/htm
109. Han PP, Shen SG, Wang HY, Sun Y, Dai YJ, Jia SR. Comparative metabolomic analysis of the effects of light quality on polysaccharide production of cyanobacterium Nostoc flagelliforme. Algal Res. 2015 May 1;9:143–50.
110. Choi CY, Kim NN, Shin HS, Park HG, Cheon SG, Kil GS. The effect of various wavelengths of light from light-emitting diodes on the antioxidant system of marine cyanobacteria, Synechococcus sp. Mol Cell Toxicol [Internet]. 2013 Sep 1 [cited 2023 Jul 4];9(3):295–302. Available from: https://link.springer.com/article/10.1007/s13273-013-0037-9
111. Bhat O, Unpaprom Y, Ramaraj R. Effect of Photoperiod and White LED on Biomass Growth and Protein Production by Spirulina. Mol Biotechnol [Internet]. 2023 Jun 21 [cited 2023 Jul 4]; Available from: http://www.ncbi.nlm.nih.gov/pubmed/37341889
112. Khajepour F, Hosseini SA, Ghorbani Nasrabadi R, Markou G. Effect of Light Intensity and Photoperiod on Growth and Biochemical Composition of a Local Isolate of Nostoc calcicola. Appl Biochem Biotechnol [Internet]. 2015 Aug 1 [cited 2023 Jul 4];176(8):2279–89. Available from: https://pubmed.ncbi.nlm.nih.gov/26100389/